

ADVANCES IN BIOPROCESSING FOR BIOLOGICS AND GENE THERAPY VECTORS

Article Collection



Sponsored by

eppendorf

**CURRENT
PROTOCOLS**

A Wiley Brand



Most Compact

QbD-driven process development with the DASbox® Mini Bioreactor System

With working volumes of 60 – 250 mL the DASbox is the optimal tool for advanced cell culture and microbial process development and Design of Experiments (DoE) applications. All critical parameters can be precisely controlled.

- > Parallel set-up of up to 24 bioreactors
- > Perfectly suited for microbial and cell culture applications
- > Liquid-free exhaust condensation
- > Fully mass flow-controlled gas mixing
- > Available with single-use vessels

Designed for stem cell process development: BioBLU 0.3sc with 8-blade impeller



www.eppendorf.com/DASbox

Eppendorf® and the Eppendorf Brand Design are registered trademarks of Eppendorf SE, Germany. DASbox® is a registered trademark of DASGIP Information and Process Technology GmbH, Juelich, Germany. All rights reserved, including graphics and images. Copyright ©2022 by Eppendorf SE.

Contents

- 4 Introduction
Jeremy Petravicz
- 5 Advances in bioreactor systems for the production of biologicals in mammalian cells
R. Sharma, S.T.L. Harrison and S.L. Tai
ChemBioEng Reviews
- 26 Advancing a rapid, high throughput screening platform for optimization of lentivirus production
S. Gopal, A.E. Osborne, L. Hock et al.
Biotechnology Journal
- 36 Production, processing, and characterization of synthetic AAV gene therapy vectors
J. El Andari and D. Grimm
Biotechnology Journal
- 50 Process evolution in cell and gene therapy from discovery to commercialization
E. Csaszar, S. Mills and P.W. Zandstra
Canadian Journal of Chemical Engineering
- 58 Bioprocess characterization of virus-like particle production with the insect cell baculovirus expression system at nanoparticle level
E. Puente-Massaguer, I. González-Domínguez, F. Strobl et al.
Journal of Chemical Technology and Biotechnology
- 68 HEK293 Suspension Cell Culture Using the BioFlo® 320 Bioprocess Controller with BioBLU® 3c Single-Use Bioreactors. Eppendorf Application Note No. 447
J.L. Escobar Ivirico and M. Sha

© 2022 Wiley-VCH GmbH
Boschstr. 12, 69469 Weinheim, Germany

Email: info@wiley-vch.de
Editors: Dr Jeremy Petravicz
Ad Sales: Bettina Willnow

Cover image © Eppendorf

Introduction

Bioprocessing is the development and manufacturing pipeline by which therapeutic agents such as engineered recombinant proteins, viral gene therapy vectors and other nanoparticle-based technologies are produced at levels required for commercial distribution. To achieve this end, large-scale cultures using engineered cell lines are grown in bioreactors or through other scalable approaches. These are constantly being refined and evolved to increase volume, product yield and stability. The goal of this article collection is to present recent advances in the bioprocessing for biologics and gene therapy vectors.

The process of growing large quantities of cells involves a precise balance between nutrient availability, temperature control and oxygen/carbon dioxide balance, among other parameters which all must be closely monitored. Bioreactors have become an industry backbone for growing vast amounts of cells to produce therapeutic agents. In Sharma *et al.* (2021), the authors review the currently existing bioreactor technologies and their use for the growth of mammalian cell lines. As part of the bioprocessing workflow the optimal condition for growth and maximal production for individual cell lines need to be determined, which can be a resource and time consuming process. The ability to test cell lines in a microscale system greatly increases the throughput of the process. Gopal *et al.* (2021) provide evidence that high-density cultures can be achieved using a microscale 96-well platform, with results comparable to larger volume platforms. Using this microscale system, optimization of conditions and biologic/viral production can be achieved rapidly and with reduced cost. To produce cell and gene therapy products, the processes utilized continue to evolve as new technologies and methodologies come online. There are many paths for this process refinement to follow. In Csaszar *et al.* (2021), the authors describe a framework for the continued evolution of the gene and cell therapy development, production and testing process based on the concept of quality by design (QbD)

which uses a multistage iterative process to gain insights as to the process and lead to further refinements.

Vaccine development that focuses on the use of engineered virus-like particles (VLPs) has recently shown significant promise as a platform. These VLPs are typically grown in the insect cell baculovirus expression vector system, which has high capacity for recombinant protein production. However, information is lacking regarding the production quality and quantity of VLPs, as well as the stability of the expression system in the context of bioreactors. Puente-Massaguer *et al.* (2021) provide characterization of two different strategies for producing VLPs through large-scale bioreactors. Gene therapy vectors have a long history of use in the development of therapeutics. Several different engineered viruses based on their wild-type sources have been used, but those derived from AAV vectors have had the most success thus far. El Andari and Grimm (2022) review the advances in downstream processing and characterization of synthetic and natural AAVs for gene therapy applications with examples of directed molecular evolution of capsid proteins. To augment this article collection, Eppendorf provides the readers with a application note to inform readers regarding their BioFlo® 320 Bioprocess Controller with BioBLU® 3c Single-Use Bioreactors for suspension-adapted HEK293 cell lines at large scale to overcome the limitations normally associated with this line for bioprocessing.

In conclusion, we hope this article collection serves to educate the reader as to the current state of bioprocessing for biologics as well as cell and gene therapy approaches. Advances in the production and processing of these agents stands to revolutionize the ability to create next generation therapies and personalized medicine, as well as vaccines for emerging infectious diseases on a rapid scale.

Jeremy Petravicz, PhD
Senior Editor, Current Protocols
Wiley

Advances in Bioreactor Systems for the Production of Biologicals in Mammalian Cells

Rajesh Sharma^[1], Susan T. L. Harrison^[1], Siew Leng Tai^{[1],*}

Abstract

With the steady advancement of medicine and the healthcare industry, the demand for recombinant biotherapeutics drugs and vaccines has increased in the last two decades. This has put substantial pressure on the biopharma industry to meet the increasing need for treatment of prevailing and new diseases. Different technologies and bioreactor designs have been developed over the years to ensure safe and economical manufacturing of biopharmaceutical products by attaining high cell densities and

longevities for extended periods of time. Bioreactors are the backbone of the bioprocessing industry albeit each bioreactor design has its advantages and disadvantages. A comprehensive design suitable for wide varieties of cell lines to produce high-yielding products with the lowest cost and risk in the shortest span of time is sought. This paper focuses on evaluating the engineering aspects of currently available bioreactor designs and their suitability for mammalian cell cultures.

Keywords: Bioreactor design, Biotherapeutic drugs, High cell density, Mammalian cell culture, Vaccines

Received: March 12, 2021; *revised:* August 16, 2021; *accepted:* October 26, 2021

DOI: 10.1002/cben.202100022

1 Introduction

Cell culture is a century-old science, pioneered by Ross Harrison in 1907 who grew frog nerve fibre on lymph fluid in vitro for weeks on coverslips. These coverslips were placed inverted in an empty hollow grounded glass slide, thoroughly sealed with paraffin wax in a hanging drop method. The results obtained through this experiment demonstrated that cells can be grown in vitro, which then laid the foundation for modern cell culture [1]. Further, developmental work with plasma clot as a medium for the growth of chick embryo in 1910 led to the gradual advancements in medium and feed development, cell line engineering and process development of biologicals. These breakthrough activities have further propelled the cell culture-based activities with the discovery of antibiotics in the 1940s and of monoclonal antibodies in the 1970s. In the 1970s, advancements in recombinant DNA (rDNA) technology led to the ability for expression of exogenous genes in microbial or mammalian cells; and in more recent years, high-throughput technologies and the advances in “omics” tools such as proteomics, genomics, metabolomics further improved the production yields and productivity [1–3].

The rise of new and emerging diseases has not only burdened the world economy but also negatively impacted the socio-economic set up of the society. Therefore, there is a need to develop and manufacture new vaccine candidates quickly, safely and at a low cost. The positive side of these emerging diseases is that it has fast-tracked the development of new vaccine

technologies such as mRNA vaccines and vector-based vaccines. It is expected that increased investment towards the development and manufacturing of new vaccines for the treatment of emerging disease will drive the global vaccines market in the near future. It is also expected that the global biopharmaceutical market will grow at a CAGR of 10.1% in the next decade, and the market may reach the mark of USD 459.81 billion by 2025 [4]. Mammalian cell lines such as Chinese hamster ovary (CHO) cells, baby hamster kidney (BHK) cells, Vero cells, human embryonic kidney (HEK) cells, mouse myeloma cells, NS0 and SP2/0 cells are used for commercial manufacturing of biologicals. For mammalian cell culture, bioreactors play an important role in the economics of product manufacturing owing to constraints on acceptable process conditions [5–7].

The key function of a bioreactor is to provide optimal cell growth conditions for high cell density and prolonged longevity of the cultures. Many bioreactor designs have been tested for the growth of mammalian cells since the 1940s. These bioreactors fall under five categories; namely, (1) bioreactors without control (e.g., tissue culture flasks, multi-tray cell factories,

^[1] Rajesh Sharma, Dr. Susan T. L. Harrison, Dr. Siew Leng Tai
Centre for Bioprocess Engineering Research (CeBER), Department of Chemical Engineering, Faculty of Engineering and the Built Environment, University of Cape Town, Private Bag, Rondebosch 7701, South Africa.
E-Mail: siew.tai@uct.ac.za

roller bottles, spinner flasks), (2) reusable bioreactors (e.g., conventional glass vessels, stainless steel stirred tank bioreactor, packed bed, pneumatically-driven bioreactors), (3) single-use bioreactors (e.g., disposable stirred tank, wave mixed, orbitally shaken, pneumatically driven and fixed bed bioreactors), (4) novel bioreactor designs with different operating principles (e.g., CelCradle, travelling wave, nucleo bioreactor with tumbling impeller, Pad bioreactor, vertical wheel and rotating wall bioreactor), and (5) membrane bioreactors (CELLine flask). In this article, these different bioreactor systems are evaluated for their suitability for process development, scale-up, and the evaluation of their engineering design for industry-specific applications and commercialization.

2 Bioreactors – The Industrial Workhorses

A bioreactor plays a dominant role in the production of biologicals, and it has been regarded as the central production wheel for the biopharmaceutical industry. The growing knowledge of the cellular behavior of different cell lines and their interaction with the macroenvironment inside the bioreactor has led to the improvement of the bioreactor design to satisfy the industry requirements. Margaritis and Wallace [8] elaborated the basic requirements for the bioreactor design as shown in Fig. 1. The design criteria takes a comprehensive approach to integrating old knowledge of bioreactor design to the new knowledge which works in unison with different process analytical tools (PAT). The PAT enables online real-time monitoring of the processes and associated process improvements by controlling

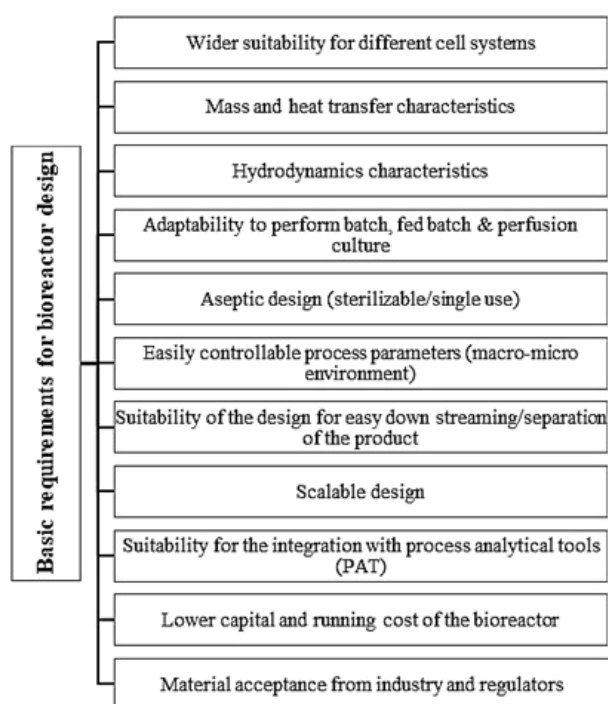


Figure 1. Basic requirements for bioreactor design – adapted from [8].

parameters stringently and reducing the risk of batch failure [9].

The first and most important aspect of bioreactor design is its wider suitability for varieties of cell systems, e.g., animal, insect, fish, plants, and human cell lines [10]. Cell lines from these sources are currently being used to produce different biological products. With the widespread knowledge and understanding of the microbiology and cell behavior of the different cell systems, one can define the nutritional requirements by a thorough understanding of the metabolic pathways and the precursors required to produce primary and secondary metabolites. This will help in achieving high cell densities and the target product concentration. Furthermore, this knowledge will enhance the culture longevity by knowing the interaction of a cell system with the surrounding macroenvironment and which would further aid in stringently maintaining and controlling the microenvironment inside the cell.

Hydrodynamic characteristics of the bioreactor play a key role in the growth of different cell lines. It directly affects the mass and heat transfer capability of the culture system. In various bioreactor designs (horizontal, vertical, or bag type), the aspect ratio of the vessel and the type of impeller used, play a crucial role in defining the hydrodynamic state of the bioreactor. The mixing profile of Newtonian fluids further affect the mass and heat transfer capability of the system. The important aspect of bioreactor design is to provide a high surface area for mass and heat transfer, an efficient mixing regime without pH, temperature, and nutritional gradient, and with low power input.

Another area of interest in the development of bioreactor design is to provide a conducive environment to the growing cells by controlling the macroenvironment surrounding the cells. This directly influences the growth kinetics and metabolic activity of the cells. Macroenvironment would further affect the microenvironment inside the cells, which would lead them to either high productivity or apoptosis. Clonal stability also plays an important role in the production of biotherapeutic proteins. Based on the clone stability, researchers can decide on the mode of operations such as batch, fed batch and continuous/perfusion. With the advancement of cutting-edge technologies in molecular level screening and cell line development, researchers lay emphasis in the development of kinetic models to predict the behavior of cell lines under investigation in a bioreactor system. With the help of kinetic models, the problem of low productivity of biotherapeutics with high cell density for prolonged viability and reduced programmed cell death can be investigated [11]. Strategies to support this include minimizing pH and temperature fluctuations using proper mixing and by reducing hydrodynamic shear by choosing the appropriate aeration-agitation regimen [12].

In addition to well-integrated bioreactor designs for the cell growth, separation of cells from the cultured broth is an important step in downstream processing (DSP). Spin filters, dialysis, gravity settlers, acoustic filters, hydrocyclones, continuous centrifuges, tangential flow filtration, and alternating tangential flow filtration are options available for separating cells from the medium [13]. Many companies have incorporated some of these separation technologies during perfusion culture in their facilities such as inclined settlers (Chiron), spin filters

(Centocor), and ultra-sound/acoustic devices (BioSep-Appikon) [14]. Cell retention by immobilization of mammalian cells has also proven to be successful in separating cells from the culture broth without additional downstream steps, thus reducing the capital and operating/running cost of the system. Ultimately, the success of the cell culture bioreactor design lies in supporting high cell densities required for high productivities, regardless of whether grown as adherent, suspension or immobilized cultured cells [15–17].

The material of construction plays an important role in designing bioreactors. The material should have regulatory acceptance as outlined by the Food and Drug Administration (FDA) in the Current Good Manufacturing Practice for Finished Pharmaceuticals guide under Subchapter C, subpart D, 21CFR211.65 [18]. It is recommended that the material used for all internal parts of the bioreactor in contact with product, culture and/or media should be constructed from 316 L passivated stainless steel. Other accessories used in the fabrication of bioreactors should support low particle generation and ease of cleanability [19]. Connectors on a bioreactor should be of clean design, with tri-clover connections, diaphragm valves, and sterilizable connections as standard features. For single-use systems, low leachability and extractability of the materials of construction are desirable, as these have negative effects on cell growth, their viability and product purity [9, 20].

The last important aspect of the successful design of a bioreactor is its capability for economical scale-up of the processes from the L to the m³ scale. It has been recommended that during the process of designing prototype bioreactors, emphasis should be given to the requirements for process development and integration of accessories for large-scale manufacturing, thus reduces the difficulties in scale up [21].

At present, various major pharmaceutical companies have bioreactors with the maximum capacity in the range of 20 to 25 m³ such as the large-scale cell culture bioreactors at Genentech, Vacaville with a capacity of 25 m³ and at Lonza, Singapore with a capacity of 20 m³ [22]. The advancement in control systems and instrumentation of these bioreactors have allowed for an optimized macroenvironment leading to higher productivity, growth kinetics and metabolic activity of the cells [19].

The peculiar feature of the mammalian cells is that they have semi-permeable outer cell membranes with the absence of a cell wall. Due to this, these cells are shear-sensitive and fragile. The fragility, large size, slow growth rates and low oxygen consumption rates make mammalian cells difficult to grow [23]. Liquid shear forces from stirring, bubble formation and direct sparging of the bioreactor have deleterious effects on the overall growth of the shear-sensitive cell lines achieving optimum cell density, viability, and productivity [13, 24, 25]. Therefore, there is a need to develop strategies which could provide adequate mass and heat transfer with low shear stress even at large scale.

Hence, several novel prototypes and bioreactor designs have been developed for shear-sensitive mammalian cells. Different designs extend different growth environments for optimal cell growth and the expression of recombinant proteins. Therefore, it is recommended to identify the critical process parameters relevant for a particular application before designing or selecting the bioreactor. These parameters such as optimum cell density (cell growth), percentage viability, cellular oxygen demand

particularly at high cell density, viscosity, foaming, the cellular settlement at the base or clumping, shear-stress sensitivity, homogenous temperature, and scalability play an important role in the selection of the bioreactor [26]. These designs combine engineering aspects and biomimicry for efficient mass and energy transfer [7, 23, 27]. These novel bioreactors, specifically designed for mammalian cell culture have different geometrical configurations and working principles; however, their design must fulfil the basic requirements as shown in Fig. 1. The data in Tab. 1 exhibits various types of bioreactor design available for mammalian cells based on their engineering characteristics. It is evident that older technology bioreactors like stirred tanks have had years of research and utilization for process improvement, while more novel bioreactors like membrane (not covered in this review) and micro bioreactors, while showing strong potential to grow mammalian cells, require further development.

3 Chronological Advancement of Bioreactors for Mammalian Cell Culture: Growth Wheel of the Biologicals Industry

Cell culture was traditionally done in glass tissue culture flasks (TC-flasks) and spinner flasks. Later, in the 1960s, disposable culture flasks made their way to the market [28]. The first use of stirred tank bioreactors for mammalian cell culture was reported in 1965 when BHK cells were grown at 30 L scale in suspension for the production of inactivated foot and mouth disease vaccine [13].

The bioreactor systems for the propagation of mammalian cells that have been developed over the last 60 or more years can be categorized in several ways. A major categorization is whether the bioreactors are reusable or single-use bioreactors (SUBs). Reusable bioreactors are vessels with rigid walls constituted of glass and/or stainless-steel and are cleaned and re-sterilized after use. Disposable reactors, on the other hand, are poly-plastic vessels which normally constitute a collapsible bag which is discarded after use. Reactors are also classified in terms of the method by which energy is introduced for mixing. Examples include mechanically agitated systems with internal energy delivery such as the stirred tank bioreactor; reactors with external pumping of liquids such as the fluidized bed bioreactor or packed bed reactor; reactors driven by external energy input such as the wave or orbitally shaken reactors; and aerated systems such as the airlift reactor or bubble column.

The details of the major reactor types and the development of bioreactors from the 1940s to 2021 has been summarized in Tab. 2 depicting the trends in the bioreactor development include single-use technology and impeller free systems with non-invasive probes for effective process control.

4 Review of Mammalian Cell Bioreactors

Mammalian cells have low oxygen demand as compared to microbial cultures, however, oxygen is still a limiting factor for

Table 1. Comparison of bioreactor systems for the growth and expression of biopharmaceutical products in mammalian cells – adapted from [26].

Parameters	Bioreactor Types									
	Re-usable stirred tank bioreactor	Single-use stirred tank bioreactor	Wave type bioreactor	Shaken bioreactor	Vertical wheel bioreactor	Rectangular bioreactor	Bubble column/airlift bioreactor	Fixed bed bioreactor	Membrane bioreactor	Micro bioreactor
O ₂ mass transfer (k_La)	+++	++/+++	++	++/+++	++	++	++	+	+	++
Mixing time	+ ¹	++ ²	++	++	++	++	++	+++/++	++	++
Shear by agitation	+++ ³	++	+	+	+	+	+	+	+	+
Shear by aeration	+++	++	+	+	+	+	+++	+	+	+
Power consumption	+++	++	++	++	++	++	+	++	+	+
Operational difficulty	++	++	++	++	++	++	+	+++	++	+
Operational flexibility	+++	++	++	++	++	++	+++	+	+	+
CIP/SIP	Yes	No	No	No	No	No	Yes	No	No	No
Max. volume	25 000 L	4000 L	2000 L	1000 L	500 L	1000 L	2000 L	30 L	Data not available	15 mL
Ease of scale up	Medium	Medium	Complex	Complex	Medium	Medium	Easy	Complex	Complex	Complex
Monitoring and control	+++	+++	+++	+++	+++	+++	+++	+	+	++
Ease of GMP compliance	+++	+++	+++	+++	+++	+++	+++	Difficult	Difficult	Data not available

¹ + Low, ² ++ Medium, ³ +++High

high-density cell cultures. The oxygen mass transfer coefficient (k_La) value of sparged stirred tank bioreactor falls between 1–15 h⁻¹ [13, 29]. Eibl et al. [28] also outlined that for a typical mammalian cell culture processes, oxygen mass transfer of 6–10 h⁻¹ is sufficient to cater the oxygen demand for middle to high cell densities, with a mixing time below 1 min and power input of 70–80 Wm⁻³.

It is the new normal for the industrial batch to achieve the cell density ranging from 5 × 10⁶–10 × 10⁶ cells mL⁻¹. Some systems have been reported to achieve even higher cell densities, especially in perfusion cultures. Most of the industrially accepted cell lines operate at a wide range of oxygen concentrations (15–90%), whereas primary cell lines prefer to grow at low oxygen concentrations mimicking in vivo conditions [30]. The typical oxygen uptake rate (OUR) of mammalian cells are in the range of 0.5 × 10⁻¹⁰–8.0 × 10⁻¹⁰ mmol cell⁻¹h⁻¹ [31]. Based on these above-mentioned OUR values, the k_La values for cell densities ranging from 1 × 10⁶–100 × 10⁶ cells mL⁻¹ were estimated to be sufficient when the dissolved oxygen concentration

was maintained at 20 to 50% of air saturation as shown in Tab. 3. For example, the oxygen mass transfer coefficient (k_La) required to prevent O₂ limitation for 10 × 10⁶ cells mL⁻¹ at 40% air saturation would fall in the range of 4.2 to 67 h⁻¹. The percentage of air saturation is also known as percentage dissolved oxygen (% DO) in the liquid phase which is given by Eq. (1).

$$\%DO = \left(\frac{C_L}{C^*} \right) \times 100 \quad (1)$$

Where, C_L is actual oxygen concentration in the liquid phase, C^* is oxygen saturation concentration at equilibrium with air [30]. The oxygen mass balance is given as the rate of change of oxygen concentration during the batch dc/dt equaling to the rate of oxygen transfer into the culture medium (OTR) minus the oxygen consumed (OUR) by the cell as shown in Eq. (2).

$$\frac{dc}{dt} = OTR - OUR \times C_x \quad (2)$$

Table 2. Chronological advancements of the bioreactors for the cell culture systems.

Bioreactor categories	1940s–1950s	1960s–1970s	1980s–1990s	2000–2004	2004–2008	2008–2012	2012–2021
Without control	Disposable blood bags (Fenwel), Glass Spinner flasks	Glass Petri plates and Roller Bottles, SU-TC flasks, SU-Multi-layered TC factories			SuperSpinner D1000 (Sartorius)	Sensolux Flasks	
Reusable	The magnetically driven rigid vessel	Stirred tank-stainless steel					
	Pneumatically driven	Cell Maker Felix (Celsius)			PBS3 (PBS biotech)		
	Hollow fibre	Cellmax				CelliGen BLU (Eppendorf)	iCELLis, Xpansion 200 (Pall)
	Packed or fixed Bed		Solid glass beads, macroporous beads (SIREN), ceramic cylinders with the uniform square channel, PE non-woven fibre (Fibra-Cel)				
Single-Use	Bioreactor for microcarrier culture		Spin filter		DE53, (Whatman) (Fibra-Cel, Eppendorf)		
	Wave mixed		Wave bioreactor		AppliFlex, (Applikon), Biostat RM (Sartorius)	CellTainer, (CELLution Biotech)	Multi-layered Tsunami Bioreactor, Allegro XRS 20 (Pall), Smart Rocker (Finesse)
	Rotationally/orbitally shaken bioreactor				Orbitally shaken helical track	CultiBag ORB (Sartorius), Orb Shake (Kuhner), BayShake (BTS)	Custom Single Run (CSR) (ABEC), Mobius 2000 (Millipore), Allegro XTR 200 (Pall)
	Mechanically driven stirred tank						Travelling wave bioreactor
Novel Design	Novel designs with the different operating principle		Rotary Cell Culture System (RCCS), (Synthecore)	Bello cells (Cesco Bioengineering)	Pad and Nucleo Bioreactor (Pall)	Dynamic Aeration System (BTS), Tide cell (Cesco Bioengineering)	
Membrane							CELLine flasks (Integra Biosciences)
Miniature/scale-down				Tube spin (TPP)	DASGIP BioLector		Ambr platform

Table 3. Estimated k_La values for various cell density at 20–50% of air saturation (supplementary dataset: DOI 10.25375/uct.12263141).

Cell densities [cells mL ⁻¹]	k_La [h ⁻¹] with air							
	20 % air saturation		30 % air saturation		40 % air saturation		50 % air saturation	
	Low	High	Low	High	Low	High	Low	High
100 × 10 ⁶	31.3	500	35.7	571.4	41.7	666.7	50	800
10 × 10 ⁶	3.1	50	3.6	57.1	4.2	66.7	5	80
5 × 10 ⁶	1.6	25	1.8	28.6	2.1	33.3	2.5	40
1 × 10 ⁶	0.3	5	0.4	5.7	0.4	6.7	0.5	8

Where C_x is the total number of cells at a given time; the oxygen transfer rate (OTR) is given by Eq. (3).

$$OTR = k_La(C^* - C_L) \quad (3)$$

The mass transfer efficiencies of different culture systems obtained through literature have been compared with respect

to their mode of aeration in Fig. 2. Mass transfer efficiency of a culture system primarily depends on the mode of aeration, mode of agitation, power input and the volume of the culture. Fig. 2 represents the indicative values of k_La of different culture system irrespective of their volumes. The cell density of 10 × 10⁶ cells mL⁻¹ is considered as an industrial benchmark for an optimized process, while 40 % air saturation is considered as

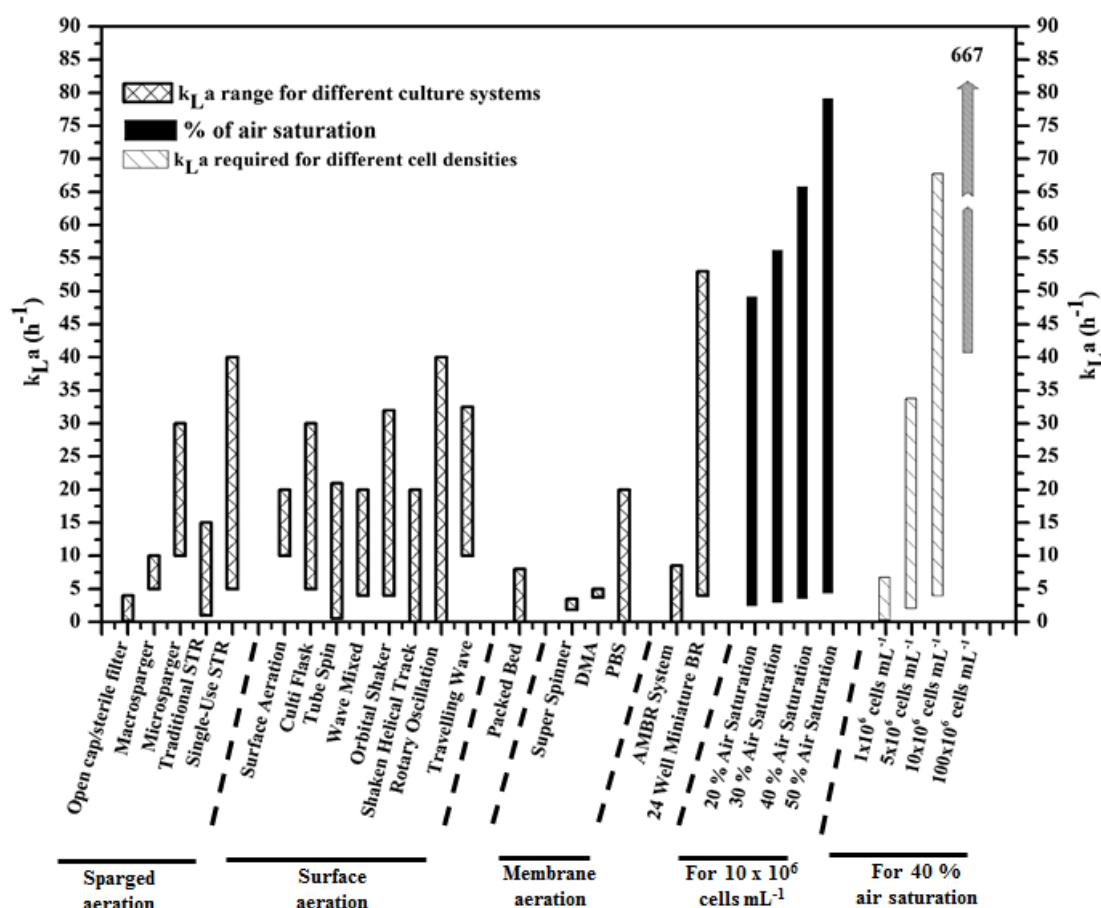


Figure 2. Indicative k_La values of different culture systems based on the methods of their aeration. Crossed columns represent k_La values of the various culture systems. Black column represents the k_La range for 10 × 10⁶ cells mL⁻¹ with varying air saturation and the striped column represent the k_La values required for different cell densities at 40% of air saturation – data taken from [13, 31, 65, 77, 83, 84, 99, 102, 122, 127–130] (supplementary dataset: DOI: <https://doi.org/10.25375/uct.12263141>).

the median oxygen saturation concentration range for established mammalian cell lines.

4.1 Bioreactors without the Control Unit

Preliminary cell culture work is performed in culture systems without any integrated control systems. The physiological condition of the growing cells is maintained by keeping the culture system inside an incubator. Such culture systems are broadly divided into the static system grown in tissue culture flasks, multi-tray culture vessels and dynamic systems typically grown in Erlenmeyer shake flasks, roller bottles and spinner flasks. These systems are typically used for initial process development such as the adaptation of cell lines, clonal selection, media and feed screening, and developing proof of concept for the processes [27].

4.1.1 Static Culture

All static cultures require a humidified CO₂ incubator to maintain suitable physicochemical conditions for the growth of mammalian cells [28]. The CO₂ incubator would provide the physiological temperature of 37 °C and around 60–80 % relative humidity. CO₂ is used for the maintenance of pH of the culture media at 7.0 ± 0.2 . The percentage of the CO₂ purged into the incubator generally falls between 5–10 % and is dependent on the concentration of bicarbonate used in the growth medium. Static cell culture work was initially carried out by using glass tissue culture flasks. In the 1960s and 70s, glass tissue culture flasks were replaced by polystyrene which led to single-use technology. These flasks provide high volume to surface area ratio and are available from 25 to 225 cm² in a single layer or up to a 5-layer format. Multi-stacked cell culture systems were then introduced for the growth of adherent cultures for the vaccine development at large scale. CellSTACK[®] from Corning and Cell Factory[™] from Nunc are available in 10 and 40 layered closed systems. They also provide a high volume to area ratio similar to tissue culture flasks (T-flask) but are very difficult to handle due to their large size and volume. The HYPER Flasks[®] system from Corning offers multi-layered culture system with 1720 cm² of surface area which is around 10 folds higher than a T-175 cm² TC-flask [32]. Since there is no mixing involved in the tissue culture flasks (TC-flasks), oxygenation of media occurs through diffusion from the headspace to the media layer. At high cell density, oxygenation is a limiting factor and accumulation of metabolic wastes have negative effects on cell growth [22]. To overcome the limitation of surface area for mass transfer, Corning introduced the 100-layered cell cube system, which provides a surface area of 85 000 cm². The liquid medium is continuously circulated through the multiple chambers of the cell cube through a media circulation pump for nutrient and oxygen supply through an inlet port at the lower corner of the plate and the media flow-out of the system from the outlet port at the top corner of the cell cube system [32]. However, it has been reported that due to the large surface area, improper fluid flow across the different layers of the cell cube can result in non-uniform cell growth and shear stress [33].

4.1.2 Dynamic Culture

Six decades ago, the polio vaccine became the first vaccine to be produced commercially where monkey kidney cells were infected with Salk poliovirus on adherent surfaces. Subsequently, the success of adapting baby hamster kidney (BHK) cells into suspension culture triggered the use of mammalian cells for the production of vaccines in a stainless steel stirred vessel [1]. Development of spinner flasks further aided the growth of mammalian cells in suspension culture. Spinner flasks and roller bottles provide the starting platform for the development of seed cultures and are currently available as reusable and disposable units. The spinner flasks consist of a culture vessel with side arms; these sidearms are used for the addition of media and cells and withdrawal of samples and for the harvesting of the culture aseptically. These flasks are kept on the magnetic stirrer inside a CO₂ incubator to provide mass and heat transfer. The oxygen mass transfer coefficient (k_{La}) in spinner flasks is reported to be in the range of 0.1–4.0 h⁻¹ [7]. Roller bottles, on the other hand, provide a much larger surface area for adherent cultures. The roller bottles are rotated horizontally such that gas exchange occurs through the liquid thin layer formed on the surface of the rotating roller bottles by diffusion [7, 22].

The new advanced culture systems developed in the first decade of the 2000s by Sartorius, such as the Sensolux flask and Super Spinner D1000 that incorporate the pre-calibrated pH and dissolved oxygen (DO) sensors for real-time monitoring of these critical process parameters. The Sensolux flasks contain pre-calibrated pH and DO sensor patches on it which would be placed on a shaker tray platform. This shaker-tray platform has optical sensors which aid in actual measurement optically and non-invasively through fluorescence. In the case of the SuperSpinner D 1000, a magnetic stirrer covered with a hollow fibrous membrane provides bubble-free aeration with gentle mixing. It has been reported that these SuperSpinner flasks support higher cell densities compared to the standard spinner and can achieve a k_{La} of 1.9–3.5 h⁻¹ [34].

4.2 Cell Culture Systems and Accessories for Microcarrier Culture

The initial concept of growing adherent cells on microcarriers as suspension culture was demonstrated by van Wezel [16]. Microcarriers are small spheres with a 90–300 μm diameter in different geometrical shapes like cylindrical (DE53, Whatman) and disk-shaped (Fibra-Cel, Eppendorf). They provide a large surface area to volume (cm²mL⁻¹) ratio and enhance mass transfer efficiency and deliver consistent product quality over static culture systems [35, 36]. Microcarriers are used to grow adherent cells for large-scale suspension culture in stirred tank bioreactors. These microcarriers are divided into two subtypes, macroporous and solid. Macroporous carriers provide a larger surface area, hence support higher cell density than solid microcarrier but yield less product than solid carriers. This is mainly due to poor mass transfer capabilities which include limited diffusion of nutrients into the center of macroporous carrier and difficulty in removing toxic metabolite, which negatively impacts the cell density and longevity of the culture [16].

4.3 Reusable Bioreactor Systems

Reusable systems are those in which culture vessels are made up of stainless steel and/or glass with a fixed vessel design and addition ports. At pilot and commercial scale, the requirements for water for injection (WFI), piping for clean steam and plant steam, cascade sparging, cooling system and cleaning-in-place/sterilization-in-place (CIP/SIP) is mandatory for the smooth operation of a large bioreactor. Reusable bioreactors typically start from 1 L (benchtop) and extend to 25 m³ in commercial scale to produce biologics from mammalian cells. Stirred tank, bubble column, airlift, packed bed bioreactors are examples of reusable bioreactors.

4.3.1 Stirred Tank Bioreactors (STRs)

Stirred tank bioreactors are the most conventional bioreactors in which energy for mass and heat transfer is introduced into the reactor mainly through the impeller shaft, driving fluid motion, and partially by sparging of gases. STRs have been engineered quite extensively. Most of the bioprocesses in the biopharmaceutical industry use the stirred tank bioreactor because of its proven and well-established track record for upstream process development and scale-up. They are the preferred production platform for the biopharmaceutical industry [37, 38].

Owing to the sensitivity of mammalian cells to shear stress caused by bursting air bubbles [39, 40], many methodologies have been developed to provide sufficient oxygen to the mitotic cells through micro and macro spargers, microporous silicone tubes and aeration through the headspace (surface aeration). High-density cultures require a high amount of oxygen supply, which often is not met by surface oxygenation methods alone. Therefore, direct sparging at large scale has proven, conventionally, to be the best suitable method of supplying oxygen to the growing cells [41]. Ozturk [41] also reported that high cell density in the bioreactor depends on the mode of aeration. Surface aeration alone (headspace) is not adequate for catering the high oxygen demand of the cells whereas membrane aeration is the most suitable mode of aeration at high density. Oxygenation of the culture media can be done internally or externally with the help of a basket (silicone tubing coiled around a stainless-steel casing) and a gas exchanger, respectively. The rate of oxygenation depends on the length of the tubing per volume. The membrane aeration has the limitation that it can only be manageable up to 200 L and support the cell density up to 10×10^6 cells mL⁻¹.

In the case of direct sparging, the type of sparger plays an important role in delivering the desired mass transfer coefficient for high cell density culture without impacting on the overall cell growth. A micro sparger provides a large surface area and high mass transfer efficiency to the high-density culture. The downside of using the micro sparger is that it also generates small bubbles (<2 mm), which create foaming and bubble bursting at the surface of the liquid [42]. In the case of macro sparger, it is reported that the high mass transfer efficiency can be achieved by providing higher gas flow rates as compared to the microsparger to achieve the same cell density. The bubbles formed in case of macro sparger are around

6–8 mm in size and do not take part in foam formation and cell death, because they travel faster upwards toward the surface and carry fewer cells attached to the bubble surface [30, 41].

The Oxygen Uptake Rate (OUR) of high cell density cultures determines the required $k_L a$ or oxygen transfer threshold of a system to support the growing cells, below which respiration becomes growth limiting. To meet this oxygen demand, different combinations of aeration-agitation regimen are tested to meet the operating window while avoiding hydrodynamic shear, bubble damage and foam formation as indicated in Fig. 3. The dotted lines in Fig. 3 represent the boundaries, that in a given system, these boundary walls are flexible. The flexibility of these boundaries depends on the type of bioreactor system used, cell type, aeration-agitation regime, and process conditions. Woodley and Titchener-Hooker [43] and Mersmann et al. [44] explained this operating window for the microbial system in general and Marks [19] for mammalian cells in particular.

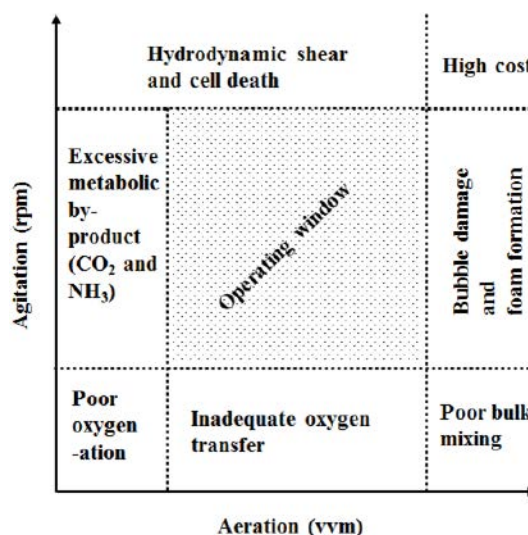


Figure 3. Sparging and agitation regimens for mammalian cells in stirred tank bioreactors – adapted from [19, 43, 44].

Mixing is necessary to keep the cells in suspension, provide homogeneity and to provide optimum mass and heat transfer. The choice of the impeller type is important in designing bioreactors for different types of cell systems. The Rushton turbine impellers exhibit radial flow which is used to maximize gas-liquid mass transfer, but this creates dispersion and shear in the reactor, hence negatively impacting the growth of shear-sensitive mammalian cells. Usually, axial flow impellers (marine or pitched blade) are used for the cultivation of mammalian cells; these induce axial flow. The motion of the fluid moves up and down along the shaft/axis assisting in effective mixing from top to bottom with low shear conditions [45]. Inappropriate mixing creates dead zones in bioreactors which would lead to low cell density and accumulation of undesired by-products which triggers necrosis and cell death by apoptosis. This would result in inconsistent batches and poor overall productivity [12]. The selection of the suitable impeller type and agitation rate mainly depends on the cell type used, the aspect ratio of

the culture vessel, the scale of the bioreactor and more importantly, the oxygen demand of the cells and the stripping of the carbon dioxide (CO₂) at the same agitation rate without compromising the shear-sensitivity of the cells [12, 46]. The removal of CO₂ from the culture system is an important parameter for the selection of the agitator while designing a bioreactor. It has been reported that the specific production rate of CO₂ for CHO cells is 4–6 pmol cell⁻¹day⁻¹ and for the efficient removal of CO₂ from the system requires a CO₂ mass transfer coefficient ($k_{La_{CO_2}}$) of 40–50 h⁻¹ for a cell density of 10 × 10⁶ cells mL⁻¹ [47].

An approach to the mitigating accumulation of undesired by-products is continuous culture systems. Continuous bioprocessing generally requires more complex integration of multiple unit operations, where the output of one unit is successfully handled by other units downstream. Continuous bioprocessing can be extended to perfusion systems. In this case, fresh media (containing nutrients, non-essential amino acids, growth factors and trace elements) are continuously fed to the bioreactor at a constant rate simultaneously with the withdrawal of the product at a rate equal to medium addition to avoid nutrient limitation and minimize metabolite accumulation but with cell retention in the bioreactor [48, 49]. Perfusion culture has gained attention from the biopharma industry to manufacture various biologicals products such as monoclonal antibodies, vaccines, and growth factors due to better process monitoring and control, high productivity, and conducive environment to the cell as compared to batch and fed-batch system [50]. The other benefit of perfusion culture is achieving industrial-scale productivity from the pilot-scale facility without using large equipment [19, 51]. However, the considerable issue regarding the use of perfusion system depends on the reliability of the cell retention devices such as spin filters, crossflow membrane, inclined settlers, continuous centrifuges, and ultrasonic separators which aid in easy product harvesting and down streaming [7, 14, 52]. The efforts should be made to use these devices optimally during the continuous operation by optimizing the perfusion rate and cell density to avoid clogging.

4.3.2 Airlift and Bubble Column Bioreactor (Pneumatically Driven Bioreactors)

The airlift and bubble column bioreactors operate pneumatically, where both oxygenation and mixing are done by rising bubbles. The stochastic movement of rising bubbles results in mass and heat transfer and mixing in these bioreactors. In airlift bioreactors, the air is sparged into only a compartment of the reactor, ascending through a riser before disengaging such that the unaerated liquid returns to the bottom of the reactor via the downcomer as a result of the density gradient, driving the recirculation of the cells and nutrient components in a circular fluid flow motion. Without impellers and a mechanical seal, these bioreactors have lower chances of contamination and facilitate easy cleaning [16]. Hydrodynamic properties of these bioreactors mainly depend on the type of sparger, gas flow rate, and liquid circulation velocity, rheology of the culture broth and most importantly the aspect ratio of the bioreactor. The typical aspect ratio of these bioreactors (height/diameter)

is in the range of 14 for small-scale and 6–7 with larger scales [7]. Airlift bioreactors have been scaled up to 2 m³ for the production of monoclonal antibodies in fed-batch mode [16, 53]. Despite good mixing and mass transfer, the design faces some limitation such as back mixing between gas and liquid phase, high-pressure drop, foaming, dead zones, bursting bubbles and bubble coalescence [21].

On the other hand, the bubble column systems represent a column with a much larger height than the diameter of the column with an internal sparger to inject gas flow inside the column. The mixing is achieved by stochastic movement of bubbles inside the column and hydrodynamic conditions mainly depend on the type of sparger, gas flow rate, column geometry and the medium rheology [7]. The bubble column bioreactor has been used to cultivate the shear-sensitive cell lines such as a hybridoma, lymphoma, BHK 21 and insect cell line Sf 21. It was concluded that in suspension culture, cell death is linked to the bubble rupture at the surface of the liquid-gas interface and significantly at the orifice of the sparger where the bubble is formed [54, 55]. Due to poor mixing, as compared to a stirred tank, the cultivation of mammalian cells in bubble column bioreactor has not been reported as yet at commercial scale [7, 56].

4.3.3 Fluidized Bed Bioreactor

The fluidized bed bioreactor is used for the cultivation of mammalian cells in suspension culture, where cells are immobilized on porous microcarriers or beads. The working principle of this type of bioreactor is that the beads with a higher density than the culture medium will be kept in suspension by the upward flow of the growth medium [16]. Fluidized bioreactors are vessels with a high aspect ratio, where solid-fluid mixing is vastly homogenous. It exhibits good mass and heat transfer due to the large surface contact area between the gas and liquid phases, hence showing good mixing and relatively low power requirements. The unique feature of fluidization of the immobilized cells depends on their settling velocity and density of the cells per bead. Heavy cells would be retained in the bioreactor due to gravity whereas free cells and debris will be washed out if their settling velocity is less than the liquid velocity [57]. Due to the high aspect ratio, the formation of oxygen gradient is a hindrance in scale-up. In an upward flow of the medium, the concentration of oxygen decreases from the bottom of the bed to the top [7]. Fluidized bioreactors exert low shear forces on the growing cells, making them a good choice for the propagation of animal and plant cells [8, 23]. Commercially available fluidized bed bioreactor systems of, up to 400 L scale are available which can support the cell density of 2 × 10⁸ cells mL⁻¹ but there are yet licensed processes that use the fluidized bed as their production platform [16].

4.3.4 Fixed or Packed Bed Bioreactor

Many cell lines are difficult to adapt to suspension cultures, for example, Vero cells. Fixed bed bioreactors have been used for the propagation of such adherent cells for the production of monoclonal antibodies, vaccines, biotherapeutics proteins, ret-

roviral vectors and the propagation of tissues for artificial organs [58–60]. Cells are immobilized or fixed either inside or outside the carrier structure (microcarriers, macroporous beads, fibrous bed) and the oxygenated medium is recirculated from the reservoir to the vessel continues to feed the growing cells. There are two aspects of the packed bed bioreactor configuration, wherein one the packed beds are outside the reservoir and the oxygenated medium is recirculated with a pump across the external bed, whereas in the other configuration, the packed bed is located inside the vessel and the oxygenated medium is circulated continuously across the internal bed [61].

Due to low hydrodynamic shear, high cell densities are attained in the packed bed bioreactor with few mammalian cells in suspension compared to stirred tank bioreactor [62]. The disadvantage of packed bed bioreactors is their low mass and heat transfer due to the low velocity of medium circulation. This low availability of oxygen, nutrients, and the limited removal of toxic metabolites limits cell growth [16, 60]. Portner et al. [63] reported that in small scale fixed-bed bioreactor with bed length up to 15 cm, media flow axially across the bed to eliminate the issue of oxygen limitation. In the case of larger fixed bed height, media was pumped radially to the bed width to overcome the oxygen demand for the growing cells [60, 63]. This problem can also be overcome by enhancing intra-particle convective flow where nutrients and oxygen are delivered to growing cells immobilized in the porous beads. This fluid flow is improved by applying pressure and controlling bulk fluid flows to enhance convection and diffusion of nutrients and oxygen into the porous bead [64]. Immobilized mammalian cells have been carried out in fixed-bed bioreactors at cell densities of 1×10^8 to 5×10^8 cells mL⁻¹ and these reactors support k_{La} values of 8.0 [65] as shown in Fig. 2. The maximum scale of fixed bed bioreactor reported to date is 30 L bed volume for the biotransformation using immobilized enzyme and in waste-water treatment [59]. Zhang et al. [17] introduced a novel fixed bed cell tank bioreactor for CHO cells expressing IgG monoclonal antibody developed by PerfuseCell, Denmark. The peculiar feature of the cell tank bioreactor is that it can support both adherent and suspension-adapted cell lines. The growing cells are retained in a non-woven polyester matrix placed in a chamber and immersed in a reservoir containing growth medium. The growth medium is delivered to the growing cells in the matrix with the help of a magnetic stirrer bead placed at the bottom of the bioreactor. The bioreactor is placed on a magnetic stirrer and the stirrer bead acts as a centrifugal pump by force circulating liquid from the media reservoir into the cassette where the matrix is suspended. The maximum cell density achieved across different runs was 200×10^6 cells mL⁻¹ and the titer of the monoclonal antibody achieved was 1.42 g in the matrix of 15 mL volume [17].

4.4 Single-Use Technology (SUT) – Broadening the Horizon of Biological Manufacturing

Disposable bioreactors use a culture bag or vessel made up of flexible plastic material [66]. In the last decade, this technology has emerged as an alternative cost-effective and flexible platform for both laboratory-scale process development and com-

mercial-scale manufacturing of biologicals. It has been estimated that setting up a new production facility based on single-use systems could lower the capital cost by 40 % as compared to commissioning a conventional hard pipe facility and it could also lower the operating cost by around 22 % per batch as compared to a batch taken in a conventional facility. The savings are mainly because of the elimination of the CIP (cleaning in place) and SIP (sterilization in place) steps, which reduces the utilization of WFI and chemicals such as phosphoric acid and sodium hydroxide which are used in conventional bioreactors. It has also been reported that the water usage in the single-use plant is 46 % lower and the carbon footprint by 35 % lower than in the traditional stainless-steel plant [9, 67–70]. Single-use technology is not only confined to the reactor component through cultivation bags but also liquid media storage bags, sampling devices, and modular facility design which includes downstream unit operation accessories like depth filters, ultrafiltration and disposable chromatography columns [9].

Disposable bioreactor systems work on a variety of operating principles such as static culture systems which includes single and multi-layered tissue culture flasks, multi-stack culture vessels, CELLLine bioreactor and dynamic culture systems which includes wave-induced mixing, use of the tumbling impeller or vibromixer to mimic stirring as in the case of STR, pneumatically-driven mixing, and shaking vessel systems. Disposable technology have many advantages over conventional bioreactors as there are no requirements for CIP and SIP, low initial capex investment, easy handling, reduced turnaround time between batches, ability to take multiple products in the same facility, minimum cross-contamination, reduced validation requirements, minimum usage of WFI and have a low carbon and energy footprint. Single-use technology, like hard piped facilities, is also easily integrated with process analytical tools (PAT) for the development of repeatable and robust processes by implementing quality by design (QbD) approach. However, compared to hard-piped stainless-steel facility which has limited scope for modularity, single-use facility can be fully modular and therefore allows for quick campaign changes, increased flexibility and improved equipment utilization, which further assist in easy validation and regulatory approvals [26, 71–73].

In pre-existing manufacturing plants with hard pipe structured facilities, there is scope for the transition to disposable technologies even with the involvement of prior capital investments, facility design and facility approval from the competent authorities. Companies carry out a step-by-step integration of the permanent hard structured facility to disposable accessories by incorporating the use of tubing, air vent capsules, TFF cassettes, preparation of seed inoculum in small bags and/or complete disposable unit operations. It has been reported that if the product has less than 50 batches annum⁻¹, single-use technology will prove economically beneficial otherwise reusable technology would still be the best option alongside hybrid facilities where part of the unit operations are carried out with disposables. Small and start-up companies have a greater interest in adopting single-use technology for a speedy pre-clinical and clinical trial material generation without compromising the sterility of the product and with a reduced product delivery span [74]. Additionally, the use of disposable technology is

50 % more energy-efficient than reusable technology. With the only energy-intensive operation on the disposal of used biohazardous bags with either incineration, chemical treatment, or through autoclaving and inactivation [71].

Despite all the benefits of disposable technology, there are concerns from industry leaders concerning the strength of the plastic material for scaling up, the accuracy of disposable non-invasive sensors, the integrity of bioreactor accessories such as sampling devices and the increased probability of extractable and leachable in the final product. Additionally, disposable technology is not environmentally friendly as it generates a large amount of non-biodegradable plastic waste [9]. Fig. 4 summarizes the holistic perspective around the use of disposable bioreactor including advantages, disadvantages, scope of improvement and the key driving factors.

Major companies dealing in single-use technology have started addressing the various drawbacks to broaden the scope of their usability. For example, Cytiva invested USD 5 million to set up a lab for the testing of extractable and leachable from the single-use consumables for the on-going support to their products [75].

The key driver for the expansion of single-use technology in biomanufacturing is their ability to extend modularity in biologicals manufacturing. Most of their components are simply “plug and play”, which assists in manufacturing multiple products in the same facility by reducing the down time. Many big companies have shifted their processes from traditional units to single-use manufacturing units. In December 2014, Amgen inaugurated its fully modular single-use technology-based biomanufacturing facility at Tuas, Singapore and Cytiva expanded

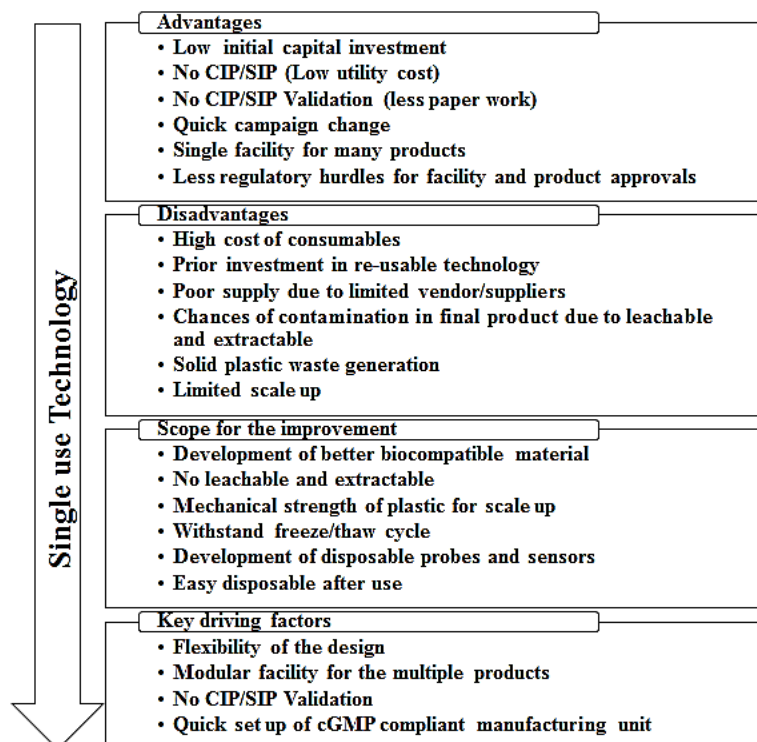


Figure 4. The advantages and disadvantages of single-use technology – adapted from [9, 27].

its single-use technology portfolio by acquiring Xcellerex, a biotechnology company dealing in single-use bioreactors (XDR series) and its accompanying Flexfactory technology for modular manufacturing platform manufacturing. Abzena has also joint-ventured with Sartorius-Stedim Biotech to equip their two integrated facilities based in Bristol, PA and San Diego, CA with single-use biomanufacturing units [75, 76].

In the last decade, many companies have ventured into the space of disposable bioreactors for the propagation of mammalian cells by developing innovative new technologies using various operating principles as shown in Tab. 4. Other designs have also demonstrated their suitability for mammalian cell culture based on various novel principles, e.g., pneumatically driven PBS bioreactor, cell tumbler (CerCell), Pad reactor with cubical design, and Bio-t bag with vibromixer technology [77]. The main players in the space of disposable bioreactors are Sartorius-Stedim (Biostat CultiBag STR), Cytiva (WAVE Bioreactor), Xcellerex (XDR), Thermo Fisher (SUB-Single-use Bioreactor), PBS Biotech (PBS Bioreactor), and Bayer Technology (Bay-Shake) [7, 28, 77, 78].

4.4.1 Wave Bioreactors

The first wave-induced bioreactor was designed by Dr. Vijay Singh in 1999; it demonstrated that wave-induced motion provides good mixing and mass transfer with minimum shear stress to the growing mammalian cultures such as Sf 9, HEK 293, and NS0 cell lines [79]. Wave bioreactors are made up of a culture bag, typically rectangular in shape, which is partially filled with growth medium and cells and inflated with a gas mixture or air. The bag is placed on a rocking platform which moves at an optimized angle and speed. The rocking movement of the platform provides sufficient agitation, mixing, heat and mass transfer. Wave and undertow bioreactors have also been developed for the production of biologicals that use different host cell systems like plant cells [80]. Oxygen is transferred from headspace to the cultured broth through entrainment of air by wave motion. It has been reported that the wave-induced culture bag has shown lower mass transfer efficiency than a stirred tank with $k_L a$ falling in the range of 4–20 h⁻¹ [81]. However, in a micro algal system, Jones et al. [82] demonstrated that the gas-liquid mass transfer in the wave bioreactor exceeds and is more energy efficient than the airlift bioreactor, with $k_L a$ values in the range of 9–150 h⁻¹.

4.4.2 Rotationally/Orbitally Shaken Bioreactor

Orbitally shaken bioreactors work on the principle of rotational motion of the culture vessel around a central axial shaft. Mass transfer of oxygen happens through surface aeration like shake flask culture systems. Zhang et al. [83] used helical tracks to improve the mass transfer efficiency of the bioreactor

Table 4. Overview of companies dealing in a single-use bioreactor in alphabetical order – adapted from [77, 81, 121].

Companies deal in SUBs	Commercial systems	Total Volume	Description
Applikon	AppliFlex	10–50 L	AppliFlex bags can use reusable, single-use and fluorophore sensors for pH and dissolved oxygen measurements. It supports CHO cells, Hybridoma cell lines and insect cells like Sf-9, Sf-21 cells. Suitable for propagating seed culture for large-scale batches.
ABEC	Custom single run	4300 L	Stirred tank bioreactor product line can be customized to fit any volume ranging from 50–3500 L.
Bayer Technology	BayShake	1000 L	Vertical orbital shaking cube-shaped bag bioreactor with the pyramidal bottom for low starting volume and full drainage, equipped with optical and fluorescence-based sensors for pH and DO measurements.
CerCell	Cell Tumbler	0.5–10 L	A rocking platform cabinet which can accommodate any commercially available wave-type bag up to 10/20 L with common drive and independent heating unit with the manually operated gas unit for air and CO ₂ .
	Cell Vessel 21 and 23 Series	2.1–75 L	Single-use bioreactor with flexibility in design customization as per the application, offering different types of impellers for mixing and mass transfer.
CELLution Biotech	CELL-tainer bag bioreactor	20–200 L	Wave style rocking platform with a box or pillow-like a bag with a pre-fixed pH and DO sensor.
Cellexus	Cell Maker	8–50 L	Airlift single-use bioreactor without agitator/rocker, suitable for a variety of cell systems.
CatchMabs	Tsunami bioreactor	6 × 160 L	Series of wave mixed bioreactor with a multi-layer platform with the same wave hydro dynamicity for cell growth.
Cytiva	Wave bioreactor systems	0.2–500 L	Well established wave systems suitable for various animal cell lines.
	Ready to process wave 25	0.3–25 L	It provides the option of single or dual culture cultivation on a single platform with different working volume. The pH, DO and pump speed can be controlled independently.
	Xcellerex XDR range	10–2000 L	Modular stirred tank disposable bioreactor system with batch, fed batch and perfusion applicability. Provide excellent mass Transfer and mixing mimicking reusable system.
Eppendorf	Celligen BLU Fixed Bed	3.75 L	Single-use stirred tank with pre-loaded Fibre-cell disks, suitable for adherent and suspension cells.
	Celligen BLU	5–50 L	Single-use bioreactor with pre-attached pitched blade impellers and Microsparger with all the other accessories required to run the batch.
Finesse	Smart Glass Vessel	0.5–2.2 L	The bioreactor provides axial and radial fluid flow by using down pumping segmented blade and bottom-mounted Rushton turbine.
	Smart Rocker Bioreactor	10–50 L	Wave platform support from gentle to vigorous rocking motion based on cell lines. The system is coming with pre-loaded SmartPuck sensors for monitoring and controlling of process parameters, also have optional load cell for fill control.
Hangzhou Am protein Bioengineering	Current bioreactor	5–300 L	Orbitally shaken single-use bioreactor with bubble and sparger free oxygen transfer from vessel surface which is made up of EVA.
Kuhner	Orb Shake Bioreactor	10–200 L	A well-established system for mammalian and plant cell cultivation.

Table 4. Continued.

Companies deal in SUBs	Commercial systems	Total Volume	Description
Merck Millipore	Mobius Cell Ready Bioreactor	3–2000 L	Mobius CellReady 2000 L joins 3, 50, and 200 L bioreactor series on June 15, 2015.
Meissner Filtration Inc.	Saltus Bioreactor	2–2000 L	The bioreactor has a vertical hollow, conical perforated disk on the shaft which provides axial motion without vortex and provides mixing and mass transfer. Due to high power consumption, it is not suitable for shear-sensitive cells.
Pall life Sciences	Allegro XRS 20	0.1–20 L	Rocker system with bi-axial motion provide shorter mixing and high mass transfer, suitable for seed development to full GMP production.
	Allegro STR	60–200 L	Squarely designed vertical bioreactor like Stainless steel bioreactor.
	Pad Reactor	10–1200 L	Cubical design bag with paddle impeller and dynamic sparger for shear-sensitive cells. Impeller and sparger is covered with ULDPE membrane.
	Xpansion multiplate	0.06–12.2 m ²	Plate system
	Nucleo Bioreactor	1000 L	It offers similar functionality as of stainless-steel bioreactor, in addition to that it has paddle impeller and dynamic sparger covered with ULDPE membrane.
PBS Biotech	Vertical wheel Bioreactor	20 mL–500 L	Airlift bioreactor where bubble aerates the vessel thus provide mixing and mass transfer. Agitation is provided by the buoyancy of gas bubble in case of air drive and magnetically coupled drive for MAG drive.
Sartorius-Stedim	Biostat CultiBag RM	300 L	Wave mixed bioreactor
	Biostat CultiBag STR	25–2000 L	Vertical stirred tank bioreactor similar to the reusable counterpart, housed in a stainless-steel chamber.
	CultiBag ORB	50–2500 L	Orbitally shaken bioreactor with surface aeration and without impeller and agitator, suitable for adherent and suspension cells.
	UniVessel SU	0.6–2.0 L	Single-use stirred tank with pre-loaded pH and DO probes, ready to use, compatible with any bio-controller brand.
Thermo Scientific	HyPerforma S.U.B. Range	25–2000 L	1st stirred tank bioreactor in the industry having the conventional geometry of the vessel. The system is compatible with other systems from Applikon, finesse etc.
Terumo BCT	Quantum Cell Xpansion	2.1 m ² culture surface	Automated flask scale cell culture process development platform based on hollow fibre system for adherent cells.
ZETA Holding GmbH	Bio-t Bag	3–1875 L	Culture bag uses vibromixer technology for mixing and aseptic handling of the process while maintaining the integrity of the bag.

by placing these tracks inside the wall of the culture vessel and with orbital motion, liquid media travels upwards along the track, thus increasing surface area for enhanced gas to liquid transfer. An increase of 5–10 fold of volumetric mass transfer coefficient has been reported due to increased liquid-gas interface, and at 1000 L scale with 39 rpm, the mass transfer coefficient of the orbitally shaken reactor with the helical track was 10 h⁻¹ with air. The $k_L a$ value in orbitally/rotationally moving bioreactor primarily depend on the shaking speed and fill volume, which increase the oxygen transfer rate. The mass transfer coefficient ($k_L a$) is inversely proportional to the working fill volume [83, 84].

4.4.3 Disposable Stirred Tank Bioreactors

As stirred tank bioreactors have an established track record in the biomanufacturing sector, the development of single-use STR bioreactor systems is an inevitable progression. Here, a plastic culture bag is mounted inside a cylindrical cabinet to support the bag as a vessel for growth. Many companies have ventured into the development of single-use stirred-tank bioreactors with internal disposable impellers such as Thermo fisher (SUB- Single-use Bioreactor), Xcellerex (XDR) and the recently launched custom single run bioreactor from ABEC which can be custom made in the range of 50 to 3500 L work-

ing volume. Thermo fisher's SUB bioreactor is equipped with a motor on the top head plate for mixing and agitation whereas XDR has a bottom driven impeller. Disposable STR bioreactors have been tested for the propagation of CHO cells. A comparative study of performance between SUB (Thermo fisher) and stainless steel STR has been done by growing CHO and NS0 cell lines. It has been demonstrated that SUB systems) successfully reproduce similar metabolic growth and product quality at production scale [85]. Disposable bioreactors have supported 20×10^6 cells mL^{-1} in fed-batch operations with the enhanced product titer of around 6.0 g L^{-1} at 1000 L scale [85].

4.4.4 Pneumatically Driven Single-use Bioreactor

A new addition on the canvas of single-use technology is pneumatically driven single-use bioreactors which primarily uses gas buoyancy as a tool for mixing and mass transfer. PBS Biotech® is the first to introduce a pneumatically driven vertical air-wheel bioreactor where a vertical wheel moves inside the liquid chamber mimicking a "merry-go-round" [86, 87]. Another addition in this class is the CellMaker series of bioreactors from Cellexus Limited. These bioreactors use the principles of airlift and mechanical agitation in unison to achieve high mixing and low shear conditions [9].

4.4.4.1 Vertical Wheel™ Bioreactor

The vertical air wheel bioreactor is an airlift bioreactor made up of single-use components. It is an impeller-less, pneumatically mixed U-shaped bioreactor, which uses gas bubbles as a mixing device by rotating the air-wheel like a "merry-go-round" with the buoyant force of the bubbles [86, 88]. This technology is patented by PBS Biotech, which uses the theory of radial-axial tangential fluid flow around a vertical rotating wheel during cell cultivation. The rotating wheel covers 85% width of the U-shaped vessel which revolves in a vertical plane on a horizontal shaft. It generates radial and axial fluid motion in the bioreactor simultaneously; radial flow in a vertical plane and the axial flow component along the horizontal axis which further supports homogeneous mixing. The energy dissipation rate (EDR) and maximum wall shear stress are reported to be $2 \times 10^3 \text{ W m}^{-3}$ and 1.7 N m^{-2} respectively, which is under the tolerance limit for mammalian cell growth [89]. The advantage of the air wheel is that it requires lesser amount of air thus increases the working volume of the batch while reducing compressor requirements. This type of bioreactor is suitable for the growth of shear sensitive mammalian and insect cell lines and is available from 3 to 2500 L in working volume [9, 87].

4.4.4.2 Cellexus System

This is a pneumatically driven (airlift) bioreactor where rising bubbles provide effective mixing, oxygen delivery and enhance mass transfer to the growing cells without a mechanical agitator. Cellexus Biosystems have introduced a novel bag geometry which facilitates the mixing. CellMaker Regular (previously

CellMaker Lite) is an inverted "L" shaped bag, where air passes through the long vertical stem and hits the deflector to provide good oxygenation and mixing. Due to the design, Cellexus systems also allows the system to be pressurized above the culture level (Overlay pressure), which in single-use systems is unique for suppressing foaming [90]. Cellexus Biosystems offer systems which can be operated on the airlift principle alone or as a hybrid system. In hybrid systems, internal impellers are fitted to give similar mixing and aeration conditions as seen in stirred tanks but with the benefits of low shear conditions similar to an airlift bioreactor [27, 91]. It has been reported that this bioreactor can provide aeration more efficiently than a very vigorously shaken culture flask. The oxygen transfer rate (OTR) is in the range of $15\text{--}30 \text{ mmol O}_2 \text{ L}^{-1} \text{ h}^{-1}$ [91]. Cellexus bioreactors are available in 3 to 50 L scale [81, 91].

4.5 Novel Cell Culture Systems

Novel bioreactor technologies are essential for the continual improvement and innovation of the bioprocess platform. Many novel bioreactors explore the concepts of biomimicry as a basis for their design. In this respect, designs are moving away from traditional air sparging which is energy-intensive and from impellers which create high hydrodynamic shear.

4.5.1 Bello Cells/CelCradle

Cesco Bioengineering Co. (Hsinchu, Taiwan) developed Bello cells which were later acquired by ESCO, Vaccixcell (Singapore) and named CelCradle. These are benchtop disposable bioreactors and come in a set of four bellow bottles with each bottle operating to a volume of 500 mL. Their working principle resembles the functionality of lungs. This bioreactor is impeller-free that works without air sparging thus provides a low shear environment and reduced foam formation. The bioreactor consists of two parts: lower hollow bellow and an upper chamber with cells immobilised on BioNOC II® made of polyester fibres. The operational mechanics of the system works in such a way that it creates cyclic oscillations by compression and release of the bellow. The oscillatory motion of the bellow moves the medium upward and downward with minimum hydrodynamic shear which is ideal for the growth of shear sensitive cell lines. One CelCradle system with 4 bellows equates to the surface area of 80 roller bottles [92]. Increase in the headspace on the upper chamber helps in gaseous exchange and high oxygen mass transfer and have achieved cell densities of $4\text{--}6 \times 10^9$ cells bottle^{-1} [93]. Research has been published on using these systems to grow Vero cells for the production of Japanese encephalitis virus and swine virus as well insect cells for the production of recombinant baculovirus [94–97].

4.5.2 Dynamic Membrane Aeration System (DMA system)

Bayer Technology Services (BTS) developed a novel aeration method, the dynamic membrane aeration method (DMA) as

reported by Frahm et al. [98] using surface aeration for the cultivation of shear sensitive cell lines with the use of microporous silicone tubing wrapped around a centrally placed star-like oscillating/tumbling stirrer. They combined rotor and stator to form a rotary oscillating stirring unit. Traditionally, the stator is a cylindrical shaped unit fixed to the head plate, onto which gas permeable silicone tubing is wrapped thoroughly. Bioreactor stirrer is placed within the hollow cylindrical space. The conventional rotor-stator combination has some limitations such as poor mass transfer capacity at high cell densities and poor scalability. These limitations have been overcome by DMA technology where mixing is generated by rotating the stator platform by 180° in a clockwise and anti-clockwise motion. This setup gives high mass transfer and a low shear condition, conducive for high cell density due to the high surface area for gaseous exchange. This DMA technology has been tested to produce blood coagulation factor VIII at 12, 20, 100 and 200 L scale. It has been reported that with the same power input of 6 W m^{-3} at 100 L scale, which is typical for cell culture applications, the mass transfer coefficient for DMA system is 35% higher than the conventional systems (stirred tank) and the cell density achieved during continuous culture at 12 L was around 15 to 20×10^9 cells mL^{-1} [98, 99].

4.5.3 Travelling Wave Bioreactor (Doughnut/Annular Shape/Toroidal Bioreactor)

Toroidal bioreactors work on the mechanism of the orbital motion of the bioreactor which creates travelling waves inside a hollow toroidal shape vessel. This travelling wave bioreactor (TWB) provides a high surface area and high surface renewal rates for oxygen mass transfer and mixing [100]. A CFD model of fluid flow has been developed with different geometries and consideration of parameters like shaking frequency, filling volume and amplitude of the moving liquid. The outcome of the computational studies has shown that travelling waves could provide a high specific surface area, low hydrodynamic shear and high mass transfer efficiency [101]. A study of growing CHO cells in the TWB achieved a cell density of 5.4×10^6 cells mL^{-1} with the viability of 95.5%. The maximum oxygen mass transfer coefficient of 32 h^{-1} was reported, which is sufficient to cater to the mean specific oxygen uptake rate of $2.5 \times 10^{-12} \text{ mg}_2 \text{ cell}^{-1} \text{ s}^{-1}$. The maximum power input was reported to be 82.2 W m^{-3} for unbaffled TWB and 86.0 W m^{-3} for baffled TWB whereas oxygen mass transfer coefficient was $10\text{--}12 \text{ h}^{-1}$ for both baffled and unbaffled bioreactor types [102].

4.5.4 Rotary Cell Culture System (RCCS)

RCCS was developed by Synthecon for the National Aeronautics and Space Administration (NASA) for the growth of stem cells and 3D cell culture [103]. This bioreactor consists of a horizontal rotating vessel filled completely with culture media and a central axis shaft covered with microporous silicone tubes for gaseous exchange. The reactor has a zero headspace, zero gravity condition for the growing cells thus exerting low hydrodynamic shear. The continuous slow rotation of the ves-

sel keeps all cells in suspension in low shear conditions and aid in forming small aggregates and cell clumps of sizes in the range of centimeter in diameter [104]. This technology, however, has some limitations with cell aggregates which limits mass transfer to cells in the inner core leading to necrosis and eventually cell death [90, 105].

4.6 Mini- and Micro-scale Bioreactors

For developing a robust and repeatable process, multiple numbers of experiments have to be validated which is time-consuming and expensive [106]. The use of quality by design (QbD) approach in the commercial manufacturing of biopharmaceutical products is gaining industry acceptance. QbD adapts scale-down or small-scale models by mimicking the commercial manufacturing process conditions [107].

To qualify for the scale-down model, it is important to compare the different scales of bioreactor operation in terms of cell growth, culture conditions (pH, DO, pCO_2 , osmolality) productivity, product quality and the level of metabolites (glucose and glutamine consumption, lactate and ammonia formation) [108]. This strategy will further test the various process conditions simultaneously and provide a huge amount of data in the shortest time interval [108, 109]. Cell line development, clonal selection, microenvironment regulation, media and feed optimization, process optimization, and process cost-effectiveness led to the uncovering of miniaturized bioreactors in 2001 [110–112]. These bioreactors provide a platform for simultaneous multiple experiments, each independent of another, whilst utilizing a minimum amount of time, chemical and consumables.

There are 4 main types of miniature systems (Tab. 5). The smallest of these systems are the micro titer plate (MTP) type bioreactors. These reactors range from 0.1 to about 7 mL. With systems of BioLector (M2P labs) and SimCell (Seahorse Biosciences), aeration is mainly achieved by surface aeration while pH and DO measurements are obtained via non-invasive methods using sensors and light scattering [113, 114]. In the 10–500 mL scale, miniature STRs type bioreactors feature as prominent scale down approach bioreactors. These bioreactors also utilize non-invasive DO and pH measurements, and mixing is mainly achieved by a magnetic stirrer, e.g., Hexascreeen (Telstar) [115] in the 10–15 mL STR bioreactor range to fixed overhead stirrers as utilized by (Eppendorf) up to the 500 mL range. Flask type high throughput bioreactors as CultiFlask 50 made by Sartorius [116] operates up to the range of 35 mL, has a centrifuge tube design and is placed in a shaker incubator. At a larger scale, Sartorius designed the SuperSpinner flask [34], which goes up to 1000 mL. Similar to the CultiFlask 50, they are disposable bioreactors, but the SuperSpinner flask is pre-assembled with a membrane stirrer for a bubble-free aeration environment. Another addition to small scale disposable bioreactor is Tubespin (TPP, Trasadingen, Switzerland), which is based on orbital shaking technology which can deliver oxygen passively through surface aeration [117]. Lastly, in the miniature bioreactor system family, are the two compartment systems. Integra Biosciences developed the CELLine bioreactor [118] where cells and medium are separated by a 10 kDa membrane to allow for high density

Table 5. Miniature systems available for high throughput process development.

Type of system	Name of system	Volume [mL]	Suppliers	Parallel units	Description/application	Ref.
MTP	Micro 24	3–7	Pall corp.	24	Deep well MTP, mass transfer by shaking and sparging.	[106, 122]
	Appikon 24	5–6	Applikon	24	Non-invasive fluorescent sensors for measurement of pH and DO, sparging through 0.2 μ membrane shaking.	[119]
	BioLector	0.1–0.2	M2P labs	48/96	Rosette shaped 48/96 well plate having dot sensor on the bottom for pH and DO, non-invasive measurement by scattering and fluorescence.	[113]
	SimCell	0.3–0.7	Seahorse Biosciences	6	Cassettes on the rotor can accommodate 1500 cells in the incubator. Each cell having patch sensor for pH, DO. k_{La} obtained is 7 h^{-1} through surface aeration.	[113, 114]
Miniature STR	ambr	10–15	TAP Biosystems	24/48	24–48 independent automated complete unit with impellers.	[114, 123]
	Dasgip/DASbox	50–500	Eppendorf	16	Fully automated with precise control of all process parameters.	[123, 124]
	Cell station	35	Fluorometrix Corp.	12	Uses optical technology for pH and DO measurements. Agitation by paddle types impeller. Each vessel is attached to a rotating platform which sampled from each vessel and monitored sequentially.	[110]
	Hexascreen	10–15	Telstar	6	Integrated system with inlet gases and non-invasive measurement of pH, DO and OD. Agitation by the magnetic pendulum-like spinner.	[115]
Flasks	CultiFlask 50	35	Sartorius	multiple	Centrifuge design with vented cap and holes for gaseous exchange, used for media screening. Each unit is independent and placed inside incubator-shaker.	[116]
	SuperSpinner flask	1000	Sartorius	1	Fully disposable and pre-assembled having unique membrane stirrer for bubble-free aeration.	[34, 121]
	Tube Spin	15/50	TPP	1	Conical tapered bottom centrifuge tubes (with vented cap) of 15, 50, and 500 mL volume with orbital shaking providing enhanced mass transfer and low shear stress	[125, 126]
Two compartment system	CELLine	350–1000	Integra Biosciences	1	Two-compartment system where medium and cell surface aerated by 10 kDa membrane which facilitates nutrients diffusion and concurrent removal of the inhibitory waste product.	[118]

cell cultures with continuous diffusion of nutrients and removal of by-products.

Although miniaturized bioreactors have performed well in developing robust processes, they have also certain shortcomings. The data obtained from these miniaturized bioreactor platforms have matched well in some cases across laboratory scale and pilot scale stirred tank systems [119], but the stirring system incorporated into the micro and mini-bioreactors are usually magnetically driven. Due to this, the fluid flow profile in these bioreactors are usually different from that of laboratory-scale bioreactors which result in different mixing patterns and mass transfer efficiencies which leads in inconsistency and non-reproducibility at larger scales [120]. The low volume also makes sampling challenging and the lack of miniaturized downstream tools also give rise to poor scalability in product recovery for production scales.

5 Conclusions

Many bioreactor designs and process development strategies have been applied to meet the continuously increasing demand for biologicals by increasing yields and productivities while reducing the batch run-time, and the cost of production. It is evident that the challenge of the ever-increasing demand for biological products has driven the quest for better-performing bioreactors for the cultivation of mammalian cells. For the last seven decades, various bioreactor designs (culture systems) have evolved, each different in operating principles and engineering characteristics, therefore exhibiting different volumetric mass transfer efficiency, power/energy input requirements, mixing time, hydrodynamic shear conditions, and fluid flow profile to support optimum cell growth and extended viability.

Most of the bioreactor designs can accommodate low to middle cell density cultures ($\leq 10 \times 10^6$ cells mL⁻¹) with 20–50% of air/air enriched with oxygen to meet the desired DO requirements. For the high cell density culture especially in the case of perfusion culture (10^9 cells mL⁻¹), the oxygen demand is high, the $k_{L,a}$ required to maintain such a high cell density falls in the range of 42–667 h⁻¹. This could be achieved by either carrying out of oxygenation of media externally or using macro sparger at high gas flow rates in combination with controlled agitation with an appropriate shear sensitive impeller. For adherent cultures, traditionally, packed bed bioreactors are used, but due to low mass transfer efficiencies and difficulties in media circulation across the bed, the maximum reported capacity of the packed bed for mammalian cultures is 30 L. These limitations were overcome by the Cell Tank bioreactor which is equally good for adherent and suspension cultures where a centrifugal pump aids in circulating fresh oxygenated media to the growing cells with low shear.

Despite the hydrodynamic limitations associated with stirred tank bioreactors, it is still a system of convenience for the cultivation of suspension culture to a scale of 25 m³. The efficient oxygen transfer rate and OD requirements at a large scale, are met by using direct sparging and efficient gas dispersion by an appropriate impeller. However, the increased mass transfer efficiency comes with the detrimental effects of high shear and

leads to sub-optimal growth conditions in STR for the sensitive mammalian cells.

This downfall has led to new bioreactor designs, many of which are inspired by nature, through biomimicry. Engineers conceptualize these designs from nature's optimal structures for growth and survival. This movement has seen the utilization of mechanical stirring and gas sparging found in STR, to airlift or fluidized bed reactors for more gentle modes of mixing and mass transfer. Bioreactors utilizing fluid motion such as the CelCradle, wave bioreactor, and travelling wave bioreactors utilizes tidal wave movements to achieve sufficiently $k_{L,a}$ for cell growth.

However, reluctance from the majority of the industry to invest in new technologies has hampered the implementation of new developments into the manufacturing line. Owing to the regulatory demands, industries are however slowly but surely increasing interest towards single-use technology (partly or fully), low energy, and low shear bioreactors. Various single-use bioreactor systems of different scales have shown promising results in culturing different cell lines, particularly mammalian cell lines. The essential pre-condition of single-use bioreactors are to operate without compromising the integrity of the system. To maintain sterility throughout the batch, irrespective of the scale, advancement in the area of pre-calibrated and non-invasive sensors have further ensured sterile conditions thus further supporting the use of single-use culture systems. The single-use bioreactors with different operating principles have also been demonstrated to impart conducive conditions for high cell density as well as improved product titer when compared to reusable systems of the same scale. The growth of single-use technologies in commercial production has already proven its worth by reducing the overall cost of production and the time for the product to reach the market, but scale-up issues of the single-use bioreactor is still a hurdle for the biological industry. The maximum scale reported in disposable bioreactor systems are 2 m³ with wave-induced bioreactor and 5 m³ in case of vertically agitated bioreactors.

Multiple experimentations are required to optimize a process, which is time-consuming and costly, and has fueled the urge to develop multiple parallel bioreactor systems which further led to the development of miniaturized bioreactors. The scale-down approach has become an essential tool for testing productivity, quality, product safety and overall efficiency of the process at a small scale (in μ L–mL scale) whilst mimicking the conditions similar to commercial-scale manufacturing by critically managing and controlling the process parameters. These bioreactors are useful in running many parallel experiments at a time. The challenges encountered in applying miniaturized bioreactors in process development is their high cost and their high failure rate in mimicking the real-time large-scale culture conditions in reusable bioreactors.

Hence, there is a need to develop a comprehensive bioreactor that can accommodate a variety of cell systems and provide physiologically favorable conditions for cell growth. Through an understanding of engineering aspects and incorporating parameters such as mass transfer, shear sensitivity, nutrient availability, and optimized process conditions either through experimental studies or modelling, refinement to the bioreactor can be done systematically. Further development of non-invasive

sensor technology and integration of process analytical technologies (PAT) in line with quality by design (QbD) principles would aid in developing robust and repeatable processes while minimizing errors (batch variability) during production.

Conflicts of Interest

The authors declare no conflict of interest.



Rajesh Sharma obtained his Masters degree in 2003 from Punjabi University, Patiala, India. Prior to joining the Chemical Engineering Department at UCT as a doctoral student in 2014, he worked in India and has more than 10 years of industrial experience in up-stream process development for the production of biologicals. His research area covers mammalian cell culture, bioreactor designing, biotherapeutic protein, and vaccines.



Susan T. L. Harrison holds a B.Sc. in Microbiology and Chemistry and a B.Sc. (Hons) degree in Microbiology from the University of Cape Town (UCT). Her Ph.D. in Chemical Engineering is from Cambridge University, U.K. She has some 30 years' experience in bioprocess engineering, gained in the industrial and academic arenas. She has held the South African research chair in Bioprocess Engineering and is

director of the Centre for Bioprocess Engineering Research in the Chemical Engineering Department and DVC: Research at UCT. Her research in bioprocess engineering spans bacterial, fungal, archaeal, and algal bioprocesses, focusing on biokinetics, maximal resource productivity, mixed microbial communities and enabling bioprocess design and bioreactor configuration.



Siew L. Tai holds a B.Eng. Hons in Chemical Engineering, University of Manchester, an M.Sc. (cum laude) in Biochemical Engineering, and a Ph.D. in Industrial Microbiology from Delft University of Technology. He carried out his post-doctoral fellowship at the University of Stellenbosch. Following that, he joined the Biovac Institute where he took part in building a vaccine manufacturing plant. His research encompasses the intricate networking between biotechnology and bioprocess engineering. His current research at UCT concentrates on the fields of bioprocess design, techno-economics, and bioproduct formation.

Acknowledgements

The authors would like to thank the National Research Foundation (NRF), South Africa for their financial support through the CSUR grant (UID90305) and SARCHI in Bioprocess Engineering (UID64778). Further, we would also acknowledge the guidance received from members of the Centre for Bioprocess Engineering Research (CeBER), Department of Chemical Engineering, University of Cape Town, South Africa.

Symbols used

C^*	[mmol L ⁻¹]	oxygen saturation concentration
C_L	[mmol L ⁻¹]	actual oxygen concentration in solution
C_X	[cells L ⁻¹]	cell density
k_{La}	[h ⁻¹]	volumetric mass transfer coefficient
OTR	[mmol _{O₂} L ⁻¹ h ⁻¹]	oxygen transfer rate
OUR	[mmol cell ⁻¹ h ⁻¹]	oxygen uptake rate
q_{O_2}	[mmol cell ⁻¹ h ⁻¹]	specific oxygen consumption rate

Abbreviations

ATF	alternating tangential flow
BHK	baby hamster kidney
BTS	Bayer Technology Services
CAGR	compound annual growth rate
CFD	computational fluid dynamics
CHO	Chinese hamster ovary
CIP	cleaning-in-place
DMA	dynamic membrane aeration
DO	dissolved oxygen

ECS	extracapillary spaces
FDA	Food and Drug Administration
GMP	good manufacturing practices
HEK	human embryonic kidney
ICS	intracapillary spaces
IgG	immunoglobulin
MBR	membrane bioreactor
MTP	micro titer plate
NASA	National Aeronautics and Space Administration
PAHO	Pan American Health Organization
PAT	process analytical technology
PE	polyester
QbD	quality by design
RCCS	rotary cell culture system
SARS-CoV-2	severe acute respiratory syndrome coronavirus 2
SIP	sterilization-in-place

References

- G. Kretzmer, *Appl. Microbiol. Biotechnol.* **2002**, *59* (2–3), 135–142. DOI: <https://doi.org/10.1007/s00253-002-0991-y>
- T. Lai, Y. Yang, S. K. Ng, *Pharmaceuticals* **2013**, *6* (5), 579–603. DOI: <https://doi.org/10.3390/ph6050579>
- M. Cuperlović-Culf, D. A. Barnett, A. S. Culf, I. Chute, *Drug Discovery Today* **2010**, *15* (15–16), 610–621. DOI: <https://doi.org/10.1016/j.drudis.2010.06.012>
- www.businesswire.com/news/home/20170613005736/en/Global-459.81-Biopharmaceutical-Market-Analysis-Trends-2014-2016 (Accessed on November 04, 2021)
- A. Kantardjiev, W. Zhou, *Mammalian Cell Cultures for Biologics Manufacturing*, Advances in Biochemical Engineering/Biotechnology, Vol. 139, Springer, Berlin **2014**.
- F. M. Wurm, *Nat. Biotechnol.* **2004**, *22* (11), 1393–1398. DOI: <https://doi.org/10.1038/nbt1026>
- D. Eibl, R. Eibl, in *Cell and Tissue Reaction Engineering*, (Eds: R. Eibl, D. Eibl, R. Pörtner, G. Catapano, P. Czermak), Principles and Practice, Springer, Heidelberg **2009**.
- A. Margaritis, J. B. Wallace, *Nat. Biotechnol.* **1984**, *2* (5), 447–453. DOI: <https://doi.org/10.1038/nbt0584-447>
- A. A. Shukla, U. Gottschalk, *Trends Biotechnol.* **2013**, *31* (3), 147–154. DOI: <https://doi.org/10.1016/j.tibtech.2012.10.004>
- J. A. Williams, *Chem. Eng. Prog.* **2002**, *98* (3), 34–41.
- B. T. Tey, M. Al-Rubeai, *Apoptosis* **2004**, *9* (6), 843–852. DOI: <https://doi.org/10.1023/B:APPT.0000045792.63249.5a>
- R. Godoy-Silva, C. Berdugo, J. J. Chalmers, in *Encyclopedia of Industrial Biotechnology: Bioprocess, Bioseparation, and Cell Technology* (Ed: M. C. Flickinger), Wiley, Hoboken **2010**.
- A. W. Nienow, *Cytotechnology* **2006**, *50* (1–3), 9–33. DOI: <https://doi.org/10.1007/s10616-006-9005-8>
- O.-W. Merten, *Cytotechnology* **2006**, *50* (1–3), 1–7. DOI: <https://doi.org/10.1007/s10616-006-9009-4>
- H. Uludag, P. De Vos, P. A. Tresco, *Adv. Drug Delivery Rev.* **2000**, *42* (1–2), 29–64. DOI: [https://doi.org/10.1016/S0169-409X\(00\)00053-3](https://doi.org/10.1016/S0169-409X(00)00053-3)
- J. N. Warnock, M. Al-Rubeai, *Biotechnol. Appl. Biochem.* **2006**, *45* (1), 1–12. DOI: <https://doi.org/10.1042/BA20050233>
- Y. Zhang, P. Stobbe, C. O. Silvander, V. Chotteau, *J. Biotechnol.* **2015**, *213*, 28–41. DOI: <https://doi.org/10.1016/j.jbiotec.2015.07.006>
- Code of Federal Regulations Title 21*, FDA, Silver Spring, MD **2016**.
- D. M. Marks, *Cytotechnology* **2003**, *42* (1), 21–33. DOI: <https://doi.org/10.1023/a:1026103405618>
- A. G. Lopes, *Food Bioprod. Process.* **2015**, *93*, 98–114. DOI: <https://doi.org/10.1016/j.fbp.2013.12.002>
- J. E. Hambor, *Bioprocess Int.* **2012**, *10* (6), 22–33.
- S. S. Ozturk, *Mammalian Cell Cultures for Biologics Manufacturing*, Advances in Biochemical Engineering/Biotechnology, Vol. 139, Springer, Berlin **2014**.
- M. K. Popović, R. Pörtner, *Bioreactors and Cultivation Systems for Cell and Tissue Culture*, Encyclopedia Life Support Systems, UNESCO, Paris **2012**.
- Y. Chisti, *Crit. Rev. Biotechnol.* **2001**, *21* (2), 67–110. DOI: <https://doi.org/10.1080/20013891081692>
- J. J. Chalmers, *Cytotechnology* **1994**, *15* (1–3), 311–320. DOI: <https://doi.org/10.1007/BF00762406>
- T.-K. Huang, K. A. McDonald, *Biotechnol. Adv.* **2012**, *30* (2), 398–409. DOI: <https://doi.org/10.1016/j.biotechadv.2011.07.016>
- R. Brecht, in *Disposable Bioreactors*, Advances in Biochemical Engineering/Biotechnology, Vol. 115, Springer, Berlin **2009**.
- R. Eibl, C. Löffelholz, D. Eibl, in *Animal Cell Biotechnology*, Springer, Berlin **2014**.
- X. Zhang, M. Stettler, D. Sanctis, M. Perrone, N. Parolini, M. Discacciati, M. Jesus, D. Hacker, A. Quarteroni, F. Wurm, in *Disposable Bioreactors*, Advances in Biochemical Engineering/Biotechnology, Vol. 115, Springer, Berlin **2009**.
- P. Czermak, R. Pörtner, A. Brix, in *Cell and Tissue Reaction Engineering*, Springer, Berlin **2009**.
- R. Pörtner, in *Animal Cell Culture* (Ed: M. Al-Rubeai), Vol. 9, Springer, Berlin **2015**.
- L. E. Gallo-Ramírez, A. Nikolay, Y. Genzel, U. Reichl, *Expert Rev. Vaccines* **2015**, *14* (9), 1181–1195. DOI: <https://doi.org/10.1586/14760584.2015.1067144>
- J. G. Aunins, B. Bader, A. Caola, J. Griffiths, M. Katz, P. Licari, K. Ram, C. S. Ranucci, W. Zhou, *Biotechnol. Prog.* **2003**, *19* (1), 2–8. DOI: <https://doi.org/10.1021/bp0256521>
- R. Heidemann, U. Riese, D. Lütkemeyer, H. Büntemeyer, J. Lehmann, *Cytotechnology* **1994**, *14* (1), 1–9. DOI: <https://doi.org/10.1007/BF00772190>
- M. Szczypka, D. Splan, H. Wools, H. Brandwein, *Bioprocess Int.* **2014**, *12* (3), 54–68.
- A. C. Schnitzler, A. Verma, D. E. Kehoe, D. Jing, J. R. Murrell, K. A. Der, M. Aysola, P. J. Rapijko, S. Punreddy, M. S. Rook, *Biochem. Eng. J.* **2016**, *108*, 3–13. DOI: <https://doi.org/10.1016/j.bej.2015.08.014>
- D. De Wilde, U. Noack, W. Kahlert, M. Barbaroux, G. Grellet, *Bioprocess Int.* **2009**, *7*, 36–41.
- L. Chu, D. K. Robinson, *Curr. Opin. Biotechnol.* **2001**, *12* (2), 180–187. DOI: [https://doi.org/10.1016/S0958-1669\(00\)00197-X](https://doi.org/10.1016/S0958-1669(00)00197-X)

- [39] D. W. Murhammer, C. F. Goochee, *Biotechnol. Prog.* **1990**, *6* (5), 391–397.
- [40] S. J. Meier, T. A. Hatton, D. I. C. Wang, *Biotechnol. Bioeng.* **1999**, *62* (4), 468–478. DOI: [https://doi.org/10.1002/\(SICI\)1097-0290\(19990220\)62:4<468::AID-BIT10>3.0.CO;2-N](https://doi.org/10.1002/(SICI)1097-0290(19990220)62:4<468::AID-BIT10>3.0.CO;2-N)
- [41] S. S. Ozturk, *Cytotechnology* **1996**, *22* (1–3), 3–16. DOI: <https://doi.org/10.1007/BF00353919>
- [42] Y. Chisti, *Trends Biotechnol.* **2000**, *18* (10), 420–432. DOI: [https://doi.org/10.1016/S0167-7799\(00\)01474-8](https://doi.org/10.1016/S0167-7799(00)01474-8)
- [43] J. M. Woodley, N. J. Titchener-Hooker, *Bioprocess Eng.* **1996**, *14* (5), 263–268. DOI: <https://doi.org/10.1007/BF00369924>
- [44] A. Mersmann, G. Schneider, H. Voit, E. Wenzig, *Chem. Eng. Technol.* **1990**, *13* (1), 357–370. DOI: <https://doi.org/10.1002/ceat.270130149>
- [45] S. Sandadi, H. Pedersen, J. S. Bowers, D. Rendeiro, S. Sandadi, J. S. Bowers, Á. D. Rendeiro, H. Pedersen, *Bioprocess Biosyst. Eng.* **2011**, *34* (7), 819–832. DOI: <https://doi.org/10.1007/s00449-011-0532-0>
- [46] A. W. Nienow, in *Encyclopedia of Industrial Biotechnology: Bioprocess, Bioseparation, and Cell Technology* (Ed: M. C. Flickinger), Wiley, Hoboken **2010**.
- [47] N. Oosterhuis, S. Junne, in *Bioreactors: Design, Operation and Novel Applications* (Ed: C.-F. Mandenius), Wiley-VCH, Weinheim **2016**.
- [48] E. S. Langer, R. A. Rader, *Bioprocess. J.* **2014**, *13*, 43–49.
- [49] C. Challener, *Bioprocess Int.* **2016**, *14* (6), 44–45.
- [50] A.-P. Zeng, W.-D. Deckwer, *Biotechnol. Prog.* **1999**, *15* (3), 373–382. DOI: <https://doi.org/10.1021/bp990040a>
- [51] S. M. Woodside, B. D. Bowen, J. M. Piret, *Cytotechnology* **1998**, *28* (1–3), 163–175. DOI: <https://doi.org/10.1023/a:1008050202561>
- [52] F. Tapia, D. Vázquez-Ramírez, Y. Genzel, U. Reichl, *Appl. Microbiol. Biotechnol.* **2016**, *100* (5), 2121–2132. DOI: <https://doi.org/10.1007/s00253-015-7267-9>
- [53] J. C. Merchuk, *Can. J. Chem. Eng.* **2008**, *81* (3–4), 324–337. DOI: <https://doi.org/10.1002/cjce.5450810301>
- [54] A. Handa-Corrigan, A. N. Emery, R. E. Spier, *Enzyme Microb. Technol.* **1989**, *11* (4), 230–235. DOI: [https://doi.org/10.1016/0141-0229\(89\)90097-5](https://doi.org/10.1016/0141-0229(89)90097-5)
- [55] J. Tramper, D. Smit, J. Straatman, J. M. Vlask, *Bioprocess Eng.* **1988**, *3* (1), 37–41. DOI: <https://doi.org/10.1007/BF00372858>
- [56] J. Varley, J. Birch, *Cytotechnology* **1999**, *29* (3), 177–205.
- [57] G. Andrews, *Biotechnol. Genet. Eng. Rev.* **1988**, *6* (1), 151–178. DOI: <https://doi.org/10.1080/02648725.1988.10647847>
- [58] Y. C. Hu, J. Kaufman, M. W. Cho, H. Golding, J. Shiloach, *Biotechnol. Prog.* **2000**, *16* (5), 744–750. DOI: <https://doi.org/10.1021/bp000112u>
- [59] F. Meuwly, P.-A. Ruffieux, A. Kadouri, U. von Stockar, *Biotechnol. Adv.* **2007**, *25* (1), 45–56. DOI: <https://doi.org/10.1016/j.biotechadv.2006.08.004>
- [60] R. Pörtner, O. B. J. P. Barradas, in *Animal Cell Biotechnology* (Ed: R. Pörtner), Humana Press, Totowa, NJ **2007**.
- [61] G. Wang, W. Zhang, C. Jacklin, D. Freedman, L. Eppstein, A. Kadouri, *Cytotechnology* **1992**, *9* (1–3), 41–49. DOI: <https://doi.org/10.1007/BF02521730>
- [62] T.-C. Zhou, W.-W. Zhou, W. Hu, J.-J. Zhong, in *Encyclopedia of Industrial Biotechnology: Bioprocess, Bioseparation, and Cell Technology* (Ed: M. C. Flickinger), Wiley, Hoboken **2010**.
- [63] R. Pörtner, O. B. Platas, D. Fassnacht, D. Nehring, P. Czermak, H. Märkl, *Open Biotechnol. J.* **2007**, *1* (1), 41–46. DOI: <https://doi.org/10.2174/1874070700701010041>
- [64] S. Park, G. Stephanopoulos, *Biotechnol. Bioeng.* **1993**, *41* (1), 25–34. DOI: <https://doi.org/10.1002/bit.260410105>
- [65] M. Shakibaie, F. Tabandeh, A. R. Zomorodipour, H. Mohamad-Beigi, S. Ebrahimi, H. Habib-Ghomi, *World Appl. Sci. J.* **2011**, *15* (11), 1568–1575.
- [66] W. Ding, J. Martin, *Bioprocess Int.* **2010**, *8* (10), 52–60.
- [67] H. L. Levine, R. Stock, J. E. Lilja, Å. Gaasvik, H. Hummel, T. C. Ransohoff, S. D. Jones, *Bioprocess Int.* **2013**, *11*, 40–45.
- [68] Rentschler Biotechnologie, *Manuf. Chem. XV.* **2015**, (October 2014), 15–16.
- [69] K. Davis, *ISPE San Francisco/Bay Area Chapter Newsletter.* **2014**, *19* (2) 18.
- [70] P. Rogge, P. D. D. Müller, *Rentschler Biotechnol.* **2014**, *20* (7–8), 20–21.
- [71] B. Rawlings, H. Pora, *Bioprocess Int.* **2009**, *7* (2), 18–26.
- [72] S. Riley, *Modular Manufacturing*, WTW Media, Cleveland, OH **2016**. www.pharmpro.com/article/2016/04/modular-manufacturing, **2016**.
- [73] E. K. Read, J. T. Park, R. B. Shah, B. S. Riley, K. A. Brorson, A. S. Rathore, *Biotechnol. Bioeng.* **2010**, *105* (2), 276–284. DOI: <https://doi.org/10.1002/bit.22528>
- [74] J. Ziemlewski, *Chem. Eng. Prog. Mag.* **2009**, *105* (7), 23–29.
- [75] F. Mirasol, *BioPharm Int.* **2018**, *31* (2), 33–35.
- [76] <https://en.antaranews.com/news/96628/amgen-opens-next-generation-biomanufacturing-facility-in-singapore> (Accessed on April 18, 2021).
- [77] C. Löffelholz, U. Husemann, G. Greller, W. Meusel, J. Kauling, P. Ay, M. Kraume, R. Eibl, D. Eibl, *Chem. Ing. Tech.* **2013**, *85* (1–2), 40–56. DOI: <https://doi.org/10.1002/cite.201200125>
- [78] R. Eibl, S. Werner, D. Eibl, in *Disposable Bioreactors, Advances in Biochemical Engineering/Biotechnology*, Vol. 115, Springer, Berlin **2009**.
- [79] V. Singh, *Cytotechnology* **1999**, *30* (1–3), 149–158. DOI: <https://doi.org/10.1023/A:1008025016272>
- [80] B. Terrier, D. Courtois, N. Hénault, A. Cuvier, M. Bastin, A. Aknin, J. Dubreuil, V. Pétiard, *Biotechnol. Bioeng.* **2007**, *96* (5), 914–923. DOI: <https://doi.org/10.1002/bit.21187>
- [81] C. Löffelholz, S. C. Kaiser, M. Kraume, R. Eibl, D. Eibl, in *Disposable Bioreactors II*, Springer, Berlin **2013**.
- [82] S. M. J. Jones, T. M. Louw, S. T. L. Harrison, *Algal Res.* **2017**, *24*, 317–324. DOI: <https://doi.org/10.1016/j.algal.2017.03.001>
- [83] X. Zhang, M. Stettler, O. Reif, A. Kocourek, M. DeJesus, D. L. Hacker, F. M. Wurm, *New Biotechnol.* **2008**, *25* (1), 68–75. DOI: <https://doi.org/10.1016/j.nbt.2008.03.001>
- [84] W. Klöckner, R. Gacem, T. Anderlei, N. Raven, S. Schillberg, C. Lattermann, J. Buchs, *J. Biol. Eng.* **2013**, *7* (1), 28. DOI: <https://doi.org/10.1186/1754-1611-7-28>
- [85] J. P. Smelko, K. R. Wiltberger, E. F. Hickman, B. J. Morris, T. J. Blackburn, T. Ryll, *Biotechnol. Prog.* **2011**, *27* (5), 1358–1364. DOI: <https://doi.org/10.1002/btpr.634>
- [86] S. C. Almo, J. D. Love, *Curr. Opin. Struct. Biol.* **2014**, *26*, 39–43. DOI: <https://doi.org/10.1016/j.sbi.2014.03.006>

- [87] B. Lee, D. Fang, M. Croughan, M. Carrondo, S.-H. Paik, *BMC Proc.* **2011**, 5, O12. DOI: <https://doi.org/10.1186/1753-6561-5-S8-O12>
- [88] www.theengineer.co.uk/culture-vulture-building-a-better-bioreactor/ (Accessed on November 04, 2021)
- [89] M. F. Q. Sousa, M. M. Silva, D. Giroux, Y. Hashimura, R. Wesselschmidt, B. Lee, A. Roldão, M. J. T. Carrondo, P. M. Alves, M. Serra, *Biotechnol. Prog.* **2015**, 31 (6), 1600–1612. DOI: <https://doi.org/10.1002/btpr.2158>
- [90] M. Eisenstein, *Nat. Methods* **2006**, 3 (12), 1035–1043. DOI: <https://doi.org/10.1038/nmeth1206-1035>
- [91] K. A. Auton, in *Cells and Culture* (Ed: T. Noll), Springer, Berlin **2010**.
- [92] https://escovaccixcell.com/tide_technology/cell_cultivation/CelCradle (Accessed on November 04, 2021)
- [93] www.cescobio.com.tw/product_detail.php?PNo=9&CNo=18 (Accessed on April 16, 2015)
- [94] H. Toriniwa, T. Komiyama, *Biologicals* **2007**, 35 (4), 221–226. DOI: <https://doi.org/10.1016/j.biologicals.2007.02.002>
- [95] Y.-C. Hu, J.-T. Lu, Y.-C. Chung, *Cytotechnology* **2003**, 42 (3), 145–153. DOI: <https://doi.org/10.1023/B:CYTO.0000015841.98225.27>
- [96] S.-C. Wu, M. Liau, Y.-C. Lin, C.-J. Sun, C.-T. Wang, *Vaccine* **2013**, 31 (6), 867–872. DOI: <https://doi.org/10.1016/j.vaccine.2012.12.017>
- [97] J.-T. Lu, Y.-C. Chung, Z.-R. Chan, Y.-C. Hu, *Biotechnol. Lett.* **2005**, 27 (15), 1059–1065. DOI: <https://doi.org/10.1007/s10529-005-8450-3>
- [98] B. Frahm, H. Brod, U. Langer, *Cytotechnology* **2009**, 59 (1), 17–30. DOI: <https://doi.org/10.1007/s10616-009-9189-9>
- [99] W. Van Hecke, D. Haltrich, B. Frahm, H. Brod, J. Dewulf, H. Van Langenhove, R. Ludwig, *J. Mol. Catal. B: Enzym.* **2011**, 68 (2), 154–161. DOI: <https://doi.org/10.1016/j.molcatb.2010.10.004>
- [100] M. Selker, B. Paldus, Disposable Bioreactor System, *US Patent 20080274541 A1*, **2008**.
- [101] S. C. Kaiser, M. Kraume, D. Eibl, *Chem. Ing. Tech.* **2013**, 85 (1–2), 136–143. DOI: <https://doi.org/10.1002/cite.201200127>
- [102] S. C. Kaiser, N. Perepelitsa, M. Kraume, D. Eibl, *Chem. Ing. Tech.* **2016**, 88 (1–2), 86–92. DOI: <https://doi.org/10.1002/cite.201500091>
- [103] D. Wang, W. Liu, B. Han, R. Xu, *Curr. Pharm. Biotechnol.* **2005**, 6 (5), 397–403. DOI: <https://doi.org/10.2174/138920105774370580>
- [104] B. Haut, H. Ben Amor, L. Coulon, A. Jacquet, V. Halloin, *Chem. Eng. Sci.* **2003**, 58 (3–6), 777–784. DOI: [https://doi.org/10.1016/S0009-2509\(02\)00607-3](https://doi.org/10.1016/S0009-2509(02)00607-3)
- [105] R. Mitteregger, G. Vogt, E. Rossmanith, D. Falkenhagen, *Int. J. Artif. Organs* **1999**, 22 (12), 816–822. DOI: <https://doi.org/10.1177/039139889902201207>
- [106] R. Bareither, D. Pollard, *Biotechnol. Prog.* **2011**, 27 (1), 2–14. DOI: <https://doi.org/10.1002/btpr.522>
- [107] R. Bhambure, K. Kumar, A. S. Rathore, *Trends Biotechnol.* **2011**, 29 (3), 127–135. DOI: <https://doi.org/10.1016/j.tibtech.2010.12.001>
- [108] F. Li, Y. Hashimura, R. Pendleton, J. Harms, E. Collins, B. Lee, *Biotechnol. Prog.* **2006**, 22 (3), 696–703. DOI: <https://doi.org/10.1021/bp0504041>
- [109] R. Legmann, H. B. Schreyer, R. G. Combs, E. L. McCormick, A. P. Russo, S. T. Rodgers, *Biotechnol. Bioeng.* **2009**, 104 (6), 1107–1120. DOI: <https://doi.org/10.1002/bit.22474>
- [110] J. I. Betts, F. Baganz, *Microb. Cell Fact.* **2006**, 5 (1), 21. DOI: <https://doi.org/10.1186/1475-2859-5-21>
- [111] J. Diao, L. Young, P. Zhou, M. L. Shuler, *Biotechnol. Bioeng.* **2008**, 100 (1), 72–81. DOI: <https://doi.org/10.1002/bit.21751>
- [112] T. V. Kirk, N. Szita, *Biotechnol. Bioeng.* **2013**, 110 (4), 1005–19. DOI: <https://doi.org/10.1002/bit.24824>
- [113] A. Amanullah, J. M. Otero, M. Mikola, A. Hsu, J. Zhang, J. Aunins, B. H. Schreyer, J. A. Hope, P. A. Russo, *Biotechnol. Bioeng.* **2010**, 106 (1), 57–67. DOI: <https://doi.org/10.1002/bit.22664>
- [114] M. H. Sani, F. Baganz, *J. Teknol.* **2012**, 59 (1). DOI: <https://doi.org/10.11113/jt.v59.1569>
- [115] A. Soley, A. Fontova, J. Gálvez, E. Sarró, M. Lecina, R. Bragós, J. J. Cairó, F. Gòdia, *Process Biochem.* **2012**, 47 (4), 597–605. DOI: <https://doi.org/10.1016/J.PROCBIO.2011.12.022>
- [116] J. Luecke, *Nat. Methods* **2007**, 4 (10), i–ii. DOI: <https://doi.org/10.1038/nmeth1007-i>
- [117] K. Xie, X.-W. Zhang, L. Huang, Y.-T. Wang, Y. Lei, J. Rong, C.-W. Qian, Q.-L. Xie, Y.-F. Wang, A. Hong, et al., *Cytotechnology* **2011**, 63 (4), 345–50. DOI: <https://doi.org/10.1007/s10616-011-9361-x>
- [118] [www.cepower.ch/view/userfiles/files/CELLLine\(3\).pdf](http://www.cepower.ch/view/userfiles/files/CELLLine(3).pdf) (Accessed on November 04, 2021)
- [119] S. Rameez, S. S. Mostafa, C. Miller, A. A. Shukla, *Biotechnol. Prog.* **2014**, 30 (3), 718–727. DOI: <https://doi.org/10.1002/btpr.1874>
- [120] M. Papagianni, *J. Microb. Biochem. Technol.* **2015**, s5 (5), 1–7. DOI: <https://doi.org/10.4172/1948-5948.S5-001>
- [121] R. Eibl, S. Kaiser, R. Lombriser, D. Eibl, *Appl. Microbiol. Biotechnol.* **2010**, 86 (1), 41–49. DOI: <https://doi.org/10.1007/s00253-009-2422-9>
- [122] J. P. J. Betts, S. R. C. Warr, G. B. Finka, M. Uden, M. Town, J. M. Janda, F. Baganz, G. J. Lye, *Biochem. Eng. J.* **2014**, 82, 105–116. DOI: <https://doi.org/10.1016/j.bej.2013.11.010>
- [123] F. Delouvroy, G. Le Reverend, B. Fessler, G. Mathy, M. Harmsen, N. Kochanowski, L. Malphettes, *BMC Proc.* **2013**, 7 (Suppl 6), P73. DOI: <https://doi.org/10.1186/1753-6561-7-S6-P73>
- [124] P. Rohe, D. Venkanna, B. Kleine, R. Freudl, M. Oldiges, *Microb. Cell Fact.* **2012**, 11 (1), 144. DOI: <https://doi.org/10.1186/1475-2859-11-144>
- [125] Q. Xie, P. O. Michel, L. Baldi, D. L. Hacker, X. Zhang, F. M. Wurm, *Biotechnol. Lett.* **2011**, 33 (5), 897–902. DOI: <https://doi.org/10.1007/s10529-011-0527-6>
- [126] M. J. De Jesus, P. Girard, M. Bourgeois, G. Baumgartner, B. Jacko, H. Amstutz, F. M. Wurm, *Biochem. Eng. J.* **2004**, 17 (3), 217–223. DOI: [https://doi.org/10.1016/S1369-703X\(03\)00180-3](https://doi.org/10.1016/S1369-703X(03)00180-3)
- [127] M. De Jesus, F. M. Wurm, *Eur. J. Pharm. Biopharm.* **2011**, 78 (2), 184–188. DOI: <https://doi.org/10.1016/j.ejpb.2011.01.005>
- [128] J. Kauling, H. Brod, M. Jenne, A. Waldhelm, U. Langer, B. Bödeker, *Chem. Ing. Tech.* **2013**, 85 (1–2), 127–135. DOI: <https://doi.org/10.1002/cite.201200155>
- [129] D. De Wilde, T. Dreher, C. Zahnow, U. Husemann, G. Grelle, T. Adams, C. Fenge, *BioProcess Int.* **2014**, 12 (8), 14.
- [130] R. Eibl, D. Eibl, *BioProcess Int.* **2009**, 7 (1), 18–23.

RESEARCH ARTICLE

Advancing a rapid, high throughput screening platform for optimization of lentivirus production

Sneha Gopal¹ | Adam E. Osborne² | Lindsay Hock² | Jill Zemianek² | Kun Fang² |
Gretchen Gee² | Ronit Ghosh¹ | David McNally² | Steven M. Cramer^{1,3} |
Jonathan S. Dordick^{1,4} 

¹ Department of Chemical and Biological Engineering, and Center for Biotechnology & Interdisciplinary Studies, Rensselaer Polytechnic Institute, Troy, New York, USA

² MassBiologics, University of Massachusetts Medical School, Mattapan, Massachusetts, USA

³ Department of Chemistry and Chemical Biology, Rensselaer Polytechnic Institute, Troy, NY 12180, USA

⁴ Departments of Biomedical Engineering and Biological Sciences, Rensselaer Polytechnic Institute, Troy, New York, USA

Correspondence

Jonathan S. Dordick, Department of Chemical and Biological Engineering, Rensselaer Polytechnic Institute, Troy, NY 12180, USA. Email: dordick@rpi.edu

Abstract

Background: Lentiviral vectors (LVVs) hold great promise as delivery tools for gene therapy and chimeric antigen receptor T cell (CAR-T) therapy. Their ability to target difficult to transfect cells and deliver genetic payloads that integrate into the host genome makes them ideal delivery candidates. However, several challenges remain to be addressed before LVVs are more widely used as therapeutics including low viral vector concentrations and the absence of suitable scale-up methods for large-scale production. To address these challenges, we have developed a high throughput microscale HEK293 suspension culture platform that enables rapid screening of conditions for improving LVV productivity.

Key Results: High density culture (40 million cells mL⁻¹) of HEK293 suspension cells in commercially available media was achieved in microscale 96-deep well plate platform at liquid volumes of 200 μL. Comparable transfection and LVV production efficiencies were observed at the microscale, in conventional shake flasks and a 1-L bioreactor, indicating that significant scale-down does not affect LVV concentrations and predictivity of scale-up. Optimization of production step allowed for final yields of LVVs to reach 1.5 × 10⁷ TU mL⁻¹.

Conclusions: The ability to test a large number of conditions simultaneously with minimal reagent use allows for the rapid optimization of LVV production in HEK293 suspension cells. Therefore, such a system may serve as a valuable tool in early stage process development and can be used as a screening tool to improve LVV concentrations for both batch and perfusion based systems.

KEYWORDS

HEK293 suspension cells, High-throughput transfection, Lentiviral titers, Lentiviral vectors

1 | INTRODUCTION

There is growing interest in developing new tools and technologies to improve and expand the use of gene therapy as a potential treatment

Abbreviations: HEK293, Human Embryonic Kidney 293; LVV, Lentiviral Vectors; PEI-Max, Polyethylenimine Max

for several genetic and degenerative diseases. Gene therapy can serve as a curative technology by replacing a defective or absent gene with a functional gene or can be used *ex vivo* for engineering immune cells for cancer therapy, for example, chimeric antigen receptor T (CAR-T) for cancer treatment.^[1,2] This requires several key steps, including identification of the critical gene of interest (GOI),^[3] the delivery method

to introduce the GOI into specific cellular targets,^[4] and the production of a suitable vector.^[5] Adenoviral vectors (AV), adeno-associated viral vectors (AAV), and lentiviral vectors (LVV) have been evaluated as delivery vectors to introduce a GOI into cellular targets.^[6-8] In particular, lentiviral vectors (LVVs) are of interest because of their ability to infect both dividing and non-dividing cells, as well as for their capacity to carry a large genetic payload size.^[9] This makes LVVs ideal delivery candidates for gene and CAR-T therapies.^[10-12]

LVVs for gene therapy applications are typically pseudotyped with vesicular stomatitis virus G (VSV-G) envelope glycoprotein, which grants these viral vectors a wider tropism.^[13] The modified LVVs are replication incompetent, which allows genetic material to integrate into the host cell genome, but prevents them from propagating.^[14] LVVs are typically generated using a host cell line that is transfected with all the components necessary for virus assembly. The most commonly used host cell is the Human Embryonic Kidney 293 (HEK293) cell line. Three different LVV generation systems (1st, 2nd and 3rd generation) have been developed that differ in the number of envelope and packaging plasmids used (from 1 to 3, respectively) and the way in which the packaging and envelope genes are split.^[15] The cells also receive a transfer vector that is packaged inside the LVV.^[16] Once the plasmids are transfected into the cell, viral assembly ensues.^[17] Subsequently, the packaged vector carrying the transfer gene is released from the cells into the medium and the supernatant is then harvested and used to transduce other cell types with the GOI.^[18]

In the current study, we used the third generation LVV system, which consists of two packaging plasmids (pMDLg/RRE and pRSV/Rev), one envelope plasmid (pMD2.g), and one transfer plasmid (pLV-EGFP). Despite the apparent relative simplicity of producing LVVs, a core challenge in LVV scale-up is the poor yield of virus present in the harvest supernatant post-collection.^[19] This could be due to several factors including the amount of plasmid DNA delivered to the cells, the transfection reagent, the ratio of DNA to cells for transfection, the HEK293 cell density, and the ratio of the four plasmids. Myriad variables can be optimized, including DNA:cell ratio, DNA:transfection reagent ratio, and cell density for transfection, all with minimal use of reagents. Studies to date have used 6-, 12-, 24-, and 96-well plate cultures for screening HEK293 suspension cells with cell densities typically less than 5×10^6 cells mL⁻¹.^[20-24] Compared to adherent-dependent HEK cells, suspension-adapted HEK293 cells allow for simpler scale-up in bioreactors where large volumes of LVV supernatant can be harvested from cells grown to high cell densities.^[25]

Herein, we employed microscale, 96-deep well plates with commercial media for cell growth and transfection. The platform used in the current work is one of the first to report high cell density growth (4×10^7 cells mL⁻¹) in a microscale platform that predicts LVV productivity in shake flasks and small bioreactors. As a result, we have developed a rapid screening tool that can be used to optimize LVV production, which may accelerate its use in gene therapy and CAR-T therapies.

2 | MATERIALS AND METHODS

2.1 | Cell lines and high-density growth in shake flasks and 96-deep well plates

A clonal line of Human Embryonic Kidney 293 (HEK293) suspension cells (derived at MassBiologics) was maintained in BalanCD HEK293 medium (Irvine Scientific), supplemented with 4 mM Glutamax, and agitated at 140 rpm in an Innova 2000 orbital shaker (Eppendorf), 19.5 mm, 37°C with 5% CO₂. Cells were seeded at 3×10^5 cells mL⁻¹ and passaged when they reached $3-5 \times 10^6$ cells mL⁻¹. HT1080 fibrosarcoma cells (CCL-121, ATCC) were cultured in Dulbecco's Modified Eagle's Medium (DMEM) (Thermo Fisher Scientific) supplemented with 10% Fetal Bovine Serum (FBS) (ThermoFisher Scientific) and 1% Penicillin Streptomycin (PenStrep, ThermoFisher Scientific), at 37°C and 5% CO₂. Commercially available viral vector producer cells (LV-Max) were obtained from Thermo Fisher Scientific and also maintained in BalanCD HEK293 supplemented with 4 mM Glutamax as indicated above.

For high-density growth of HEK293 suspension cells in shake flasks, the cells were seeded at 3×10^5 cells mL⁻¹ in 30 mL of medium. On day 3 post-seeding, when cell density reached approximately $2-4 \times 10^6$ cells mL⁻¹, the culture volume was reduced to 10 mL per 125 mL shake flask and media exchange was performed daily until cells reached maximum density. For 96-deep well plates, the cells were incubated in 500 μ L/well in 2 mL Axygen well plates (Corning) with square walls and sealed with a gas-permeable sealing membrane. The plates were maintained in an orbital shaker (3 mm diameter) and agitated at up to 1000 rpm. For high-density growth in 96-deep well plates, the total culture volume was reduced to 200 μ L/well.

2.2 | Transfection

Third-generation packaging and envelope plasmids included pRSV-Rev (Addgene plasmid #12253), pMDLg-RRE (Addgene plasmid #12251) and pMD2.g (Addgene plasmid #12259), respectively, and were a gift from Didier Trono (Ecole Polytechnique Fédérale de Lausanne). The transfer plasmid pLV-EGFP (Addgene plasmid #36083) was a gift from Pantelis Tsoulfas (University of Miami). Transfections were performed with DNA solution added to OptiPro Serum-Free medium at a ratio of total starting culture volume to medium volume of 15. Polyethyleneimine-Max (PEI-Max, Polysciences), 40 kD, a commonly used linear polymer that is cost-effective and scalable for HEK293 transfections,^[26,27] was added to an equal volume of OptiPro Serum-Free medium at various ratios. The two mixtures were combined and allowed to complex for 15 min. The resulting mixture was then added to the cells.

HEK293 suspension cells were seeded in all wells of a 96-deep well plate at 3×10^5 cells mL⁻¹ excluding the 36 edge wells to avoid a higher rate of evaporation. The cells were grown to the desired cell density and then transfected with a single pLV-EGFP plasmid at

0.5–7.0 pg DNA/cell and at PEI:DNA ratios of 2:1, 3.5:1, and 5:1. Transfections were run in duplicate. The cells were harvested after 48 h, washed with Dulbecco's Phosphate Buffered Saline (DPBS), and resuspended in DPBS. The transfection efficiency was then measured using BD LSR II flow cytometer (Becton-Dickinson).

2.3 | Lentiviral production in 96-deep well plates and scaled-up bioreactor system

For LVV production at low cell density, cells were seeded at 5×10^5 cells mL^{-1} at day 0. At day 1, the packaging, envelope and transfer plasmids (Cell Biolabs) were transfected into HEK293 suspension cells using PEI-Max (1 mg mL^{-1}) at a mass ratio of 6:4:6:1 (pRSVRev:pMDL:pLVGFP:pMD2g). Medium exchange was performed 24 h post-transfection followed by the addition of 5 mM sodium butyrate. The LVV supernatant was then collected 48 h post-media exchange, filtered through a $0.45 \mu\text{m}$ polyethersulfone (PES) filter (Millipore Sigma) and frozen for titration. A 1-L DasGip bioreactor (Eppendorf), working volume of 0.8 L, was inoculated with 5×10^5 cells mL^{-1} 24 h prior to transfection. Cells were cultured in BalanCD medium supplemented with 4 mM L-glutamine (Gibco Life Technologies) at pH 7.3, 40% dissolved O_2 , 36.5°C , 120 rpm, and 0.5 L h^{-1} air flow. Transfection was performed using 1.9 pg/cell plasmid DNA at the aforementioned ratio, complexed with 4 mg mL^{-1} PEI at a ratio of 1:3.5 DNA:PEI. Complexation of plasmid DNA was performed for 15 min before being injected into the bioreactor by syringe. Sodium butyrate (5 mM final concentration) was added 24 h post-transfection. A sample was also taken to establish the efficiency of transfection by GFP fluorescence, and the culture was harvested 72 h post-transfection. The cells were pelleted at $200 \times g$ for 7 min in a swinging bucket centrifuge. The clarified media was frozen at -80°C or used for the titration infectivity assay.

2.4 | Titration of lentiviral supernatant with HT1080 cells

Lentiviral vector titration with an infectivity assay was performed using two methods—flow cytometry and high content imaging. For the former, HT1080 cells were seeded at 5×10^4 cells/well in a 12-well plate. After 24 h, the harvested LVV supernatant was serially diluted in DMEM + 10% FBS + 1% PenStrep and added to the cells with $8 \mu\text{g mL}^{-1}$ of polybrene. The cells were assayed for EGFP expression using a BD LSR II flow cytometer 48 h post-transduction. A threshold transduction efficiency was set at 30% to discard multiple infections and LVV concentration was calculated according to Equation 1.

LVV Concentration

$$= \frac{\%GFP \text{ Positive} * \text{Number of Cells Transduced} * \text{Dilution Factor}}{\text{Culture Volume}} \quad (1)$$

For high content imaging, HT1080 cells were seeded at 2×10^4 cells/well in 96-well plates. After 24 h, the harvested supernatant was serially diluted in DMEM + 10% FBS + 1% PenStrep, and added to cells with $8 \mu\text{g mL}^{-1}$ of polybrene. After 48 h, cell nuclei were stained with $5 \mu\text{g mL}^{-1}$ of Hoechst 33342 (Thermo Fisher Scientific) and imaged using a Cellomics ArrayScan XTI (Thermo Fisher Scientific). Transduction efficiency was calculated using the Target Activation Bioapplication feature.

2.5 | RT-qPCR and p24 sandwich ELISA

Viral RNA was extracted from harvest supernatant using the Pure-Link Viral RNA/DNA Extraction Kit (Thermo Fisher Scientific) according to the manufacturer's instructions (see Supporting Information for details). A p24 sandwich ELISA assay was performed using a commercially available DuoSet p24 sandwich ELISA kit (R&D Systems) as detailed in Supporting Information.

2.6 | Statistical analysis

A parametric unpaired student's t-test was used to determine statistical significance ($p < 0.05$) of transfection efficiency between shake flasks and 96-deep well plates, and among different media. All analyses were performed using GraphPad Prism 9.

3 | RESULTS

3.1 | Growth and transfection of HEK293 suspension cells in commercial media

Cell growth (30 mL culture volume) was evaluated in four commercially available media—CDM4HEK293, CDM4Permab, BalanCD HEK293 and HyCell TransfX—to identify an optimal medium for HEK293 suspension cells (Figure 1A). These cells were previously identified to be high producing clones for AAVs, and were considered to be a useful starting cell line for this study. The maximum growth rates were all within a factor of 2; $0.013\text{--}0.026 \text{ h}^{-1}$ (Table S1). While CDM4Permab exhibited the highest maximum growth rate with a relatively high cell density, neither it nor CDM4HEK293 supported transfection with PEI-Max as no EGFP fluorescence was observed 48 h post-transfection (Figure S1, Figure S3). BalanCD, however, did support transfection with PEI-Max (Figure S1, Figure S3) and CDM4Permab supported transfection with non-PEI reagents (Figure S2). Clearly, interactions among media composition and the chemical nature of cationic polymers and cationic lipid transfection reagents impact transfection efficiency.^[28,29] However, we chose BalanCD for further experiments, since PEI-Max is a highly scalable transfection reagent.

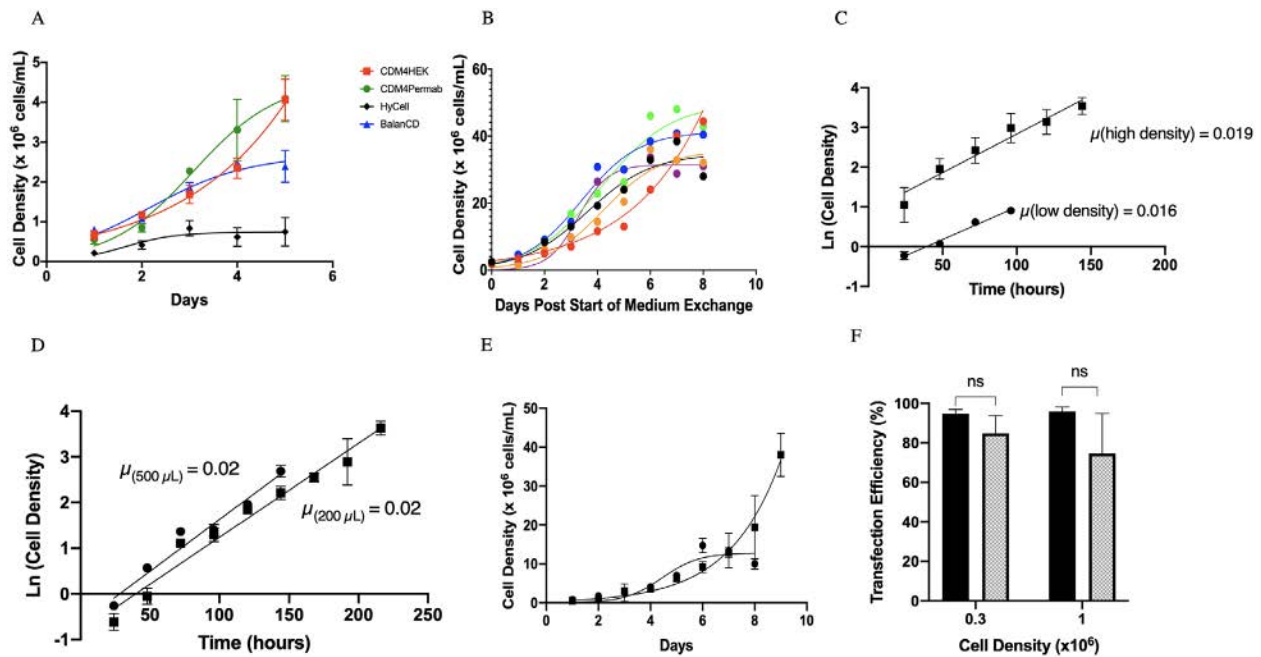


FIGURE 1 Influence of culture media on HEK293 suspension cell growth. (A) Cell growth in 125 mL shake flasks (30 mL liquid volume) by seeding 3×10^5 cells mL^{-1} on day 0. Cell growth was evaluated in four different commercially available media: CDM4HEK293 (\square), CDM4Permab (\bullet), BalanCD HEK293 (\blacktriangle), and HyCell TransfX (\blacklozenge). A logistic growth curve model was fit through the data points. Error bars represent standard deviation across replicates. High Density HEK293 suspension cell growth in BalanCD HEK293. (B) Cells were grown in BalanCD HEK293 to high densities in 125 mL shake flasks (10 mL liquid volume). Medium exchange occurred daily after three days. A logistic growth line of best fit was drawn through the points. Each run of six replicates is shown. (C) Exponential growth for high-density (\blacksquare) and low-density (\bullet) cultures of HEK293 suspension cells in 125 mL shake flasks (10 mL liquid volume). The slopes represent the growth rate (μ) of HEK293 suspension cells. (D) Exponential growth for high density cultures in 96-deep well plates at 500 μL (\bullet) and 200 μL (\blacksquare). (E) Growth of HEK293 suspension cells in 96-deep well plates at 500 μL (\bullet) and 200 μL (\blacksquare). A logistic growth line of best fit was drawn through the points. The error bars represent standard deviation across three replicates ($N = 3$). (F) HEK293 suspension cells cultured in BalanCD HEK293 were transfected with a single pLV-EGFP plasmid at 3×10^5 cells mL^{-1} and 1×10^6 cells mL^{-1} in shake flasks (filled bars) and 96-deep well plates (dotted bars). The transfection efficiency of the cells was measured after 48 h using a flow cytometer. A Students t -test was used to compare the transfection between shake flasks and 96-deep well plates at each density ($*p < 0.05$, $**p < 0.01$, $***p < 0.001$, $****p < 0.0001$, ns (not significant $p > 0.05$). Error bars represent standard deviation across three replicates ($N = 3$)

3.2 | High-density growth and transfection of HEK293 suspension cells in BalanCD in shake flasks and deep well plates

In the absence of medium exchange, the maximum cell density in BalanCD was approximately 2.5×10^6 cells mL^{-1} (Figure 1A), likely due to glucose limitations.^[30,31] Thus, HEK293 suspension cells were seeded at 3×10^5 cells mL^{-1} in 30 mL of BalanCD medium (in 125 mL shake flasks) supplemented with 4 mM Glutamax. A “mock” perfusion was then initiated on day 3 when the cells were collected, spun down, and resuspended daily to replace depleted nutrients. We also reduced the liquid culture volume to 10 mL per 125 mL shake flask to provide increased headspace for higher oxygen transfer.^[32] This methodology led to improved cell densities of up to $4.0 (\pm 6.9) \times 10^7$ cells mL^{-1} (error based on standard deviation) across six independent runs (Figure 1B). The average maximum growth rate was 0.018 h^{-1} for high cell density (Figure 1C), which is very similar to the maximum growth rate at lower cell densities.

We then performed nearly 100-fold scale-down to 96-deep well plates for optimization studies. Two culture volumes, 500 and

200 μL /well, were used in square-walled 96-deep well plates create a baffling effect known to enhance oxygen transfer in the wells.^[20] Cells were seeded at 3×10^5 cells mL^{-1} and medium was exchanged daily starting on day 3. Growth rates (Figure 1D) and cell numbers were comparable in both volumes up to approximately 5 days (Figure 1E). However, the maximum cell density attained at 500 μL was $\sim 1.5 \times 10^7$ cells mL^{-1} , while with 200 μL /well, cell densities up to at least 4.0×10^7 cells mL^{-1} were achieved (Figure 1E).

The oxygen transfer rate (OTR) is affected by the oxygen mass transfer coefficient, the area of mass transfer and the concentration gradient for oxygen between the culture medium and air as shown by Equation 2^[33]

$$\text{OTR} = k_L a (C^* - C) \quad (2)$$

Where k_L is the oxygen mass transfer coefficient, a is the surface area of the air-medium interface, C^* is the saturation oxygen concentration in the medium,^[34] and C is the concentration of oxygen in the medium. The maximum oxygen transfer rate (OTR_{max}) occurs when C is zero. The $k_L a$ can be experimentally modified since it is strongly

TABLE 1 Lentiviral titers in 96-deep well plates

LVV production at 1×10^6 cells mL ⁻¹ in 96-deep well plates				
Method used	Replicate 1	Replicate 2	Replicate 3	Mean \pm SD
p24 sandwich ELISA [pg mL ⁻¹]	1.3×10^3	1.1×10^3	1.4×10^3	$1.3 \times 10^3 \pm 17$
RT-qPCR [copies mL ⁻¹]	5.8×10^7	2.8×10^7	6.4×10^7	$5.0 \times 10^7 \pm 1.9 \times 10^7$
Infectivity titer [TU mL ⁻¹]	2.4×10^5	1.8×10^5	1.4×10^5	$1.9 \times 10^5 \pm 5.0 \times 10^4$

affected by the liquid culture volume, the agitation rate and the shape of the culture vessel.^[20,35] Using k_L correlations for deep-well plates and shake flasks (see Supporting Information), calculated k_L values obtained in 125 mL shake flasks agitated at 140 rpm and maintained at 37°C were ~ 55 and ~ 30 h⁻¹ for liquid volumes of 10 and 30 mL, respectively. For 96-deep well plates, the closest approximation to our system was developed for liquid volumes of 600–1000 μ L using sulfite oxidation in the absence of cells and cell culture medium.^[20] Using this correlation, we calculated k_L values of ~ 150 and ~ 120 h⁻¹ for 200 and 500 μ L culture volumes, respectively.

The oxygen uptake rate (OUR) of a HEK293 suspension cell has been estimated to be 335 μ mol (gDCW⁻¹h⁻¹).^[36] At the start of “mock perfusion,” the cell density is approximately 2×10^6 cells mL⁻¹ and the maximum density obtained is 4×10^7 cells mL⁻¹, or 1.0 and 21 g L⁻¹ for the starting and maximum cell densities, respectively. This further corresponds to calculated OURs of 335 and 7035 μ M h⁻¹, respectively. Based on this calculation for shake flask cultures, the OTR is not limiting at the cell concentration at the start of mock perfusion, but becomes limiting at the maximum cell density for 30 mL liquid volume (Table S2). This is not the case with 10 mL shake flask liquid volume. Oxygen transfer is not limiting in either liquid volumes of 96-deep well plates. These results indicate that HEK293 suspension cultures can be scaled down approximately 150-fold and reach cell densities similar to those in shake flasks. Indeed, the maximum cell growth rate, 0.020 h⁻¹ for 200 μ L/well, was similar to that obtained in shake flasks.

We then compared transfection efficiency of HEK293 suspension cells in shake flasks and 96-deep well plates for single plasmid transfection of pLV-EGFP. HEK293 suspension cells were transfected at 3×10^5 and 1×10^6 cells mL⁻¹ in shake flasks and 96-deep well plates, respectively, using PEI-Max. The transfection efficiency at 48 h post-transfection was determined using flow cytometry. No significant difference in transfection efficiency was observed between shake flasks and 96-deep well plates at both densities (Figure 1F and Figure S3–S4). This indicates that culture scale-down did not alter transfection behavior.

3.3 | Comparison of LVV production between 96-deep well plates and scaled-up batch systems

We transfected the four lentiviral plasmids at a ratio of 6:4:6:1 (pRSVRev:pMDL:pLV-EGFP:pMD2g) into HEK293 suspension cells

with PEI-Max at a cell density of 1×10^6 cells mL⁻¹. This plasmid ratio was chosen based on a previous protocol, but was modified slightly to ensure that the amount of the envelope plasmid (pMD2g) was set as the lowest amount due to potential toxicity associated with VSV glycoprotein.^[37,38] Transfections were first performed in 96-deep well plates. LVV concentrations were analyzed by RT-qPCR, infectivity assays using HT1080 cells (via flow cytometry) and p24 sandwich ELISA (Table 1). Multiple wells were transfected for each replicate and pooled to ensure that sufficient sample was available to be analyzed by the three methods. Highly reproducible LVV particle concentrations were observed for three replicates across each of the three assay types. LVVs in a 1-L bioreactor using the aforementioned plasmid ratio and transfection condition, but using both infectivity and RT-qPCR measurements, which resulted in 6.9×10^4 TU mL⁻¹ and 2×10^8 copies mL⁻¹, respectively. Both infectivity and RT-qPCR values were similar to those obtained with the 96-deep well plate; the ratio of infectivity in the 96-deep well plate to 1-L bioreactor was only 2.75 despite the 1600-fold scale-up performed. Since we were able to show that LVV concentrations obtained after a reduction of scale was similar to the concentrations obtained in bioreactors, we proceeded to conduct multiple screens with HEK293 suspension cells at the microscale to optimize viral vector production.

3.4 | Identification of optimal PEI:DNA and DNA/cell density for transfection

A combinatorial screen was performed to identify optimal transfection conditions of HEK293 suspension cells across a wide range of cell densities. The cells were seeded at 3×10^5 cells mL⁻¹ and allowed to grow to 4×10^7 cells mL⁻¹. When the cells reached discrete cell densities they were transfected with pLV-EGFP over a range of DNA amount/cell and PEI/DNA ratios. Three heat maps were generated at PEI/DNA ratios of 2:1, 3.5:1, and 5:1 (Figure 2). The transfection efficiencies could be divided into two regimes; a low cell density regime ($< 5 \times 10^6$ cells mL⁻¹) and a high cell density regime ($\geq 5 \times 10^6$ cells mL⁻¹).

The behavior of the cells at low cell density can be further subdivided into three regions, each corresponding to low (Figure 2A), medium (Figure 2B) and high (Figure 2C) PEI/DNA ratios. At low PEI/DNA ratios (Figure 2A), increasing the amount of DNA per cell increased the transfection efficiency. Higher concentrations of

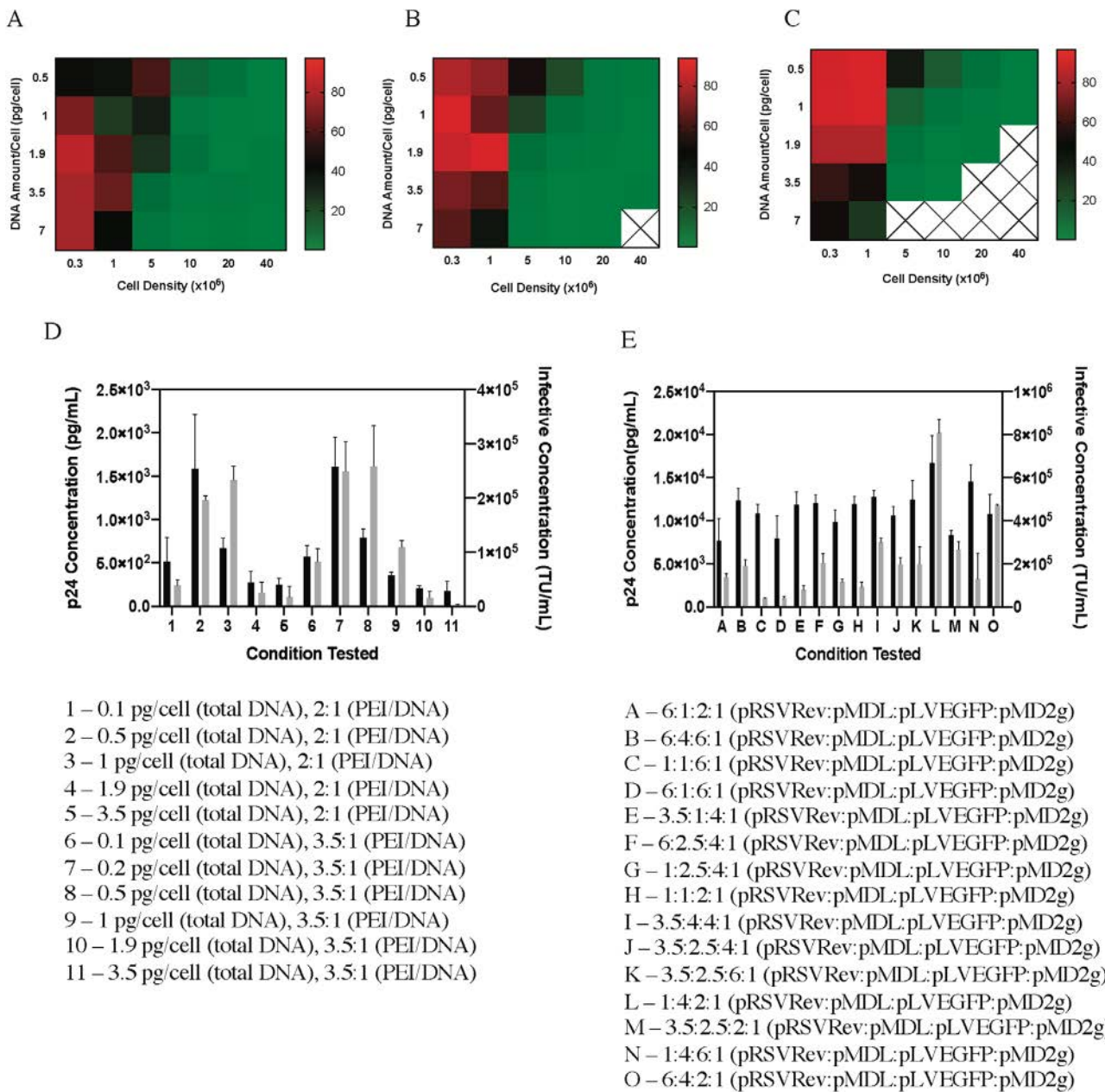


FIGURE 2 Transfection and LVV production optimization in HEK293 suspension cells performed in 96-deep well plates in duplicate. The three different PEI:DNA ratios of (A) 2:1, (B) 3.5:1 and (C) 5:1 are plotted as three separate heat maps. The redder the square the higher the transfection efficiency. X indicates conditions where no significant events were recorded due to cell death resulting from PEI toxicity. (D) Screen to identify optimal DNA amount/cell and PEI/DNA for lentivirus production at 2×10^7 cells mL^{-1} . Both p24 concentration in pg/mL (gray bars) and infectivity in TU mL^{-1} (black bars) were measured. (E) Screen to identify optimal plasmid ratio (pRSVRev:pMDL:pLVEGFP:pMD2g) for lentivirus production at 2×10^7 cells mL^{-1} . The conditions tested are shown below the figures. The error bars represent standard deviation across three replicates

PEI:DNA complex increased the chances of a cell taking up the complex, becoming transfected to express GFP, and this led to higher measured transfection efficiency. At high PEI/DNA ratios (Figure 2C), increasing the amount of DNA per cell reduced the transfection efficiency, possibly due to cytotoxicity associated with excess PEI. Cytotoxicity was most evident at higher cell densities when no transfection events were recorded (marked by X in Figure 2) corresponding to very high concentrations of PEI. In addition, at a specific DNA concentration and cell density, an increase in the PEI/DNA ratio from

2:1 to 5:1 increased the transfection efficiency with up to 3.5 pg DNA/cell.

Increased PEI:DNA ratio is known to increase the N/P ratio (the moles of amine groups in PEI to moles of phosphate groups in DNA) in a transfection complex.^[39] The increase in transfection efficiency up to 3.5 pg DNA/cell is consistent with a higher N/P ratio causing higher transfection efficiency.^[40] Above 3.5 pg DNA/cell, cytotoxicity impacted transfection efficiency. However, for an intermediate PEI/DNA ratio of 3.5:1 (Figure 2B), there was a range of DNA

concentrations between 0.5 and 3.5 pg/cell where transfection efficiency was optimal. This indicates that a combination of specific DNA content, N/P ratio, and reduced cytotoxicity, results in optimal transfection efficiency. For low cell density transfections, a PEI/DNA ratio of 3.5:1 is optimal with 0.5 to 3.5 pg DNA/cell, while at high cell densities, higher transfection efficiencies occurred with lower DNA amounts at all PEI/DNA ratios as a result of lower concentration of PEI and lower cytotoxicity.

3.5 | Identification of optimal 4-plasmid ratio

A second screen was performed with four plasmids at a ratio of 6:4:6:1 (pRSVRev:pMDL:pLVEGFP:pMD2g) in 96-deep well plates to identify optimal DNA/cell and PEI/DNA ratios using HEK293 suspension cells at 2×10^7 cells mL^{-1} . Final LVV concentration was determined using the infectivity assay in HT1080 cells (via high content imaging) and p24 sandwich ELISA (Figure 2D). Infectivity is a more accurate measure of LVV concentration than p24 sandwich ELISA, since it relates directly to functional LVV concentration. The concentration of p24 protein, however, does not necessarily correlate to the concentration of infective particles. This can be seen best at Condition 3 where despite exhibiting one of the highest p24 concentrations (~ 1500 pg/cell), infectivity was nearly two-thirds lower than in Condition 2. This may be due to the presence of free p24 as well as p24 associated with non-functional viral vector. Hence, our screening assays were primarily focused on functional viral vector concentration. Based on the results depicted in Figure 2D, the highest functional LVV concentrations were observed with Conditions - 2 and 7, corresponding to 0.5 pg DNA/cell, 2:1 PEI/DNA and 0.2 pg DNA/cell, 3:5:1 PEI/DNA, respectively. For all conditions tested, higher functional LVV concentration was obtained at the 2:1 PEI/DNA ratio. However, as the PEI content is increased, the amount of DNA that is needed can be reduced. This is seen with Condition 7, where it was possible to reduce the ratio of DNA/cell while maintaining the higher PEI/DNA ratio. This is likely due to the presence of more PEI/DNA complexes allowing for more efficient transfection. Nonetheless, the two top conditions still generated only $\sim 2\text{--}3 \times 10^5$ TU mL^{-1} . Hence we proceeded to evaluate the effect of changing the ratio of the four plasmids for LVV production.

To this end, HEK293 suspension cells at a cell density of 2×10^7 cells mL^{-1} were transfected in 96-deep well plates with all four plasmids. Fifteen conditions were tested (Figure 2E). Based on the previous screen (Condition 7), the total DNA amount was fixed at 0.2 pg/cell and a PEI/DNA ratio of 3.5:1 was used. The resulting concentration of LVV particles was measured using both infectivity (via high content imaging) and p24 sandwich ELISA. Condition L exhibited the highest concentration of viral particles at 6.7×10^5 TU mL^{-1} . However, rather surprisingly, there was only an approx. two-fold increase from lowest functional titer (Condition A) to highest (Condition L). Moreover, comparison of Condition B, which is identical in the 4-plasmid ratio to that used for lower cell densities (10^6 cells mL^{-1} ; Table 1), the functional LVV concentration increased only 3.6-fold, yet there was

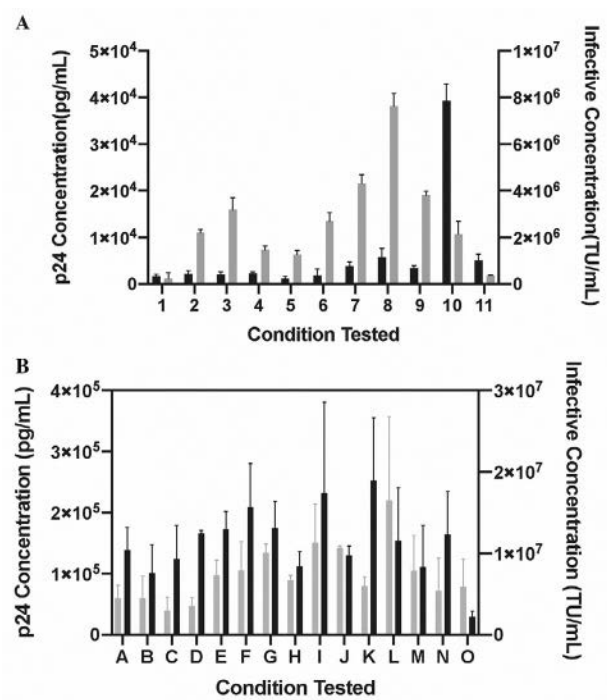


FIGURE 3 Lentivirus vector production optimization in LV-Max Cells. Both p24 concentration in pg/mL (gray bars) and infectivity in TU mL^{-1} (black bars) were measured. (A) Screen to identify optimal DNA amount/cell and PEI/DNA for lentivirus production at 2×10^7 cells mL^{-1} . (B) Screen to identify optimal plasmid ratio (pRSVRev:pMDL:pLVEGFP:pMD2g) for lentivirus production at 2×10^7 cells mL^{-1} . The conditions tested are shown in Figure 2D,E. The error bars represent standard deviation across three replicates

a 20-fold increase in cell density. This drop in specific productivity at high cell density could be due to the chosen cell clone.

3.6 | Evaluation of commercially available LV-Max cell line

To establish generality and to increase LVV concentrations, we transitioned to the LV-Max cell line. The same two screens were performed as with the HEK293 suspension cells. The harvest supernatant was collected at 48 h and used to measure the functional LVV concentration with both infectivity (high content imaging) and p24 sandwich ELISA assays (Figure 3A). Unlike with HEK293 suspension cells, there was a clear peak at 1.9 pg DNA/cell and PEI/DNA of 3.5:1 where the functional LVV concentration was maximized. In addition, there was a significant increase in the yield of the LVV particles from $\sim 10^5$ TU mL^{-1} to $\sim 8 \times 10^6$ TU mL^{-1} (Figure 3A). Therefore, we used Condition 10 (1.9 pg/cell at PEI/DNA of 3.5:1) in the 4-plasmid, 15-Condition screen with LV-Max cells (Figure 3B). By modifying the concentration of plasmids during transfection, functional yields reached approx. 2×10^7 TU mL^{-1} (Condition K). Clearly, the cell clone used for viral vector production significantly impacted LVV productivity.

As a final validation step, we scaled up LV-Max Condition K for use in 125 mL shake flasks to confirm whether similar scalability from 96-deep well plates as observed with the HEK 293 suspension cells would translate to LV-Max cells. The LV-Max cells were transfected with all four plasmids at a ratio of 3.5:2.5:6:1 (pRSVRev:PMDL:pLVEGFP:pMD2g) and the harvest supernatant was collected 48 h post-transfection. The LVV concentration was then measured using both the infectivity and p24 assays. Infectivity values across all three replicates in shake flasks were similar to the values in 96-deep well plates (Table S3). Therefore, the 96-deep well plate platform could serve as a useful tool to screen conditions for production of LVVs at high cell density.

4 | DISCUSSION

Both gene therapy and CAR-T applications are emerging tools to help treat several degenerative diseases and cancer, and both rely on efficient and targeted delivery of therapeutic genes to cells of interest. LVVs are a promising delivery vehicle due to their large tropism and their ability to cause genomic integration of a gene of interest. However, low viral amounts and lack of scalability have largely prevented their more widespread use for gene therapy and CAR-T applications. Several factors can be addressed further during the manufacturing process to improve the yield and scalability of LVVs. These include culture format of host cells (e.g., suspension vs. adherent), medium for cell growth and transfection, transfection reagent, and quantity and number of plasmids. However, a major bottleneck remains a lack of throughput to test these myriad conditions. To address this challenge, we developed a screening platform using conventional square-walled 96-deep well plates that enable high cell density using commercially available media. This platform can be used to screen a wide range of conditions without the need for large amounts of reagents and plasmids.

BalanCD supported high density cell growth in shake flasks and in 96-deep well plates with cells reaching a maximum density of up to 4×10^7 cells mL⁻¹ in both formats with comparable growth rates and transfection efficiencies with a single *Egfp* gene-containing plasmid. While our transfection experiments were focused primarily on using PEI-Max due to its scalability, similar transfection experiments can be performed with other reagents. Furthermore, novel transfection reagents can be tested with relative ease over a wide range of densities without consuming large reagent amounts. To this end, we performed two proof-of-concept screening studies to highlight the range of conditions that can be evaluated with the 96-deep well plate platform for suspension adapted cells. The first screen identified optimal DNA amount/cell and PEI/DNA ratio, while the second screen identified the optimal four-plasmid ratio. A schematic of how these two screens were used to guide LVV production in scale-up systems is shown in Figure S5.

Three methods are commonly used to measure LVV concentration obtained in the harvest supernatant—p24 sandwich ELISA, RT-qPCR and infectivity assays.^[41] Of the three, the infectivity assay allows for direct quantification of functional viral particles.^[42] In the presence of a fluorescent transfer plasmid (i.e., pLV EGFP), the percentage of cells

that are transduced by the LVV (carrying the EGFP construct) can be measured using flow cytometry. Since LVVs are often introduced to target cells at different dilutions, the starting viral concentration can be determined by using Equation (1). Both p24 sandwich ELISA and RT-qPCR, however, are metrics of physical viral vector concentration and often overestimate the number of viral particles.^[43] On the other hand, infectivity assays are a more useful metric as they allow for the measurement of truly functional particles. Hence, vector copy number measurements are also used, wherein transduced cells are maintained in culture long-term and the percentage of cells that have integrated a copy of the target gene can be measured using PCR. In future work, a longer-term infectivity study would be beneficial to demonstrate the influence of LVV production conditions on the infective properties of the LVVs. Nonetheless, for the current study, we focused only on a short-term fluorescent reporter-based infectivity assay, since we were primarily interested in performing a rapid screen to identify an optimal condition for LVV production from a library of conditions. We were able to show that the same LVV productivity was obtained in shake flasks and 1-L bioreactor after short-term culture. A long-term stable transduction experiment should reveal similar trends, since both 96-deep well plates and shake flasks, as well as bioreactors, start with the same concentration of LVV in the harvest.

The relatively low infective concentration obtained with the HEK293 suspension cell line is clearly a function of the cell clone used. This was demonstrated by transitioning to an LV-Max cell line, which increased functional LVV concentrations nearly 100-fold. Importantly, in both cell lines, the ratios of DNA/cell and PEI/DNA dominate over the ratios of the four plasmids. The approach taken in the current study supports the ability of a simple, microscale 96-deep well plate platform to predict scale-up to shake flask scale and possibly increased bioreactor scales.

In summary, the methodology developed herein may help guide LVV and other viral vector manufacturing in bioreactor scale-up models that can then be used for different therapeutic applications. Importantly, the high cell densities and high oxygen transfer rates in microwell systems mimic conditions in larger-scale bioreactors. This will accelerate bioprocess optimization of viral vector production for therapeutic applications. Moreover, even smaller systems may be envisioned, including microarrays that can mimic high oxygen transfer due to very small diffusion path lengths.^[44] As a result, very high-throughput optimization of LVV production, as well as other viral vectors produced in HEK293 or other cell lines, may be envisioned.

ACKNOWLEDGMENTS

This work was performed under a Project Award Agreement from the National Institute for Innovation in Manufacturing Biopharmaceuticals (NIIMBL) and financial assistance award 70NANB17H002 from the U.S. Department of Commerce, National Institute of Standards and Technology. The authors acknowledge the collaboration with Michael Betenbaugh and Pranay Ladiwala (Johns Hopkins University).

CONFLICT OF INTEREST

The authors declare no conflict of interest.

AUTHOR CONTRIBUTIONS

Sneha Gopal: formal analysis; investigation; methodology; writing-original draft; writing-review & editing. Lindsay Hock: resources. Jill Zemianek: resources. Kun Fang: resources. Gretchen Gee: resources. Ronit Ghosh: methodology; resources. David McNally: funding acquisition; project administration. Adam Osborne: resources. Steven Cramer: funding acquisition; project administration. Jonathan Dordick: writing-review & editing; funding acquisition; project administration.

DATA AVAILABILITY STATEMENT

The data that support the findings of this study are available from the corresponding author upon reasonable request.

ORCID

Jonathan S. Dordick  <https://orcid.org/0000-0001-7802-3702>

REFERENCES

- Kalos, M., Levine, B. L., Porter, D. L., Katz, S., Grupp, S. A., Bagg, A., & June, C. H. (2011). T Cells with chimeric antigen receptors have potent antitumor effects and can establish memory in patients with advanced leukemia. *Science Translational Medicine*, 3, 95ra73.
- Nobles, C. L., Sherrill-Mix, S., Everett, J. K., Reddy, S., Fraietta, J. A., Porter, D. L., Frey, N., Gill, S. I., Grupp, S. A., Maude, S. L., Siegel, D. L., Levine, B. L., June, C. H., Lacey, S. F., Melenhorst, J. J., & Bushman, F. D. (2020). *Journal of Clinical Investigation*, CD19-targeting CAR T cell immunotherapy outcomes correlate with genomic modification by vector integration. 130, 673.
- Goswami, R., Subramanian, G., Silayeva, L., Newkirk, I., Doctor, D., Chawla, K., Chattopadhyay, S., Chandra, D., Chilukuri, N., & Betapudi, V. (2019). *Frontiers in Oncology*, 9.
- Gonçalves, G. A. R., & de Paiva, M. A. R. (2017). Gene therapy: advances, challenges and perspectives. *Einstein*, 15, 369.
- van der Loo, J. C. M., & Wright, J. F. (2016). Progress and challenges in viral vector manufacturing. *Human Molecular Genetics*, 25(R1), R42–R52.
- Cao, H., Ouyang, H., Grasmann, H., Bartlett, C., Du, K., Duan, R., Shi, F., Estrada, M., Seigel, K. E., Coates, A. L., Yeager, H., Bear, C. E., Gonska, T., Moraes, T. J., & Hu, J. (2018). Transducing airway basal cells with a helper-dependent adenoviral vector for lung gene therapy. *Human Gene Therapy*, 29, 643–652.
- Matkar, P. N., Leong-Poi, H., & Singh, K. K. (2016). Cardiac gene therapy: are we there yet? *Gene Therapy*, 23, 635–648.
- Parr-Brownlie, L. C., Bosch-Bouju, C., Schoderboeck, L., Sizemore, R. J., Abraham, W. C., & Hughes, S. M. (2015). Lentiviral vectors as tools to understand central nervous system biology in mammalian model organisms. *Frontiers in Molecular Neuroscience*, 8, 14.
- Naldini, L., Trono, D., & Verma, I. M. (2016). Lentiviral vectors, two decades later. *Science*, 353, 1101–1102.
- Harms, A. S., Barnum, C. J., Ruhn, K. A., Varghese, S., Treviño, I., Blesch, A., & Tansey, M. G. (2011). Delayed dominant-negative TNF gene therapy halts progressive loss of nigral dopaminergic neurons in a rat model of Parkinson's disease. *Molecular Therapy*, 19, 46–52.
- Marquez Loza, L. I., Yuen, E. C., & McCray, P. B. (2019). Lentiviral vectors for the treatment and prevention of cystic fibrosis lung disease. *Genes*, 10, 218.
- Picanço-Castro, V., Moço, P. D., Mizukami, A., Vaz, L. D., de Souza Fernandes Pereira, M., Silvestre, R. N., de Azevedo, J. T. C., de Sousa Bomfim, A., de Abreu Neto, M. S., Malmegrim, K. C. R., Swiech, K., & Covas, D. T. (2020). Establishment of a simple and efficient platform for cart cell generation and expansion: From lentiviral production to in vivo studies. *Hematology, Transfusion and Cell Therapy*, 42(2), 150–158.
- Schlingens, R., Howard, J., Wooley, D., Thompson, M., Baden, L. R., Yang, O. O., Christiani, D. C., Mostoslavsky, G., Diamond, D. V., Duane, E. G., Byers, K., Winters, T., Gelfand, J. A., Fujimoto, G., Hudson, T. W., & Vyas, J. M. (2016). Risks associated with lentiviral vector exposures and prevention strategies. *Journal of Occupational and Environmental Medicine*, 58, 1159–1166.
- Ranzani, M., Cesana, D., Bartholomae, C. C., Sanvito, F., Pala, M., Benedicenti, F., Gallina, P., Sergi, L. S., Merella, S., Bulfone, A., Doglioni, C., von Kalle, C., Kim, Y. J., Schmidt, M., Tonon, G., Naldini, L., & Montini, E. (2013). Lentiviral vector-based insertional mutagenesis identifies genes associated with liver cancer. *Nature Methods*, 10, 155–161.
- Park, J., Inwood, S., SKruthiventi, J. J., Shiloach, J., & Betenbaugh, M. (2018). Progressing from transient to stable packaging cell lines for continuous production of lentiviral and gammaretroviral vectors. *Current Opinion in Chemical Engineering*, 22, 128–137.
- Do Minh, A., Tran, M. Y., & Kamen, A. A. (2020). *Chimeric antigen receptor T cells: Development and production*, New York City, NY: Springer.
- McCarron, A., Donnelley, M., McIntyre, C., & Parsons, D. (2016). Challenges of up-scaling lentivirus production and processing. *Journal of Biotechnology*, 240, 23–30.
- Kennedy, A., & Cribbs, A. P. (2016). *Lentiviral vectors and exosomes as gene and protein delivery tools*, New York City, NY: Springer.
- Rout-Pitt, N., McCarron, A., McIntyre, C., Parsons, D., & Donnelley, M. (2018). *Journal of Biological Methods*, 5, e90.
- Bos, A. B., Luan, P., Duque, J. N., Reilly, D., Harms, P. D., & Wong, A. W. (2015). Optimization and automation of an end-to-end high throughput microscale transient protein production process. *Biotechnology and Bioengineering*, 112, 1832–1842.
- Davies, A., Greene, A., Lullau, E., & Abbott, W. M. (2005) Optimisation and evaluation of a high-throughput mammalian protein expression system. *Protein Expression and Purification*, 42, 111–121.
- Vink, T., Oudshoorn-Dickmann, M., Roza, M., Reitsma, J. J., & de Jong, R. N. (2014). A simple, robust and highly efficient transient expression system for producing antibodies. *Methods*, 65, 5–10.
- Schlaeger, E.-J., & Christensen, K. (1999). Transient gene expression in mammalian cells grown in serum-free suspension culture. *Cytotechnology*, 30, 71–83.
- Raymond, C., Tom, R., Perret, S., Moussouami, P., L'Abbé, D., St-Laurent, G., & Durocher, Y. (2011). A simplified polyethylenimine-mediated transfection process for large-scale and high-throughput applications. *Methods*, 55, 44–51.
- Merten, O.-W., Hebben, M., & Bovolenta, C. (2016) Production of lentiviral vectors. *Molecular Therapy-Methods & Clinical Development*, 3, 16017.
- Delafosse, L., Xu, P., & Durocher, Y. (2016). Comparative study of polyethylenimines for transient gene expression in mammalian HEK293 and CHO cells. *Journal of Biotechnology*, 227, 103–111.
- Longo, P. A., Kavran, J. M., Kim, M.-S., & Leahy, D. J. (2013). Transient mammalian cell transfection with polyethylenimine (PEI). *Methods in enzymology*, 529, 227–240.
- Masotti, A., Mossa, G., Cametti, C., Ortaggi, G., Bianco, A., Grosso, N. D., Malizia, D., & Esposito, C. (2009). Comparison of different commercially available cationic liposome-DNA lipoplexes: Parameters influencing toxicity and transfection efficiency. *Colloids and Surfaces B: Biointerfaces*, 68, 136–144.
- Zhu, L., & Mahato, R. I. (2010). Lipid and polymeric carrier-mediated nucleic acid delivery. *Expert Opinion on Drug Delivery*, 7, 1209–1226.
- Vallée, C., Durocher, Y., & Henry, O. (2014). Exploiting the metabolism of PYC expressing HEK293 cells in fed-batch cultures. *Journal of Biotechnology*, 169, 63–70.
- Song, M., Raphaelli, K., Jones, M. L., Aliabadi-Zadeh, K., Leung, K. M., Crowley, D., Hughes, B., Mahler, S., Gray, P. P., Huang, E. P., & Chin, D. Y. (2011). Clonal selection of high producing, stably transfected HEK293 cell lines utilizing modified, high-throughput FACS screening. *Journal of Chemical Technology and Biotechnology*, 86, 935–941.

32. Wagner, B. A., Venkataraman, S., & Buettner, G. R. (2011). *Biology and Medicine*, 51, 700–712.
33. Micheletti, M., Barrett, T., Doig, S. D., Baganz, F., Levy, M. S., Woodley, J. M., & Lye, G. J. (2006). Fluid mixing in shaken bioreactors: Implications for scale-up predictions from microlitre-scale microbial and mammalian cell cultures. *Chemical Engineering Science*, 61, 2939–2949.
34. Place, T. L., Domann, F. E., & Case, A. J. (2017). Limitations of oxygen delivery to cells in culture: An underappreciated problem in basic and translational research. *Free Radical Biology and Medicine*, 113, 311–322.
35. Hermann, R., Lehmann, M., & Büchs, J. (2003). Characterization of gas-liquid mass transfer phenomena in microtiter plates. *Biotechnology and Bioengineering*, 81, 178–186.
36. Dietmair, S., Hodson, M. P., Quek, L.-E., Timmins, N. E., Gray, P., & Nielsen, L. K. (2012). A multi-omics analysis of recombinant protein production in Hek293 cells. *Plos One*, 7, e43394.
37. Hu, S., Li, M., & Akkina, R. (2019). *Viral vectors for gene therapy: Methods and protocols*, New York City, NY: Springer, 125–134.
38. Qiao, J., Moreno, J., Sanchez-Perez, L., Kottke, T., Thompson, J., Caruso, M., Diaz, R. M., & Vile, R. (2006). VSV-G pseudotyped, MuLV-based, semi-replication-competent retrovirus for cancer treatment. *Gene Therapy*, 13, 1457–1470.
39. Zhao, Q.-Q., Chen, J.-L., Lv, T.-F., He, C.-X., Tang, G.-P., Liang, W.-Q., Tabata, Y., & Gao, J.-Q., (2009) N/P ratio significantly influences the transfection efficiency and cytotoxicity of a polyethyleneimine/chitosan/DNA complex. *Biological & Pharmaceutical Bulletin*, 32, 706–710.
40. Intra, J., & Salem, A. K. (2008). Characterization of the transgene expression generated by branched and linear polyethyleneimine-plasmid DNA nanoparticles in vitro and after intraperitoneal injection in vivo. *Journal of Controlled Release*, 130, 129–138.
41. Lizée, G., Aerts, J. L., Gonzales, M. I., Chinnasamy, N., Morgan, R. A., & Topalian, S. L. (2003). Real-time quantitative reverse transcriptase-polymerase chain reaction as a method for determining lentiviral vector titers and measuring transgene expression. *Human Gene Therapy*, 14, 497–507.
42. Geraerts, M., Willems, S., Baekelandt, V., Debyser, Z., & Gijsbers, R. (2006). *BMC Biotechnology [Electronic Resource]*, 6, 34.
43. Barczak, W., Suchorska, W., Rubiś, B., & Kulcenty, K. (2015). Universal real-time PCR-based assay for lentiviral titration. *Molecular Biotechnology*, 57, 195–200.
44. Meli, L., Barbosa, H. S. C., Hickey, A. M., Gasimli, L., Nierode, G., Diogo, M. M., Linhardt, R. J., Cabral, J. M. S., & Dordick, J. S. (2014). Three dimensional cellular microarray platform for human neural stem cell differentiation and toxicology. *Stem Cell Research*, 13, 36–47.

SUPPORTING INFORMATION

Additional supporting information may be found online in the Supporting Information section at the end of the article.

How to cite this article: Gopal, S., Osborne, A. E., Hock, L., Zemianek, J., Fang, K., Gee, G., Ghosh, R. McNally, D., Cramer, S. M., & Dordick, J. S. (2021). Advancing a rapid, high throughput screening platform for optimization of lentivirus production. *Biotechnol. J.*, 16, e2000621.
<https://doi.org/10.1002/biot.202000621>

Production, Processing, and Characterization of Synthetic AAV Gene Therapy Vectors

Jihad El Andari and Dirk Grimm*

Over the last two decades, gene therapy vectors based on wild-type Adeno-associated viruses (AAV) are safe and efficacious in numerous clinical trials and are translated into three approved gene therapy products. Concomitantly, a large body of preclinical work has illustrated the power and potential of engineered synthetic AAV capsids that often excel in terms of an organ or cell specificity, the efficiency of in vitro or in vivo gene transfer, and/or reactivity with anti-AAV immune responses. In turn, this has created a demand for new, scalable, easy-to-implement, and plug-and-play platform processes that are compatible with the rapidly increasing range of AAV capsid variants. Here, the focus is on recent advances in methodologies for downstream processing and characterization of natural or synthetic AAV vectors, comprising different chromatography techniques and thermostability measurements. To illustrate the breadth of this portfolio, two chimeric capsids are used as representative examples that are derived through forward- or backwards-directed molecular evolution, namely, AAV-DJ and Anc80. Collectively, this ever-expanding arsenal of technologies promises to facilitate the development of the next AAV vector generation derived from synthetic capsids and to accelerate their manufacturing, and to thus boost the field of human gene therapy.

1. Introduction


Since the dawn of the era of human gene therapy research in the 1970s, hardly any vehicle for therapeutic gene transfer has attracted more attention than the Adeno-associated virus (AAV). As a non-pathogenic member of the *Parvoviridae* family, AAV is composed of a single-stranded DNA genome encapsidated in a 23–28 nm, $T = 1$, non-enveloped capsid. Arguably, the greatest and perhaps also a unique asset of AAV is its extreme amenability to genetic engineering and repurposing of the viral genome and capsid. This flexibility enables not only the construction of recombinant vectors encoding an assortment of therapeutic cargos, but it also facilitates the rational design or molecular evolution of novel capsids with enhanced organ or cell specificity, transduction efficiency and/or lower reactivity with anti-AAV immunity.^[1–3] To this end, a vast collection of technologies for capsid engineering have been invented and applied over the years, ranging from site-directed mutagenesis of individual amino

acids in the capsid, or insertion of retargeting peptides or larger moieties, to the creation of chimeric capsids composed of multiple parental subunits derived from natural viruses or designed in silico.

As these techniques have been reviewed extensively by others and us before,^[2–7] and as a more detailed discussion is outside our current scope, we will merely highlight two specific strategies and prototypes of synthetic AAV capsids that assume an exemplary role in this article. The first strategy harnesses the principle of DNA family shuffling to create chimeric AAV capsids that are built from blocks derived from a set of two or more input viruses with different properties. Therefore, the parental *cap(sid)* genes of ≈ 2.2 kilobases (kb) are first fragmented into ≈ 100 to 800-base pair (bp) long pieces using a controlled DNaseI digest. Next, these are forced to recombine in a primer-less PCR reaction, in which the individual fragments self-prime enabled by the typically greater than 70% DNA homology of most AAV isolates. A subsequent second PCR is then used to amplify the pool of chimeric *cap* genes for subcloning into a replication- and packaging-competent AAV plasmid. The latter also contains the AAV *rep* gene and inverted terminal repeats (ITRs), which are required for encapsidation of the chimeric sequences. The ensuing plasmid library of usually more than a million different capsid variants is used to produce a corresponding viral library, which

Dr. J. El Andari, Prof. D. Grimm
Dept. of Infectious Diseases/Virology
Medical Faculty
University of Heidelberg
69120 Heidelberg, Germany
E-mail: dirk.grimm@bioquant.uni-heidelberg.de

Dr. J. El Andari, Prof. D. Grimm
BioQuant
Cluster of Excellence CellNetworks
University of Heidelberg
69120 Heidelberg, Germany
Prof. D. Grimm
German Center for Infection Research (DZIF) and German Center for Cardiovascular Research (DZHK)
partner site Heidelberg
69120 Heidelberg, Germany

 The ORCID identification number(s) for the author(s) of this article can be found under <https://doi.org/10.1002/biot.202000025>

© 2020 The Authors. *Biotechnology Journal* published by Wiley-VCH GmbH. This is an open access article under the terms of the Creative Commons Attribution License, which permits use, distribution and reproduction in any medium, provided the original work is properly cited.

DOI: 10.1002/biot.202000025

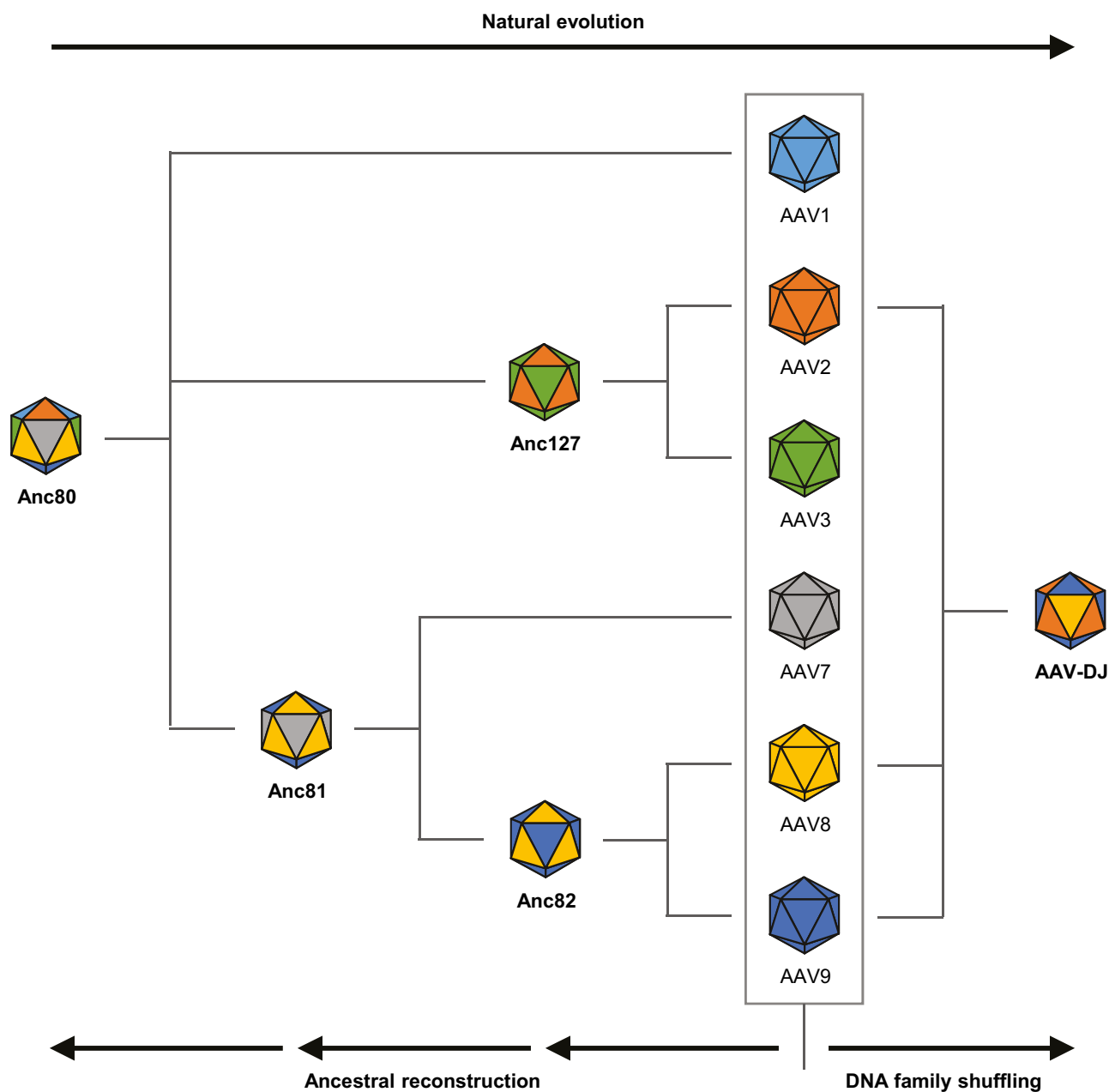


Figure 1. Evolution of synthetic AAV capsids AAV-DJ (right) and Anc (left). Shown in the box are the six AAV wild-types that form the basis for all synthetic capsids depicted in this figure and discussed in the text. AAV-DJ was derived by DNA family shuffling of AAV serotypes 2, 8, and 9, that is, through forward-directed molecular evolution. The Anc family (Anc80-82, 127) was in silico designed using ancestral reconstruction, that is, through backwards-directed molecular evolution starting with all shown six wild-types. Note that this is not a genuine phylogenetic tree and that evolutionary relationships have been simplified. The actual phylogeny is depicted in the original work by Zinn et al.^[20]

is finally interrogated in cultured cells or animal tissues *in vivo* through two to five iterative cycles of infection, the rescue of *cap* sequences from the on-target cells, re-cloning, and production of a secondary library for the next round.

In the 2008 study from the Kay lab that pioneered the use of this technique for AAV capsid evolution^[8] and that was quickly succeeded by similar work from the Samulski^[9] and Schaffer^[10] labs, a chimeric AAV capsid called AAV-DJ was molecularly evolved in cultured human liver cells in the presence of

neutralizing anti-AAV antibodies. From the eight distinct AAV serotypes that formed the initial capsid library, five were eliminated during the iterative selection, leaving fragments of AAV2, 8, and 9 that had recombined to yield AAV-DJ (Figure 1, right). As shown in this work and many follow-up studies,^[11–13] AAV-DJ mediates highly efficient and specific gene transfer to the mouse liver following peripheral administration, as initially hoped for. Interestingly, it also turned out to be an excellent candidate for gene transfer into other cell types *in vitro* and *in vivo*, explaining

why AAV-DJ has been widely used to date for numerous applications and in various models of human gene therapy.^[11,14–17] Moreover, its structure was resolved by cryo-electron microscopy at 4.5 Å resolution,^[18] or, more recently, even at 2.8 Å resolution in complex with a heparan sulfate analog.^[19] Because of its interesting properties, its broad use and the advanced knowledge of its structure and biology, we will use AAV-DJ as the prototype of a synthetic AAV capsid in this article that was created by forward-directed molecular evolution.

Complementing this strategy is another powerful and original technology that was pioneered by Luk Vandenberghe and his team in 2015 and that is called "ancestral reconstruction".^[20] As the name implies, in contrast to AAV DNA family shuffling, this methodology goes back in natural evolution by computationally predicting and then experimentally recreating ancestors of contemporary AAV capsids that may or may not have existed, but when developed as vectors can display unique and interesting properties. The best-known example in the field is Anc80L65, which is a specific variant of a node called Anc80 that represents the ancestor of a variety of present AAV serotypes including AAV1, 2, 8, and 9 (Figure 1, left). Akin to AAV-DJ, Anc80L65 also excels in many clinically relevant cells and tissues in comparison to widely used other capsids such as AAV8, comprising the liver of mice and monkeys, or hair cells in the murine cochlea.^[5,20–23] Thus, for the same rationale that applies to AAV-DJ, Anc80L65 and some of its closely related siblings that were also derived by backwards-directed molecular evolution will be used as a second class of prototypes of synthetic AAV capsids in the following.

Notably, while these capsids were evolved with two opposed technologies, they can be produced as recombinant gene therapy vectors using the identical protocol. This is due to one of the many strengths of the AAV vector system, which is the fact that the only component that requires adaptation for the production of a new viral capsid variant is the *cap* gene itself. In contrast, all other pivotal factors such as the AAV *rep* gene (typically derived from AAV2) as well as adenoviral helper functions remain unchanged. Consequently, irrespective of the origin—natural or synthetic—of a new capsid type, of its sequence and structure, and of the technology that was employed for its creation, the protocol for AAV vector production only requires a marginal amendment in the form of the cloning of the desired *cap* gene into the AAV helper construct.^[24] This is strikingly different, however, for all subsequent steps in the protocol that follow downstream of the initial vector production scheme, that is, viral particle purification and characterization. One reason is that a significant proportion of the respective technologies that have been developed and reported over the last decades were specifically designed for a subset of AAV isolates. This includes purification methods that are based on virus affinity for a given receptor, such as AAV2 purification via heparin affinity chromatography^[25] or protocols for AAV particle characterization that harness serotype-specific monoclonal antibodies, such as capsid ELISAs for selected serotypes.^[26,27] Moreover, the often limited understanding of the biology of new capsids and their biophysical properties hampers the rational selection of a suited protocol for purification and/or characterization from the arsenal of conventional strategies, thus requiring trial-and-error or necessitating the establishment of the novel, capsid-tailored methodologies.

Here, we will use the aforementioned AAV-DJ and Anc family as representative examples to illustrate the flurry of recent activities that aim to expand our options for downstream processing and characterization of synthetic AAV capsid variants, while remaining compatible with (pre-) clinical demands including high yield, purity, quality, and consistency. Thereby, this article intends to complement a collection of excellent previous reviews by our colleagues who have comprehensively discussed more traditional technologies for AAV manufacturing. In particular, for further reading, we recommend the overview articles by Ayuso, Mingozzi, and Bosch,^[28] Clement and Grieger,^[29] or Aponte-Ubillus et al.,^[30] among others.^[31–33] Also, we will start by briefly highlighting interesting recent progress in the upscaling of the upstream AAV production process as it goes hand in hand with downstream optimization. Finally, we will exemplify other technological advances that are related to the progress in AAV downstream processing, comprising latest improvements in AAV characterization through mass spectrometry or thermostability measurement, or in detection and removal of contaminants. An overview of the different methodologies discussed in this article including a selection of pros and cons and representative examples from the literature is given in Table 1.

2. Manufacturing of Synthetic AAV Vectors

As noted above, AAV production can easily be adapted to newly discovered wild-type isolates or synthetically engineered capsids, by simply replacing the *cap* gene in the preferred AAV helper construct. This is particularly straightforward in the case of protocols based on transient plasmid transfection,^[34] in which *cap* is encoded on an AAV helper plasmid and typically co-transfected with the AAV vector and another plasmid providing all adenoviral helper functions; the latter can also be combined with the AAV *rep* and *cap* genes on a single construct.^[24,35–37] It is more labor- and time-intensive in the case of stable AAV producer cell lines or scalable systems based on heterologous viruses such as baculoviruses,^[38] yet the overall principle remains identical. Nonetheless, we note that, to our best knowledge, these alternative systems remain to be harnessed for the production of synthetic AAV capsids. In particular, in the case of the baculovirus system, this may then require additional optimization of the AAV expression cassettes including promoters to maintain a correct stoichiometry and splicing of all capsid mRNAs and proteins as well as other biological AAV properties.^[28,39]

Of note, stable lines or helpervirus infection are not the only means of up-scaling AAV production; instead, numerous groups have succeeded at adapting HEK293 cells (a human embryonic kidney cell line that is typically used for AAV manufacturing) to growth in suspension. One example has recently been provided by Blessing and colleagues who cultured an adapted HEK293 suspension cell clone called HEKExpress under serum-free conditions in orbitally shaken bioreactors (OSRs). The latter combine efficient gas transfer with high cell viability and can be scaled up to 1000 liters.^[40,41] Using transient transfection with polyethylenimine (PEI) and POROS CaptureSelect resins for AAV purification via immunoaffinity chromatography, the authors managed to achieve AAV8 and AAV9 production with a significant recovery (>35%).^[40] While not demonstrated in the original report,

Table 1. Methodologies for production, purification, and characterization of synthetic AAV capsids.

Step	Technology	Pros	Cons	AAV-DJ	Anc
Production	Transient plasmid DNA transfection	<ul style="list-style-type: none"> easy and cheap to adapt to new AAVs possible in each lab high particle yields 	<ul style="list-style-type: none"> difficult to scale up vast plasmid DNA amounts needed for larger vector batches 	8	20
	Stable cell lines	<ul style="list-style-type: none"> reproducible scalable up to clinical manufacturing 	<ul style="list-style-type: none"> hard to customize potential cellular instability over time may require helper virus 	Not yet reported	Not yet reported
	Helper viruses	<ul style="list-style-type: none"> scalable (especially with baculoviruses and suspension insect cells) high particle yields 	<ul style="list-style-type: none"> contaminating virus instability of helper virus biological AAV properties may be altered 	Not yet reported	Not yet reported
Purification	Crude lysates	<ul style="list-style-type: none"> quick, cheap and easy to generate compatible with any AAV capsid variant 	<ul style="list-style-type: none"> various contaminants stocks usually not titrated unclear ratios of full:empty capsids 	103	20
	CsCl (cesium chloride) density gradients	<ul style="list-style-type: none"> good separation of full:empty capsids high purity versatile 	<ul style="list-style-type: none"> cumbersome hard to scale up open system prone to contaminations time-consuming toxicity 	8	Not yet reported
	Iodixanol density gradients	<ul style="list-style-type: none"> versatile decent purity enrichment of full capsids less toxic than CsCl 	<ul style="list-style-type: none"> difficult to scale up open system prone to contaminations time-consuming 	11	84
	IEC (ion-exchange chromatography)	<ul style="list-style-type: none"> ability to separate full and empty capsids in large scale easily scalable versatile 	different physicochemical AAV properties require adaptation	80	Not yet reported
	IAC (immunoaffinity chromatography)	<ul style="list-style-type: none"> very specific easily scalable high yields and purity 	<ul style="list-style-type: none"> serotype-selective (lesser concern with AAVX) antibody leaching no removal of empty capsids 	13	84
Characterization	MS	<ul style="list-style-type: none"> enables detection of post-translational capsid modifications useful for lot-to-lot control can distinguish AAV serotypes and genomes 	<ul style="list-style-type: none"> requires special, expensive equipment as well as experience often demands large sample volumes yields no data on capsid structure 	Not yet reported	Not yet reported
	Thermostability	<ul style="list-style-type: none"> simple, cheap, robust and fast can distinguish serotypes independent of specific instrumentation 	<ul style="list-style-type: none"> not all serotypes can be segregated sensitive to changes in buffer and pH 	Not yet reported	20

Note that this table merely summarizes the subset of technologies that are discussed in this article and that only one representative example (numbers are literature references) is always listed for the use of these techniques in the context of AAV-DJ and/or Anc capsids. For more comprehensive overviews of these and other methodologies including additional pros and cons, we refer the reader to excellent previous reviews and original articles as referenced in the text. The numbers indicated are related to the corresponding references.

this scalable production and purification system can likely be harnessed for synthetic AAV capsids as well.

The latter was shown in a similar study by Grieger and colleagues^[42] in which the authors managed to adapt adherent HEK293 cells to grow in suspension under animal component- and antibiotic-free conditions in shaker flasks and WAVE bioreactors. On top, a pipeline was established and optimized that involves triple-transfection of these cells using PEI Max, followed by a combination of discontinuous iodixanol gradient purification and ion-exchange chromatography (IEC). Remarkably, tweaking of the chromatography conditions enabled the

removal of frequently observed contamination in parvoviral vectors stocks, namely, ferritin. Further notable is the successful up-scaling of the transfection and culturing conditions into WAVE bioreactors of up to 20 liters, frequently resulting in the production of around 1×10^5 vector particles per cell and a total of greater than 1×10^{14} highly pure and >90% full vector particles of various serotypes (AAV1–6, 8, 9). Important to the current article, this method is fully compatible with synthetic AAV capsids, as demonstrated with AAV variants 2i8^[43] and 2.5.^[44] Finally, it was shown that vector yields can be increased through continuous harvest from the medium over 120 hours. As a whole, this

technology is very encouraging owing to its universal nature and its ensuing compatibility with synthetic capsids, as well as because virus yields per cell match or surpass those obtained with other HEK293 cell-based systems^[42,45–47] or those using herpes simplex viruses^[48] or baculoviruses.^[49]

Also, we note further interesting studies by, for instance, Emmerling et al. who managed to adapt HEK293T cells to growth in fully-controlled, single-use iCELLis Nano bioreactors and who obtained substantial AAV2 yields that approximated those achieved in more conventional cell factories.^[50] Finally, we highlight comprehensive recent work by the Mingozzi lab in which Collaud et al. harnessed a 10–200 L suspension cell-based production system to scale up AAV8 vector manufacturing for good laboratory practice toxicology-biodistribution studies.^[51] While these and other similar reports used wild-type AAV variants, there is a high chance that these new and optimized AAV production systems are compatible with synthetic capsid variants as well and can thus ideally synergize with large-scale downstream processing.

3. Methods for AAV Vector Purification

Today, the AAV field has a plethora of methodologies at its disposal for the harvesting of vector particles from producer cells and/or the culture media and for their subsequent purification, whose description would be beyond the scope of this article; rather, we again refer the reader to seminal previous reviews for details.^[28–33] Here, we will briefly recapitulate two of the oldest and most conventional technologies for AAV purification, that is, by cesium chloride (CsCl) or iodixanol density gradient centrifugation.^[52] These protocols are used abundantly because they allow, at least to some extent, for the separation of full (i.e., vector DNA-containing) and empty particles, and because they are largely independent of the capsid. In direct comparison, CsCl-based purification requires more time and work,^[53–55] but a major benefit is a significantly lower proportion of remaining empty particles (<2%) in contrast to iodixanol (\approx 20%).^[33,53] Vice versa, CsCl is more toxic than iodixanol and can induce adverse effects in animals, thus raising a need for dialysis with physiological buffers before use in *in vivo* studies. Toxicity is a lesser concern with iodixanol owing to its inert and non-ionic nature, permitting the immediate use of iodixanol-purified AAV vectors *in vivo*,^[56,57] although the safety in patients with compromised kidney functions is unclear.^[58] Either way, rebuffing of iodixanol-purified AAV particles for *in vivo* studies may be indicated because of the relatively high viscosity of the 40% iodixanol phase in which the full particles accumulate and which may hamper vector injection. To this end, a variety of techniques have been tried, including ultrafiltration/concentration with Amicon Ultra-15, 100 kDa MWCO centrifugation tubes, size-exclusion chromatography with desalting columns, hollow-fiber tangential flow ultrafiltration, or polyethylene glycol (PEG)-8000 precipitation and concentration. Based on data by Strobel et al.,^[53] ultrafiltration may be most efficient and least time-consuming, and it also yielded highest particle recovery and was most effective at removing iodixanol traces.^[53] Still, it remains debated controversially whether CsCl or iodixanol purification results in higher AAV vector bioactivity and product quality. For example, while Zolotukhin et al. reported higher transduction with vectors

purified with iodixanol,^[52] Strobel et al. found slightly higher potency of AAV vectors that were purified with CsCl.^[53] In general, multiple factors may govern transduction efficiency comprising cellular impurities such as ferritin,^[42,55,59,60] prolonged exposure to CsCl that can reduce infectivity,^[61] the proportion of full and empty particles,^[62] repetitive freezing and thawing of vector stocks,^[63] or precipitation methods,^[53] which all require further characterization and standardization.

Next to density gradient centrifugation, column-based chromatography has become a popular technology for downstream AAV purification, as it can effectively discriminate AAV particles from impurities including host cell proteins, nucleases, detergents and residual DNA, and can concurrently be used to re-buffer AAV vector samples. Importantly, while AAV purification via chromatography offers less flexibility than the more universal gradient centrifugation technology, it is easily tailored for large-scale production and is compatible with other purification methods, explaining the wide use and frequent commercialization of these techniques.^[28–32,64–70]

A first important category is IEC, in which AAVs interact with the column matrix by electrostatic interactions of net surface charges on the viral particle and ion resins in the IEC column. As this interaction depends on the isoelectric point (pI) of the capsids and the pH of the buffers, increasing ion strength via higher salt concentrations in elution buffers enables the efficient recovery of column-bound vector particles. A pivotal asset of IEC is its capacity to remove empty capsids at large scale and under optimized elution conditions, based on the small but significant differences in pI between empty (6.3) and full (5.9) capsids.^[71–73] To date, a variety of different anion- or cation-exchange chromatography resins have been developed, many of which are already commercially available. For instance, anion and cation exchangers such as POROS HQ and SP sepharose, respectively, were used for the purification of multiple wild-type AAV serotypes.^[32,71,74,75] Additional benefits of using IEC technology for AAV purification comprise its reproducibility and compatibility with automation and upscaling, the independence from chemical reagents (that could represent unwanted impurities in the final product), and the lack of leaching (i.e., detaching of capturing reagents such as anti-AAV antibodies, which is often observed in affinity-based AAV purification methods). Notably, though, IEC cannot discriminate assembled capsids from protein impurities that show a similar pI and thus usually requires a subsequent step using an alternative matrix with distinct pH and salt conditions.^[31] Furthermore, the effectiveness of IEC is readily influenced by the characteristics of the input material, and the method cannot be standardized for all AAV capsids including synthetic variants due to their different physicochemical properties.

A second category is affinity chromatography, which exploits either specific AAV substrates that mimic cellular receptors, or which—in immunoaffinity chromatography (IAC)—harnesses monoclonal antibodies or nanobodies that recognize AAV outer shell proteins. Either way, this technique is typically capable of differentiating assembled capsids from free viral proteins and impurities.^[35] One of the earliest examples in this category is heparin-based affinity column chromatography, which was established soon after the AAV2 membrane-associated heparan sulfate proteoglycan receptor had been identified.^[25,76] Although this

method is, in principle, also compatible with AAV6 or AAV1 (after a single amino acid change),^[77] it is mainly used to purify the AAV2 serotype.^[29] Moreover, it is feasible to engineer heparin-binding domains into other AAV capsid variants, but this may interfere with their transduction potency or titers as found with multiple capsids and in various cells.^[8,78] Similarly, AAV2 affinity chromatography purification based on the monoclonal antibody A20 has been reported,^[26] which specifically recognizes assembled AAV2 capsids and can thus be used for concurrent capsid purification and depletion of free capsid proteins. However, due to the restriction to AAV2 (and AAV3, which is also recognized by A20) and the dependency on a purified monoclonal antibody that is rate-limiting, this technology was not developed further.

Instead, another notable example of an affinity chromatography medium that has already been used extensively for over a decade and that is commercially available is AVB Sepharose High Performance. The ligands in this resin are highly stable, single-domain antibody fragments from the family *Camelidae*, which were isolated from llamas that were naturally infected with AAVs and which are fused to *N*-hydroxysuccinimide (NHS)-activated Sepharose High Performance.^[28] This approach has gained popularity and is relevant for this article since it enables the purification of multiple AAV variants including synthetic capsids (e.g., AAV1-8, AAVrh8R, AAVrh10, AAV12, and AAV6.2) and since it is characterized by a large vector binding capacity, acceptable levels of concentration and recovery, as well as a moderate linear flow-rate.^[51,62,69,79,80] At least one AVB-binding epitope (amino acid sequence SPAKFA) was identified in the AAV capsid, and its transfer from AAV3B (where it was discovered initially) into other serotypes such as AAV8, rh.64R1, AAV9^[81] or into the synthetic AAV-DJ or AAV-DJ/8^[80] improved binding of the ensuing modified capsids to the AVB resin without compromising transduction efficiency. Interestingly, the O’Riordan lab reported preliminary evidence that the AAV-DJ-SPAKFA mutant not only binds to AVB but also tends to produce more genome-containing particles and to yield better transduction than AAV-DJ in cultured Huh7 cells.^[80]

The discovery of this AVB-binding epitope and the conservation of its function after transfer into multiple AAV capsid variants is critical for at least two reasons. First, it may allow us to predict the suitability of the AVB resin for purification of other AAV capsid variants, natural, or synthetic, purely based on the primary amino acid sequence. This would greatly facilitate the selection of capsid variants in cases where the ease and/or scale of purification are crucial factors. Second, capsids lacking this epitope may be engineered and transformed into AVB binders upon grafting of the epitope, as demonstrated by Wang et al.^[81] or Nass et al.,^[80] highlighting the potential of AVB technology for purification of increasingly diverse AAV capsid variants.

Conversely, a disadvantage of AVB that may hamper its wider use especially for clinical-grade AAV vector purification is the immense costs of the resin material that can rapidly become rate-limiting, in particular when contemplating the purification of multi-liter, bioreactor-derived vector stocks. Moreover, as noted, the AVB resin fails to capture some of the widely used AAV variants such as wild-type AAV9 or the synthetic AAV-DJ capsid (in its unmodified form, see above).^[80,81] Another general drawback of affinity chromatography over IEC^[75,82,83] is its inability to separate full and empty capsids, which is not surpris-

ing considering their identical amino acid composition.^[28,29,80] Importantly, Qu et al. were able to discriminate between the two populations of AAV2 capsids based on slight differences in charge using IEC.^[71] Similarly, the O’Riordan lab has recently shown that combining affinity chromatography and subsequent IEC can result in a significant reduction in empty capsids, enabling the enrichment of up to 80% full, genome-containing capsids depending on the AAV serotype.^[80]

In addition to AVB affinity columns, other commercially available immunoaffinity resins have recently gained increasing attention and are capable of purifying synthetic AAV capsids, such as POROS AAV9 and AAV8 CaptureSelect Affinity matrices. Here, the ligand is covalently bound to Polystyrene-Divinylbenzene (POROS) beads that have a high capacity of AAV particle binding ($\approx 10^{14}$ vector genomes per ml of resin).^[31] Moreover, POROS resins can effectively reduce impurities within a single run and can resist mechanical pressure of up to 10 Mpa, which in combination with AKTA devices allows for the processing of large volumes of AAV vectors.^[40] Their potential was comprehensively demonstrated by Nass et al., who reported that AAV8 (80%) and AAV9 (73%) were efficiently recovered from their respective specific resins.^[80] Interestingly, sequence similarity may not be a strong predictor of compatibility with a particular POROS resin, as demonstrated with AAVrh8R that was successfully purified with POROS AAV8 but not POROS AAV9, despite its higher similarity to AAV9. Similarly, albeit AAV-DJ is largely homologous to AAV8, it could not be purified via the POROS AAV8 resin (and also not AVB, see above). Accordingly, until the specific epitopes that are recognized by the POROS systems have been identified, the compatibility of a given AAV variant has to be tested and rational epitope grafting strategies such as reported for the AVB resin remain impossible. Nonetheless, the experience with isolates such as AAVrh8R implies that the increasing collection of off-the-shelf serotype-specific affinity resins may offer sufficient variety to enable the purification of a wealth of AAV capsid variants. Along these lines, the recent release of yet another commercially available resin, POROS AAVX CaptureSelect, is encouraging as it is supposed to display a broad affinity towards numerous AAV serotypes and synthetic capsids.^[84]

Noteworthy, chromatography technologies are also useful for quality control (QC) of vector stocks as they allow to determine the ratio of full and empty (F:E) capsids,^[62] partially packaged capsids, and other protein contaminants.^[42,85] Knowledge of this ratio is critical given the accumulating and controversially discussed^[86–88] evidence that, on the one hand, the presence of empty capsids may impair transduction efficiencies and exacerbate adverse side effects.^[89] On the other hand, it was proposed that empty capsids may be beneficial by acting as decoys for anti-AAV antibodies and by thus helping to overcome preexisting humoral immunity to AAV.^[90] For these reasons, a large body of techniques has been devised in the past to measure the F:E ratio, comprising analytical ultracentrifugation (AUC), cryo-electron microscopy, UV spectrophotometry, anion-exchange high-performance liquid chromatography (AEX), or charge detection mass spectrometry (CDMS). We also note other technologies such as ELISA combined with PCR, or transmission electron microscopy (TEM), but point out that use of TEM alone is insufficient to determine F:E ratios, and that both, ELISA and qPCR, possess an inherent degree of variability which may

be exacerbated during their combination and result in a significant over- or underrepresentation of packaging efficiencies. Particularly notable in the context of the present review is recent work by Wang et al., who demonstrated the power of AEX using POROS 50 HQ and CIMac columns to separate full and empty capsids of the synthetic variant AAV6.2.^[62] Impressively, following the optimization of various experimental parameters such as salts and buffering agents, the final method was shown to be accurate, linear, reproducible and sensitive, permitting the detection of low proportions (2.9%) of empty AAV6.2 capsids using relative UV measurements at 260/280 nm. Compared to AUC, one of the most commonly used approaches to determine F:E ratios based on sedimentation velocity, AEX gave a slightly lower resolution and failed to detect a peak of partially packaged AAV capsids. Still, this may be outweighed by the benefits of AEX, especially its compatibility with automatization and its ease-of-use.^[62]

Finally, we note a recent study by Arden and Metzger, who reported a simple, cost-effective, and serotype-independent AAV purification protocol that is merely based on PEG precipitation and two centrifugation steps.^[91] Proof-of-concept comprised its application for purification of the AAV variant AAVM41, that is, a myocardium-tropic, synthetic AAV created by DNA family shuffling of serotypes 1, 6, 7, and 8.^[92] Albeit raw data were only shown for another AAV serotype, AAV6, AAVM41 yields and purity obtained with this streamlined protocol were reported to be high, and in vivo bioactivity in mice was preserved. This implies that this inexpensive methodology is well suited to complement existing AAV purification technology based on gradient centrifugation or affinity column purification, albeit it may not be easily scalable.

4. Purification of AAV-DJ

A good example of a synthetic AAV capsid that has been successfully purified using a number of the technologies highlighted above and others is AAV-DJ, the prototype of a capsid generated by DNA family shuffling, that is, the forced recombination of capsid DNA fragments from multiple parental AAV isolates (here, AAV2, 8, and 9).^[8] Therefore, in this chapter, we will harness this specific capsid to exemplify the diversity of technologies that exists and that has already been exploited for purification of synthetic AAV capsids. Importantly, in Table 1, this will be complemented by an overview of the use of the same technologies for Anc capsids, that is, the family of synthetic capsids created through ancestral reconstruction including Anc80L65.

In the initial report of AAV-DJ,^[8] CsCl density gradient centrifugation was used for purification, followed by later studies that used the same protocol^[14,16,19,93] or iodixanol density gradient centrifugation.^[11,15,94–97] Notably, AAV-DJ contains the heparin-binding domain from one of its parents, AAV2, which tempted Liu and Moon to try and purify AAV-DJ via heparin affinity column chromatography.^[13] Indeed, a relatively small, 5 mL heparin column in combination with FPLC was sufficient to enable the purification of 3×10^{13} particles from 150 15 cm dishes of triple-transfected HEK293 cells. However, this method was incompatible with the purification of vector particles that had been secreted into the media during production due to column contamination with proteins in the cell culture medium, resulting in a loss of $\approx 40\%$ of produced particles. The utility of heparin

affinity columns for AAV-DJ purification was also independently verified by Xie et al.,^[19] who combined this with three rounds of CsCl density gradient centrifugation in order to purify empty virus-like particles of AAV-DJ and to resolve their structure bound by a heparinoid pentasaccharide. Also, Candelas et al. used heparin column-purified AAV-DJ to investigate the role of the T-type calcium channel Cav3.2 in lamina II neurons of the spinal cord in mice.^[98]

In another study,^[99] Hashimoto and colleagues compared all four combinations of two plasmid transfection (calcium phosphate co-precipitation and lipofectamine) and two purification methodologies (CsCl and iodixanol density gradient centrifugation), to produce a derivative of AAV-DJ called AAV-DJ/8, in which the aforementioned heparin-binding domain from AAV2 was replaced with the corresponding sequence of AAV8.^[8] This showed that the combination of lipofectamine and iodixanol purification may be best suited to obtain high titers of AAV-DJ/8, albeit questions about the scalability of lipofectamine transfection remained. In line with work by Strobel and colleagues who independently also compared the two purification technologies,^[53] the choice of method did not affect in vitro or in vivo vector bioactivity.

Both synthetic AAV capsids, AAV-DJ and its derivative AAV-DJ/8, were also studied by Kimura et al. who implemented an original purification protocol based on PEG precipitation, aqueous two-phase partitioning (previously also reported by Guo et al.^[100]) and iodixanol density gradient centrifugation.^[101] To this end, vector particles were produced using a likewise optimized triple-transfection protocol whose hallmarks were a reduction in medium glucose and a pH stabilization, resulting in overall titers of up to 1×10^{14} highly pure AAV vector particles per mL. As in the work of Hashimoto et al.,^[99] in vivo mouse studies served to confirm that the bioactivity of vectors purified with this improved, rapid and economical protocol was maintained.

Similarly, Yu et al. reported a protocol for AAV purification based on three-phase partitioning (TPP) combined with CsCl density gradient centrifugation,^[102] which is capable of separating full from empty particles and of removing 90% of cellular proteins, while concurrently increasing the capacity of ultracentrifugation by up to 10-fold, depending on the AAV serotype. TPP is a non-chromatographic methodology that is based on the separation of tertiary butanol into two phases upon mixing with ammonium sulfate, and the additional separation of target proteins such as AAV particles into a third phase between the other two. The impressive proof-of-concept data included purification of synthetic AAV-DJ particles from a 25 L production run, resulting in a total of $\approx 5 \times 10^{15}$ vector genomes and an $\approx 80\%$ recovery rate. The fact that next to AAV-DJ, the method was also validated with numerous wild-type AAVs suggests that it is widely applicable and, based on the authors' calculation, useful for stocks in the 10^{17} vector genome-scale.

A special variation of a protocol for AAV-DJ purification was reported by Kukisi and colleagues,^[103] who used this vector to selectively and artificially activate specific neural circuits in the medial amygdala of mice, to study the role of olfactory signals for sexual behavior. To this end, cells transfected with the AAV helper and vector plasmids were collected, suspended in artificial cerebrospinal fluid and subjected to four freeze-thaw cycles. Subsequently, the cell lysate was treated with benzonase and

centrifuged twice at $16.000 \times g$ for 10 min, yielding a supernatant that was directly used for the *in vivo* experiments.

Finally, we note a study by Lakhan and colleagues who used AAV-DJ vectors to deliver the *COX2* gene to fracture sites in a mouse femoral fracture model, where it effectively transduced mesenchymal stem cells.^[17] For vector purification, the authors harnessed the AAV Purification Kit from Cell Biolabs Inc., which is based on an affinity matrix that is not further specified but suitable for AAV2 and AAV-DJ, and which claims to yield >60% recovery and >95% purity following a 3 h protocol (<https://www.cellbiolabs.com/aav-purification-standard-kit>). The same kit was also used by Yoo et al. in a study where they harnessed AAV-DJ to express a cocktail of heart reprogramming and regeneration factors *in vitro* and *in vivo*.^[104]

5. Methods for AAV Vector Characterization

Akin to the arsenal of technologies for AAV vector purification, there is a wealth of reported strategies for the subsequent characterization of vector particles, whose comprehensive discussion would be beyond our present scope. Therefore, in the following, we will restrict ourselves to a selection of methodologies that we deem particularly interesting and promising for their (future) application to synthetic AAV capsids, and that, to the best of our knowledge, have not been reviewed extensively before. We apologize to all other authors who have developed an alternative, sensitive and powerful techniques that we cannot review in great detail here for space reasons, such as SDS capillary gel electrophoresis.^[105]

5.1. Mass Spectrometry

Over the last 1.5 decades, mass spectrometry (MS) has been used to characterize AAV capsid protein integrity and post-translational modifications, as well as to identify contaminating cellular proteins in AAV vector preparations (see next chapter). Concurrently, it has also been recognized as a versatile and powerful technology to confirm AAV serotype identity and as an assay for lot release testing. Among the first to apply MS for the study of AAV capsid biology were Salganik et al., who harnessed MS to identify proteolytic cleavage sites in the AAV1 capsid.^[106] Capsid modifications were also studied by Murray and colleagues, who specifically assessed the glycosylation of AAV2 capsids and reported evidence that this particular post-translational modification may not occur,^[107] a conclusion that was later confirmed by Jin et al.^[85]

However, the general view of AAV as a non-glycosylated virus changed with more recent studies, for example, a 2018 report by the Xiao group who used MALDI-time-of-flight (TOF) and high-resolution LC/MS to identify *N*-glycosylation on amino acid N499 of the AAV8 capsid, at least in a fraction of the stock they investigated.^[108] Interestingly, the same amino acid was also among the numerous asparagine residues on the AAV8 capsid that Giles et al. discovered to be deaminated by LC tandem-mass MS, and it was the one showing the greatest stock-to-stock variation in terms of deamidation level, for reasons unknown.^[109] As shown in the same study, the phenomenon of deamidation is not unique to AAV8 but was also observed for seven other isolates,

that is, AAV1, AAV3 to 5, AAV7, AAVrh32.33 and AAV9, and may negatively affect capsid assembly, transduction efficiency, tissue tropism and immunoreactivity. An interesting concept with relevance for AAV manufacturing that emerged from this work is that of a "deamidation clock", according to which progressing deamidation correlates with losses in vector activity, thus providing an advantage to freshly translated virions for transduction.^[109] Hence, MS-based analysis of capsid deamidation may become an important part of future workflows to quantify consistency and lot-to-lot reproducibility during AAV vector manufacturing.

Likewise, Mary et al. used MALDI-TOF/TOF analysis as well as a combination of nanoUPLC and Triple-TOF MS analysis to identify post-translational modifications in ten AAV serotypes, AAV1 through 9 and AAVrh10, and detected a variety of such events including glycosylation, phosphorylation, acetylation, ubiquitination and SUMOylation.^[110] Interestingly, while some of these occurred at evolutionarily largely conserved residues in multiple serotypes, others were specific for one or more viral isolates, implying their potential for identification or confirmation of particular capsids during vector manufacturing. The fact that LC/MS but not MALDI-TOF analysis revealed *N*- and *O*-glycosylation in AAV2 adds to the controversy about this specific post-translational modification in AAV2 and concurrently highlights the importance of using utmost sensitive detection technology. Similar to the deamidation events reported by the Wilson group,^[109] the broad spectrum of modifications detected here could affect immune recognition of the capsid as well as its stability, cellular entry and trafficking, or other aspects of its intracellular fate.^[110] Of note, using LC-MS, Jin et al. also independently detected acetylation on the VP1 and VP3 *N*-termini of six different AAV serotypes, that is, AAV1, 2, 5, 7, 9, and rh10, and speculated on a link to capsid protein degradation or ubiquitination.^[85] The second conclusion of this work with relevance for the topic of the present article was that the unanimous determination of VP1, VP2, and VP3 masses could serve as a generic but highly specific and rapid method for capsid serotype identity testing and to ensure product consistency during AAV manufacturing, even though its usefulness for synthetic AAV variants remains to be demonstrated to date.

Until then, the great potential of MS technology for confirmation of AAV serotype identity and batch release testing has already been exemplified in 2009 in a comprehensive study by Van Vliet et al., who developed a protocol involving VP protein separation by gel electrophoresis, band excision, trypsin digestion, and LC/MS/MS.^[111] As demonstrated in various proof-of-concept experiments, this workflow was capable of separating closely related serotypes AAV1, 2, and 8 from each other as well as from the more distinct AAV4 and 5. Moreover, it also enabled the recognition of a point mutation in the AAV4 capsid at VP1 position 544 (K544E) that had previously been detected by conventional Sanger sequencing, even though the two AAV4 variants were indistinguishable *in vivo* in the mouse retina.

The usefulness of MS techniques for identification and quantification of AAV capsids and their components was further validated in three later studies, including work by Snijder et al. who illustrated the power of high-resolution Orbitrap MS for the study of VP protein stoichiometry in assembled AAV1 capsids.^[112] Intriguingly, their data suggest that AAV1 exists in a total of eight stoichiometries, composed of 0-2 copies of VP1, 8-11 of VP2, and

48-51 of the major capsid protein VP3. In turn, this implies that AAV(1) capsid assembly is a stochastic rather than a predefined process whose outcome depends on the expression levels of each capsid protein. This idea of inherent variability between individual particles is an appealing hypothesis that could readily explain the inability of even atomic-level crystallography approaches to precisely resolve the unique regions of VP1 and VP2.

Subsequently, Pierson and colleagues harnessed charge detection (CD)MS to dissect the DNA content of AAV8 vectors containing single- or double-stranded genomes, permitting them to demonstrate its power to quantitatively and rapidly characterize various subpopulations comprising particles with a full or partial genome, empty capsids as well as impurities.^[113] With this resolution and these features, CDMS seems well suited to complement the other technologies, especially since it allows to monitor not only capsid but also genome integrity.

Finally, another useful addition has more recently been reported by Zhang et al. who applied a novel, automated, microfluidic ZipChip CE/MS methodology to identify AAV2 capsid proteins within a very short period (4 min) and from a minimal sample volume of 5 nL.^[114] To illustrate the resolution of this technology, the authors successfully distinguished wild-type AAV2 from a triple point mutant of the same serotype, reminiscent of the data by Van Vliet et al.^[111] but achieved in much shorter processing time. Notably, this study also again confirmed the single N-terminal acetylation on VP1 and VP3 that has been reported previously.^[85,109]

5.2. Capsid Thermostability

The MS-based technologies highlighted above allow to distinguish capsid serotypes including variants with minimal sequence divergence, and are thus, in principle, useful to validate proper labeling and batch-to-batch consistency of AAV vector stocks for clinical use. However, most of the reported protocols may have limited applicability for a variety of reasons, including the requirement for large substrate volumes or for special instrumentation, and their inability to yield higher-level structural information beyond primary capsid protein sequence.

These and other gaps can potentially be filled by another technology that was introduced into the AAV field in 2013 by Rayaprolu et al.^[115] and then extensively and independently validated in two publications by the groups of Luk Vandenberghe, Eduard Ayuso, and Mavis Agbandje-McKenna in 2017.^[116,117] The hallmark of this powerful biophysical technique, called differential scanning fluorimetry (DSF) or AAV-ID,^[117] is its ability to rapidly, easily, and accurately measure AAV capsid thermostability (melting temperature, T_m), by monitoring capsid unfolding in real-time in response to temperature gradients in the presence of SYPRO Orange. The latter is a hydrophobic dye whose fluorescence at 570 nm is quenched by solvent molecules but which starts to fluoresce once it binds to hydrophobic pockets, such as those that are normally located inside the AAV capsid and become exposed during heat-induced denaturing. Already in 2013, the McKenna and Bothner labs recognized the potential of DSF to determine AAV capsid T_m and to then use these values to unambiguously identify divergent serotypes, as exemplified using AAV1, 2, 5, and 8.^[115] Intriguingly, recording of thermal denaturation

curves using DSF revealed distinct and narrow transition temperatures that were characteristic for each serotype, with the lowest observed for AAV2 ($\approx 70^\circ\text{C}$) and the highest for AAV5 ($\approx 90^\circ\text{C}$). Further analysis showed that these T_m are neither determined by capsid protein VP1 nor by the presence of an AAV genome inside the capsid, which was later confirmed in the aforementioned follow-up studies.^[116,117] Importantly, the authors also performed a first mixing experiment in which AAV2 and AAV5, the two serotypes with the greatest difference in T_m , were pooled and analyzed by DSF. This yielded two distinct and serotype-specific peaks, and thus illustrated the power of this technique to concurrently identify and resolve at least two different capsid variants.

The latter was subsequently extended and much more profoundly demonstrated by Pacouret et al., who used DSF to analyze a collection of 67 AAV stocks and who convincingly showed its ability to discriminate six different serotypes by their T_m fingerprint, namely, AAV1, 2, 5, 6.2, 8, and 9.^[117] In line with the data from Rayaprolu et al.,^[115] T_m were largely independent of the presence or size of an encapsidated genome, as well as of production (mammalian versus insect cells) or purification protocols (iodixanol versus POROS). Moreover, the methodology—called AAV-ID here—is highly robust, as illustrated via its reproducible application in two different labs. Also interesting is that the signal amplitude at the apex of the T_m peak correlated with vector dose in a linear fashion over at least one order of magnitude, illustrating the ability of AAV-ID to provide information on particle concentration. Furthermore, Pacouret and colleagues showed that the thermostability measure is strongly affected by the pH of the AAV vector formulation buffer in a serotype-dependent manner, providing clues about a link between capsid stability and cellular mechanisms affecting AAV genome release, including acidification in the endosome. However, the finding that in some cases, fluorescence transition was obscured by contaminants, implied that AAV-ID may be limited to AAV stocks above a certain purity threshold. Finally, reminiscent of the MS data by Van Vliet et al.,^[111] AAV-ID was shown to be able to distinguish various pairs of AAVs that differ in a few residues, such as AAV1 and 6.2.

These conclusions were essentially mirrored in the work by Bennett et al.,^[116] who studied ten different AAV serotypes (AAV1 through 9, AAVrh.10) and who showed that most of them can be distinguished by their unique T_m , except AAV7, 9, and rh.10 whose T_m was in a very similar range around 77°C . Also in this work, melting temperatures were affected by buffer formulation and pH in a serotype-specific manner, but not by the presence or absence of a genome inside the particles. Notably, the method proved to be very sensitive and capable of detecting as little as 5×10^{11} purified AAV5 (the most stable serotype) particles in 25 μL . Extending the previous studies,^[115,117] Bennett and colleagues demonstrated that the VP3 capsid protein is the sole determinant of thermostability (and sufficient to assemble capsids). Finally, akin to Pacouret et al.,^[117] it was shown that DSF can distinguish a pair of AAV serotypes differing in single amino acid, by swapping residue E/K531 between AAV1 and AAV6, respectively.

Of interest for this article, the same lab has applied various techniques including DSF to also assess the thermostability of synthetic AAV capsids, especially variants that were designed in silico through ancestral reconstruction.^[20] Specifically, Zinn et al. determined the T_m of their lead AAV candidate, Anc80L65, to be $\approx 92^\circ\text{C}$ and thus 15–30 $^\circ\text{C}$ higher than that of AAV2 or AAV8. This

came as a surprise considering the relatively poor vector yields that were obtained with Anc80L65 as compared to AAV8, but it may imply that higher activation energy is required not only to disassemble but also to assemble Anc80L65 capsids, albeit this needs to be validated. An even further increase was noted for another reconstructed capsid from the AAV1-3 lineage, Anc127, whereas two others, Anc81 and Anc82 (Figure 1), had a lower T_m than Anc80. The fact that the latter two are evolutionary intermediates between Anc80 and extant serotypes illustrates the power of DSF to not only distinguish synthetic AAV variants based on T_m , but to also gain insights into natural virus evolution.

Last but not least, we highlight a recently reported alternative technology dubbed intrinsic (i)DSF, which provides remarkable precision and sensitivity (down to 2×10^{11} AAV particles) in the absence of external dyes such as SYPRO Orange.^[118] Briefly, this approach relies on the inherent red-shift of tryptophan residues under UV light when exposed to a hydrophilic rather than a hydrophobic environment, as is the case during AAV capsid disassembly. Similar to the preceding studies using SYPRO Orange-dependent DSF, also iDSF was shown to enable the discrimination of various natural serotypes (albeit not all; e.g., the AAV3/AAV8 pair could not be distinguished) and to yield similar T_m values. Notably, iDSF is relatively simple, fast and inexpensive, making it attractive for high-throughput screening and sample monitoring during the purification process. Finally, albeit not demonstrated in the pilot study by Rieser and colleagues, the fact that tryptophan residues within AAV capsids are largely conserved across serotypes implies great usefulness of this method also for synthetic AAV capsid variants in the future.

5.3. Bacterial and Cellular Contaminants

Frequent and usually adverse contamination of AAV vector stocks is endotoxin, that is, a lipopolysaccharide (LPS) found in the outer membrane of Gram-negative bacteria. Particularly concerning is that even minute amounts of LPS can trigger severe adaptive immune responses in intravenously injected mammals including humans and potentially lead to an inflammatory response, sepsis, multi-organ failure and, ultimately, death. Exacerbating this concern is that bacteria are found almost everywhere in a laboratory setting, including in buffers, on lab-ware and surfaces as well as in the plasmid DNA that is produced and used for AAV vector production. Moreover, proteins such as the AAV capsid shell tend to readily interact with LPS over a broad range of isoelectric points, implying that AAV serotypes and natural or engineered capsid variants may all display at least some degree of affinity toward endotoxin.

Therefore, we consider a recent study by Kondratova and colleagues from the Zolotukhin lab that tackled this particular AAV contaminant as important, timely and worth highlighting.^[119] In this work, the authors succeeded at establishing a new, rather simple but very effective protocol that permits to reduce the endotoxin content of AAV stocks to virtually undetectable levels of <2.5 endotoxin units [EU] mL^{-1} , which complies well with the FDA-recommended upper limit of 5 EU kg^{-1} body weight for intravenously injected biopharmaceuticals.^[119,120] Briefly, the hallmarks of this protocol are the initial treatment of AAV stocks with mild detergent, followed by a series of buffer

exchange and concentration steps under experimental conditions that prevent adverse AAV particle aggregation. Importantly, a thorough analysis of the final products yielded no evidence for perturbations of transduction efficiency, capsid thermostability, protein composition or capsid morphology. Even more important in the context of the present article is that the authors successfully validated their new technology with eight different AAV capsid variants, including wild-types AAV2, AAV5, AAV8, AAV9, and AAVrh10 as well as synthetic capsids, such as AAV-DJ^[8] and AAV-TT.^[121] Also very encouraging are the high recovery rates of between 50% and 96% of starting material, which surpass the low yields of typically $<10\%$ that are often observed with commercial LPS removal kits.

Collectively, these advantageous properties make this new protocol highly attractive especially for academic laboratories who work with different AAV capsid variants and who will thus benefit most from the combination of inexpensive, off-the-shelf reagents, quick turn-around time, high recovery, versatility and effectiveness at LPS removal. However, its scalability to large(r) volumes has remained unclear to date and should be established in future work.

Of note, bacterial endotoxins are not the only contaminants that have been detected in AAV preparations, but others have likewise reported the presence of cellular proteins. In one notable 2014 study, Dong and colleagues used a combination of two proteomics approaches, gel electrophoresis liquid chromatography-mass spectrometry (GeLC-MS) and two-dimensional gel electrophoresis, to assess the purity of cesium chloride gradient-purified AAV2 vectors and detected 13 co-purifying cellular proteins, including known AAV host factors such as nucleolin and nucleophosmin.^[87] One of them, protein SET, was also found in stocks of serotypes AAV5, 6, 8, and 9 that were purified with the same method. Interestingly, though, it was absent from AAV2 stocks that were purified using IEC, and it seemed to specifically co-purify with full, DNA-containing AAV2 capsids, but not with the excess of empty particles, for reasons unclear. This work and related other studies (see below) are intriguing because the data have multiple implications for AAV biology and vector manufacturing. First, such identification of contaminating or co-purifying (under specific conditions) host cell proteins is highly informative as it expands our still limited understanding of natural AAV biology, which may ultimately allow to rationally engineer better vectors and/or to improve manufacturing protocols. There is evidence that cellular contaminants may actually enhance AAV vector transduction^[55,122] (unpublished own observations), and there are also numerous reports of mammalian serum proteins that interact with AAV capsids and affect their properties (Fakhiri et al., submitted). Accordingly, it may not necessarily be desirable to comprehensively eliminate all cellular factors from AAV vector preparations during purification, in particular not those that could act as transduction enhancers. Secondly, considering the speed of many proteomics technologies, the rapid and robust detection of contaminating proteins by these methodologies could well be implemented as a routine procedure for AAV quality control.

Similar findings and conclusions were also reached by Strobel et al. in a 2015 study where they compared two methodologies for AAV purification by density gradient centrifugation (see also above) and used nanoscale liquid chromatography-tandem

mass spectrometry (nanoLC-MS/MS) analysis to investigate the identity of 13 additional protein bands in purified AAV8 vector preparations.^[53] Notably, these authors identified several proteins that overlapped with those from the Dong et al. study,^[87] including SET, nucleolin, mitochondrial single-stranded DNA-binding protein and nucleophosmin, and the latter two were independently also detected as proteins that co-purified with AAV8 by Aloor et al.,^[108] which emphasizes their role in the AAV life cycle. Also noteworthy is that some of the contaminants in the work by Strobel and colleagues,^[53] such as nucleolin and nucleophosmin, were specifically detected in the CsCl-purified samples but absent from the iodixanol-purified batches, which could inform future purification protocols

Finally, in another noteworthy example, the Samulski lab utilized mass spectrometry to identify a small contaminating protein of around 20 kDa, that is, ferritin, which they observed in AAV stocks of multiple serotypes that were purified by iodixanol density gradient chromatography followed by IEC.^[42] In negatively stained transmission electron microscopy pictures, this protein formed small, circular structures of up to 10 microns, which were independently detected in an AAV5 stock in a more recent study from the Zolotukhin lab.^[59] Ferritin was also among the contaminating proteins in AAV8 stocks that were investigated earlier by the Lamla lab.^[53] Besides, our lab has recently observed the presence of ferritin protein and structures in various recombinant AAV and bocaviral vector preparations (Fakhiri and Grimm, manuscript in preparation). As noted above, unlike endotoxins, the presence of ferritin will most likely not interfere with AAV (or bocaviral) functionality and is thus a lesser concern. Moreover, if desired, it can be removed by tweaking the IEC conditions, as illustrated by Grieger et al.^[42]

6. Conclusions

It may seem ironic that the smallest of all viruses that are being developed and evaluated as vectors for human gene therapy, AAV, has rapidly become the biggest and undisputed star that continues to enjoy the limelight. The reasons for this astounding success are manifold but are largely based on the ever-expanding portfolio of ingenious, versatile and powerful techniques for AAV vector manufacturing, ranging from methodologies for high-throughput capsid diversification and large-scale vector production, to tailored and innovative concepts for AAV particle purification, characterization and quality control for lot releases. Not surprisingly, most of the technologies for downstream AAV vector processing had originally been developed for and validated with wild-type AAV serotypes due to their long availability and our advanced understanding of their biology. Importantly, though, their development has also paved the way for the implementation of new manufacturing technology that is compatible with the many rapidly emerging, non-natural viral variants, too. Concurrently, this process is fostered by our steadily increasing knowledge of the function and properties of natural versus synthetic AAV capsids, which will ideally allow the adaptation of existing technology to future capsids once their structural and biophysical characteristics have been unraveled. These aspects were in the center of the present article, but we acknowledge that owing to the sheer complexity of this research field and the flurry of activities by academic and industrial entities, we

could only offer a glimpse into the relevant advances, and we, unfortunately, had to omit important and informative work by other colleagues for reasons of space and clarity. Nonetheless, we at least want to mention that the strategies highlighted in the present article synergize with, and are perfectly complemented by, a wealth of other, equally important and informative approaches. Examples of such work that we could not discuss here despite its relevance for synthetic AAV capsids include the investigation of methodologies for cell harvest and lysate clarification, comprising a large variety of chemical or physical approaches such as freeze-thawing and low-speed centrifugation, which is particularly suitable for small-scale preparations and has thus been used preferably in our recent comparison of libraries of synthetic AAV capsid variants in cultured cells.^[123] In contrast, other technologies such as microfluidization or lysis with detergents such as Triton X-100 are better suited for large-scale manufacturing of natural or synthetic AAV capsids, albeit the use of chemicals necessitates their subsequent monitoring in the final product as potential impurities.^[28,33] Moreover, we note the emerging use of deep sequencing techniques for analyses of the contents of AAV vector particles (plasmid backbones, cellular DNAs, fragmented genomes).^[124] This comprises non-selective but sensitive single-stranded DNA virus sequencing (SSV-Seq) technology for detection of illegitimate residual cellular or plasmid DNA as reported by the Ayuso lab^[125] or Fast-Seq methodology from the Paulk lab.^[126] Techniques such as the latter are becoming increasingly important as more and more AAV gene therapies including synthetic capsid-based stratagems are being tested in patients, raising a need for new and robust processes to detect, quantify, and eliminate product impurities, as comprehensively reviewed by Penaud-Budloo and colleagues^[33] as well as Ayuso, Mingozzi, and Bosch.^[28] Along the same lines, we note exciting new insights into the role of primary or secondary sequence elements in the vector genome that govern replication and/or encapsidation as well as AAV vector DNA integrity.^[127] Combined with the advanced technologies that were summarized here and with further ongoing innovations in the field of AAV capsid evolution, including rational design^[128] and machine learning,^[129] this offers plenty of reason to be optimistic about the future of AAV vector biomanufacturing and its continued contribution to the success story of human gene therapy.

Acknowledgements

The authors are very grateful for the funding and other support from the MYOCURE project. MYOCURE has received funding from the European Union's Horizon 2020 research and innovation program under grant agreement No 667751. D.G. is thankful for support by the German Center for Infection Research (DZIF, BMBF; TTU-HIV 04.803 and TTU-HIV 04.815). D.G. acknowledges additional funding by the German Research Foundation (DFG) through the Cluster of Excellence CellNetworks (EXC81) and the Collaborative Research Centers SFB1129 (Projektnummer 240245660) and TRR179 (Projektnummer 272983813).

Open access funding enabled and organized by Projekt DEAL.

Data Availability Statement

Data sharing not applicable — no new data generated.

Conflict of Interest

D.G. is a co-founder, shareholder and designated chief scientific officer (CSO) of AvaiGen GmbH. J.E.A. declares that he has no conflict of interest.

Keywords

Adeno-associated virus, gene therapy, manufacturing, viral vector

Received: June 4, 2020

Revised: September 13, 2020

Published online: October 7, 2020

- [1] H. C. Verdera, K. Kuranda, F. Mingozzi, *Mol. Ther.* **2020**, *28*, 723.
- [2] D. Wang, P. W. L. Tai, G. Gao, *Nat. Rev. Drug Discovery* **2019**, *18*, 358.
- [3] D. Grimm, S. Zolotukhin, *Mol. Ther.* **2015**, *23*, 1819.
- [4] C. Li, R. J. Samulski, *Nat. Rev. Genet.* **2020**, *21*, 255.
- [5] J. Weinmann, D. Grimm, *Virus Genes* **2017**, *53*, 707.
- [6] H. Buning, A. Srivastava, *Mol. Ther. Methods Clin. Dev.* **2019**, *12*, 248.
- [7] M. A. Kotterman, D. V. Schaffer, *Nat. Rev. Genet.* **2014**, *15*, 445.
- [8] D. Grimm, J. S. Lee, L. Wang, T. Desai, B. Akache, T. A. Storm, M. A. Kay, *J. Virol.* **2008**, *82*, 5887.
- [9] W. Li, A. Asokan, Z. Wu, T. Van Dyke, N. DiPrimio, J. S. Johnson, L. Govindaswamy, M. Agbandje-McKenna, S. Leichter, D. E. Redmond, Jr., T. J. McCown, K. B. Petermann, N. E. Sharpless, R. Jude Samulski, *Mol. Ther.* **2008**, *16*, 1252.
- [10] J. T. Koerber, J. H. Jang, D. V. Schaffer, *Mol. Ther.* **2008**, *16*, 1703.
- [11] J. Wei, G. Ran, X. Wang, N. Jiang, X. Lin, C. Ling, *J. Biol. Chem.* **2019**, *294*, 14096.
- [12] R. D. Hickey, J. B. Lillegard, J. E. Fisher, T. J. McKenzie, S. E. Hofherr, M. J. Finegold, S. L. Nyberg, M. Grompe, *Hepatology* **2011**, *54*, 1351.
- [13] J. Liu, Y. A. Moon, *Yonsei Med. J.* **2016**, *57*, 790.
- [14] S. P. Melo, L. Lisowski, E. Bashkirova, H. H. Zhen, L. Lisowski, E. Bashkirova, H. H. Zhen, K. Chu, D. R. Keene, M. P. Marinkovich, M. A. Kay, A. E. Oro, *Mol. Ther.* **2014**, *22*, 725.
- [15] K. A. Danilov, S. G. Vassilieva, A. V. Polikarpova, A. V. Starikova, A. A. Shmidt, I. I. Galkind, A. A. Tsitrin, T. V. Egorova, S. N. Orlov, Y. V. Kotelevtsev, *Exp. Cell Res.* **2020**, *392*, 112033.
- [16] Y. Katada, K. Kobayashi, K. Tsubota, T. Kurihara, *PeerJ* **2019**, *7*, e6317.
- [17] R. Lakhan, D. J. Baylink, K. H. Lau, X. Tang, M. H.-C. Sheng, C. H. Rundle, X. Qin, *Gene Ther.* **2015**, *22*, 721.
- [18] T. F. Lerch, J. K. O'Donnell, N. L. Meyer, Q. Xie, K. A. Taylor, S. M. Stagg, M. S. Chapman, *Structure* **2012**, *20*, 1310.
- [19] Q. Xie, J. M. Spear, A. J. Noble, D. R. Sousa, N. L. Meyer, O. Davulcu, F. Zhang, R. J. Linhardt, S. M. Stagg, M. S. Chapman, *Mol. Ther. Methods Clin. Dev.* **2017**, *5*, P1.
- [20] E. Zinn, S. Pacouret, V. Khaychuk, H. T. Turunen, L. S. Carvalho, E. Andres-Mateos, S. Shah, R. Shelke, A. C. Maurer, E. Plovie, R. Xiao, L. H. Vandenberghe, *Cell Rep.* **2015**, *12*, 1056.
- [21] J. Suzuki, K. Hashimoto, R. Xiao, L. H. Vandenberghe, M. C. Liberman, *Sci. Rep.* **2017**, *7*, 45524.
- [22] L. D. Landegger, B. Pan, C. Askew, S. J. Wassmer, S. D. Gluck, A. Galvin, R. Taylor, A. Forge, K. M. Stankovic, J. R. Holt, L. H. Vandenberghe, *Nat. Biotechnol.* **2017**, *35*, 280.
- [23] B. Pan, C. Askew, A. Galvin, S. Heman-Ackah, Y. Asai, A. A. Indzhykulyan, F. M. Jodelka, M. L. Hastings, J. J. Lentz, L. H. Vandenberghe, J. R. Holt, G. S. Géléoc, *Nat. Biotechnol.* **2017**, *35*, 264.
- [24] D. Grimm, M. A. Kay, J. A. Kleinschmidt, *Mol. Ther.* **2003**, *7*, 839.
- [25] K. R. Clark, X. Liu, J. P. McGrath, P. R. Johnson, *Hum. Gene Ther.* **1999**, *10*, 1031.
- [26] D. Grimm, A. Kern, M. Pawlita, F. K. Ferrari, R. J. Samulski, J. A. Kleinschmidt, *Gene Ther.* **1999**, *6*, 1322.
- [27] D. Kuck, A. Kern, J. A. Kleinschmidt, *J. Virol. Methods* **2007**, *140*, 17.
- [28] E. Ayuso, F. Mingozzi, F. Bosch, *Curr. Gene Ther.* **2010**, *10*, 423.
- [29] N. Clement, J. C. Grieger, *Mol. Ther. Methods Clin. Dev.* **2016**, *3*, 16002.
- [30] J. J. Aponte-Ubillus, D. Barajas, J. Peltier, C. Bardliving, P. Shamlou, D. Gold, *Appl. Microbiol. Biotechnol.* **2018**, *102*, 1045.
- [31] M. Hebben, *Cell Gene Ther. Insights* **2018**, *4*, 131.
- [32] W. Qu, M. Wang, Y. Wu, R. Xu, *Curr. Pharm. Biotechnol.* **2015**, *16*, 684.
- [33] M. Penaud-Budloo, A. Francois, N. Clement, E. Ayuso, *Mol. Ther. Methods Clin. Dev.* **2018**, *8*, 166.
- [34] J. F. Wright, *Hum. Gene Ther.* **2009**, *20*, 698.
- [35] D. Grimm, A. Kern, K. Rittner, J. A. Kleinschmidt, *Hum. Gene Ther.* **1998**, *9*, 2745.
- [36] T. Matsushita, S. Elliger, C. Elliger, G. Podsakoff, L. Villarreal, G. J. Kurtzman, Y. Iwaki, P. Colosi, *Gene Ther.* **1998**, *5*, 938.
- [37] X. Xiao, J. Li, R. J. Samulski, *J. Virol.* **1998**, *72*, 2224.
- [38] M. Urabe, C. Ding, R. M. Kotin, *Hum. Gene Ther.* **2002**, *13*, 1935.
- [39] O. Kondratov, D. Marsic, S. M. Crosson, H. R. Mendez-Gomez, O. Moskalenko, M. Mietzsch, R. Heilbronn, J. R. Allison, K. B. Green, M. Agbandje-McKenna, S. Zolotukhin, *Mol. Ther.* **2017**, *25*, 2661.
- [40] D. Blessing, G. Vachey, C. Pythoud, M. Rey, V. Padrun, F. M. Wurm, B. L. Schneider, N. Déglon, *Mol. Ther. Methods Clin. Dev.* **2019**, *13*, 14.
- [41] H. Zhang, J. Xie, Q. Xie, J. M. Wilson, G. Gao, *Hum. Gene Ther.* **2009**, *20*, 922.
- [42] J. C. Grieger, S. M. Soltys, R. J. Samulski, *Mol. Ther.* **2016**, *24*, 287.
- [43] A. Asokan, J. C. Conway, J. L. Phillips, C. Li, J. Hegge, R. Sinnott, S. Yadav, N. DiPrimio, H.-J. Nam, M. Agbandje-McKenna, S. McPhee, J. Wolff, R. J. Samulski, *Nat. Biotechnol.* **2010**, *28*, 79.
- [44] D. E. Bowles, S. W. McPhee, C. Li, S. J. Gray, J. J. Samulski, A. S. Camp, J. Li, B. Wang, P. E. Monahan, J. E. Rabinowitz, J. C. Grieger, L. Govindasamy, M. Agbandje-McKenna, X. Xiao, R. J. Samulski, *Mol. Ther.* **2012**, *20*, 443.
- [45] Y. Durocher, P. L. Pham, G. St-Laurent, D. Jacob, B. Cass, P. Chahal, C. J. Lau, J. Nalbantoglu, A. Kamen, *J. Virol. Methods* **2007**, *144*, 32.
- [46] M. Hildinger, L. Baldi, M. Stettler, F. M. Wurm, *Biotechnol. Lett.* **2007**, *29*, 1713.
- [47] J. Y. Park, B. P. Lim, K. Lee, Y. G. Kim, E. C. Jo, *Biotechnol. Bioeng.* **2006**, *94*, 416.
- [48] D. L. Thomas, L. Wang, J. Niamke, J. Liu, W. Kang, M. M. Scotti, G.-J. Ye, G. Veres, D. R. Knop, *Hum. Gene Ther.* **2009**, *20*, 861.
- [49] M. G. Aucoin, M. Perrier, A. A. Kamen, *Biotechnol. Adv.* **2008**, *26*, 73.
- [50] V. V. Emmerling, A. Pegel, E. G. Milian, A. Venereo-Sanchez, M. Kunz, J. Wegele, A. A. Kamen, S. Kochanek, M. Hoerer, *Biotechnol. J.* **2016**, *11*, 290.
- [51] F. Collaud, G. Bortolussi, L. Guianvarc'h, S. J. Aronson, T. Bordet, P. Veron, S. Charles, P. Vidal, M. S. Sola, S. Rundwasser, D. G. Dufour, F. Lacoste, C. Luc, L. V. Wittenberghe, S. Martin, C. Le Bec, P. J. Bosma, A. F. Muro, G. Ronzitti, M. Hebben, F. Mingozzi, *Mol. Ther. Methods Clin. Dev.* **2019**, *12*, 157.
- [52] S. Zolotukhin, B. J. Byrne, E. Mason, I. Zolotukhin, M. Potter, K. Chesnut, C. Summerford, R. J. Samulski, N. Muzyczka, *Gene Ther.* **1999**, *6*, 973.
- [53] B. Strobel, F. D. Miller, W. Rist, T. Lamla, *Hum. Gene Ther. Methods* **2015**, *26*, 147.
- [54] J. C. Grieger, V. W. Choi, R. J. Samulski, *Nat. Protoc.* **2006**, *1*, 1412.
- [55] L. Tenenbaum, M. Hamdane, M. Pouzet, B. Avalosse, A. Stathopoulos, F. Jurysta, C. Rosenbaum, C. O. Hanemann, M. Levivier, T. Velu, *Gene Ther.* **1999**, *6*, 1045.

- [56] W. T. Hermens, O. ter Brake, P. A. Dijkhuizen, M. A. Sonnemans, D. Grimm, J. A. Kleinschmidt, J. Verhaagen, *Hum. Gene Ther.* **1999**, *10*, 1885.
- [57] L. E. Larsen, I. F. Heglund, R. Fabian, P. Walday, W. F. Blazak, *Acta Radiol. Suppl.* **1995**, *36*, 238.
- [58] M. Andreucci, T. Faga, R. Serra, G. De Sarro, A. Michael, *Drug. Healthc. Patient Saf.* **2017**, *9*, 25.
- [59] S. M. Crosson, P. Dib, J. K. Smith, S. Zolotukhin, *Mol. Ther. Methods Clin. Dev.* **2018**, *10*, 1.
- [60] R. O. Snyder, J. Francis, *Curr. Gene Ther.* **2005**, *5*, 311.
- [61] G. Chadeuf, C. Ciron, P. Moullier, A. Salvetti, *Mol. Ther.* **2005**, *12*, 744.
- [62] C. Wang, S. H. R. Mulagapati, Z. Chen, J. Du, X. Zhao, G. Xi, L. Chen, T. Linke, C. Gao, A. E. Schmelzer, D. Liu, *Mol. Ther. Methods Clin. Dev.* **2019**, *15*, 257.
- [63] D. B. Howard, B. K. Harvey, *Hum. Gene Ther. Methods* **2017**, *28*, 39.
- [64] K. Tamayose, Y. Hirai, T. Shimada, *Hum. Gene Ther.* **1996**, *7*, 507.
- [65] D. Debelak, J. Fisher, S. Iuliano, D. Sesholtz, D. L. Sloane, E. Matkinson, *J. Chromatogr. B. Biomed. Sci. Appl.* **2000**, *740*, 195.
- [66] G. Gao, G. Qu, M. S. Burnham, J. Huang, N. Chirmule, B. Joshi, Q. C. Yu, J. A. Marsh, C. M. Conceicao, J. M. Wilson, *Hum. Gene Ther.* **2000**, *11*, 2079.
- [67] C. R. O'Riordan, A. L. Lachapelle, K. A. Vincent, S. C. Wadsworth, *J. Gene Med.* **2000**, *2*, 444.
- [68] N. Brument, R. Morenweiser, V. Blouin, E. Toublanc, I. Raimbaud, Y. Chérel, S. Folliot, F. Gaden, P. Boulanger, G. Kroner-Lux, P. Moullier, F. Rolling, A. Salvetti, *Mol. Ther.* **2002**, *6*, 678.
- [69] R. H. Smith, J. R. Levy, R. M. Kotin, *Mol. Ther.* **2009**, *17*, 1888.
- [70] R. H. Smith, L. Yang, R. M. Kotin, *Methods Mol. Biol.* **2008**, *434*, 37.
- [71] G. Qu, J. Bahr-Davidson, J. Prado, A. Tai, F. Cataniag, J. McDonnell, J. Zhou, B. Hauck, J. Luna, J. M. Sommer, P. Smith, S. Zhou, P. Colosi, K. A. High, G. F. Pierce, J. F. Wright, *J. Virol. Methods* **2007**, *140*, 183.
- [72] T. Okada, M. Nonaka-Sarukawa, R. Uchibori, K. Kinoshita, H. Hayashita-Kinoh, Y. Nitahara-Kasahara, S. Takeda, K. Ozawa, *Hum. Gene Ther.* **2009**, *20*, 1013.
- [73] M. Urabe, T. Nakakura, K. Q. Xin, Y. Obara, H. Mizukami, A. Kume, R. M. Kotin, K. Ozawa, *J. Virol.* **2006**, *80*, 1874.
- [74] M. Urabe, K. Q. Xin, Y. Obara, T. Nakakura, H. Mizukami, A. Kume, K. Okuda, K. Ozawa, *Mol. Ther.* **2006**, *13*, 823.
- [75] N. Kaludov, B. Handelman, J. A. Chiorini, *Hum. Gene Ther.* **2002**, *13*, 1235.
- [76] C. Summerford, R. J. Samulski, *J. Virol.* **1998**, *72*, 1438.
- [77] Z. Wu, A. Asokan, J. C. Grieger, L. Govindasamy, Z. Wu, A. Asokan, J. C. Grieger, L. Govindasamy, M. Agbandje-McKenna, R. Jude Samulski, *J. Virol.* **2006**, *80*, 11393.
- [78] N. K. Paulk, K. Pekrun, E. Zhu, S. Nygaard, B. Li, J. Xu, K. Chu, C. Leborgne, A. P. Dane, A. Haft, Y. Zhang, F. Zhang, C. Morton, M. B. Valentine, A. M. Davidoff, A. C. Nathwani, F. Mingozzi, M. Grompe, I. E. Alexander, L. Lisowski, M. A. Kay, *Mol. Ther.* **2018**, *26*, 289.
- [79] M. Mietzsch, S. Grasse, C. Zurawski, S. Weger, A. Bennett, M. Agbandje-McKenna, N. Muzyczka, S. Zolotukhin, R. Heilbronn, *Hum. Gene Ther.* **2014**, *25*, 212.
- [80] S. A. Nass, M. A. Mattingly, D. A. Woodcock, B. L. Burnham, J. A. Ardinger, S. E. Osmond, A. M. Frederick, A. Scaria, S. H. Cheng, C. R. O'Riordan, *Mol. Ther. Methods Clin. Dev.* **2018**, *9*, 33.
- [81] Q. Wang, M. Lock, A. J. Prongay, M. R. Alvira, B. Petkov, J. M. Wilson, *Mol. Ther. Methods Clin. Dev.* **2015**, *2*, 15040.
- [82] A. M. Davidoff, C. Y. Ng, S. Sleep, J. Gray, S. Azam, Y. Zhao, J. H. McIntosh, M. Karimipoor, A. C. Nathwani, *J. Virol. Methods* **2004**, *121*, 209.
- [83] M. Lock, M. R. Alvira, J. M. Wilson, *Hum. Gene Ther. Methods* **2012**, *23*, 56.
- [84] P. F. Schmit, S. Pacouret, E. Zinn, E. Telford, F. Nicolaou, F. Broucque, E. Andres-Mateos, R. Xiao, M. Penaud-Budloo, M. Bouzelha, N. Jaulin, O. Adjali, E. Ayuso, L. H. Vandenberghe, *Mol. Ther. Methods Clin. Dev.* **2020**, *17*, 107.
- [85] X. Jin, L. Liu, S. Nass, C. O'Riordan, E. Pastor, X. K. Zhang, *Hum. Gene Ther. Methods* **2017**, *28*, 255.
- [86] T. R. Flotte, *Hum. Gene Ther.* **2017**, *28*, 147.
- [87] B. Dong, X. Duan, H. Y. Chow, L. Chen, H. Lu, W. Wu, B. Hauck, F. Wright, P. Kapranov, W. Xiao, *PLoS One* **2014**, *9*, e86453.
- [88] C. Vandamme, O. Adjali, F. Mingozzi, *Hum. Gene Ther.* **2017**, *28*, 1061.
- [89] K. Gao, M. Li, L. Zhong, Q. Su, J. Li, S. Li, R. He, Y. Zhang, G. Hendricks, J. Wang, G. Gao, *Mol. Ther. Methods Clin. Dev.* **2014**, *1*, 9.
- [90] F. Mingozzi, X. M. Anguela, G. Pavani, Y. Chen, R. J. Davidson, D. J. Hui, M. Yazicioglu, L. Elkouby, C. J. Hinderer, A. Faella, C. Howard, A. Tai, G. M. Podsakoff, S. Zhou, E. Basner-Tschakarjan, J. F. Wright, K. A. High, *Sci. Transl. Med.* **2013**, *5*, 194ra92.
- [91] E. Arden, J. M. Metzger, *J. Biol. Methods* **2016**, *3*, 38.
- [92] L. Yang, J. Jiang, L. M. Drouin, M. Agbandje-McKenna, C. Chen, C. Qiao, D. Pu, X. Hu, D.-Z. Wang, J. Li, X. Xiao, *Proc. Natl. Acad. Sci. U. S. A.* **2009**, *106*, 3946.
- [93] Y. Mao, X. Wang, R. Yan, W. Hu, A. Li, S. Wang, H. Li, *BMC Biotechnol.* **2016**, *16*, 1.
- [94] L. R. Lee, L. Peacock, L. Lisowski, D. G. Little, C. F. Munns, A. Schindeler, *Mol. Ther. Methods Clin. Dev.* **2019**, *15*, 101.
- [95] E. Senís, L. Mosteiro, S. Wilkening, E. Wiedtke, A. Nowrouzi, S. Afzal, R. Fronza, H. Landerer, M. Abad, D. Niopek, M. Schmidt, M. Serrano, D. Grimm, *Nat. Commun.* **2018**, *9*, 2651.
- [96] C. Yin, T. Zhang, X. Qu, Y. Zhang, R. Putatunda, X. Xiao, F. Li, W. Xiao, H. Zhao, S. Dai, X. Qin, X. Mo, W.-B. Young, K. Khalili, W. Hu, *Mol. Ther.* **2017**, *25*, 1168.
- [97] M. Jang, S. E. Lee, I. H. Cho, *Front. Cell. Neurosci.* **2018**, *12*, 157.
- [98] M. Candelas, A. Reynders, M. Arango-Lievano, C. Neumayer, M. Candelas, A. Reynders, M. Arango-Lievano, C. Neumayer, A. Fruquière, E. Demes, J. Hamid, C. Lemmers, C. Bernat, A. Monteil, V. Compan, S. Laffray, P. Inquimbert, Y. Le. Feuvre, G. W. Zamponi, A. Moqrich, E. Bourinet, P.-F. Méry, *Sci. Rep.* **2019**, *9*, 3112.
- [99] H. Hashimoto, T. Mizushima, T. Chijiwa, M. Nakamura, H. Suemizu, *Virus Res.* **2017**, *238*, 63.
- [100] P. Guo, X. Xiao, Y. El-Gohary, J. Paredes, K. Prasadana, C. Shiota, J. Wiersch, C. Welsh, G. K. Gittes, *Bioengineered* **2013**, *4*, 103.
- [101] T. Kimura, B. Ferran, Y. Tsukahara, Q. Shang, S. Desai, A. Fedoce, D. R. Pimentel, I. Luptak, T. Adachi, Y. Ido, R. Matsui, M. M. Bachschmid, *Sci. Rep.* **2019**, *9*, 13601.
- [102] Z. Yu, S. Zhou, N. Luo, C. Y. Ho, M. Chen, H. Chen, *Mol. Ther. Methods Clin. Dev.* **2020**, *17*, 34.
- [103] T. Kikusui, M. Kajita, N. Otsuka, T. Hattori, K. W. A. Kumazawa, M. Nagasawa, A. Inutsuka, A. Yamanak, N. Matsuo, H. E. Covington, K. Mogi, *Behav. Brain Res.* **2018**, *346*, 96.
- [104] S. Y. Yoo, S. N. Jeong, J. I. Kang, S. W. Lee, *ACS Omega* **2018**, *3*, 5918.
- [105] C. X. Zhang, M. M. Meagher, *Methods Mol. Biol.* **2019**, *1972*, 263.
- [106] M. Salganik, B. Venkatakishnan, A. Bennett, B. Lins, J. Yarbrough, N. Muzyczka, M. Agbandje-McKenna, R. McKenna, *J. Virol.* **2012**, *86*, 11877.
- [107] S. Murray, C. L. Nilsson, J. T. Hare, M. R. Emmett, A. Korostelev, H. Ongley, A. G. Marshall, M. S. Chapman, *J. Virol.* **2006**, *80*, 6171.
- [108] A. Aloor, J. Zhang, E. A. Gashash, A. Parameswaran, M. Chrzanowski, C. Ma, Y. Diao, P. G. Wang, W. Xiao, *Viruses* **2018**, *10*, 644.
- [109] A. R. Giles, J. J. Sims, K. B. Turner, L. Govindasamy, M. R. Alvira, M. Lock, J. M. Wilson, *Mol. Ther.* **2018**, *26*, 2848.
- [110] B. Mary, S. Maurya, S. Arumugam, V. Kumar, G. R. Jayandharan, *FEBS J.* **2019**, *286*, 4964.
- [111] K. Van Vliet, Y. Mohiuddin, S. McClung, V. Blouin, F. Rolling, P. Moullier, M. Agbandje-McKenna, R. O. Snyder, *J. Virol. Methods* **2009**, *159*, 167.

- [112] J. Snijder, M. van de Waterbeemd, E. Damoc, E. Denisov, D. Grinfeld, A. Bennett, M. Agbandje-McKenna, A. Makarov, A. J. R. Heck, *J. Am. Chem. Soc.* **2014**, *136*, 7295.
- [113] E. E. Pierson, D. Z. Keifer, A. Asokan, M. F. Jarrold, *Anal. Chem.* **2016**, *88*, 6718.
- [114] Y. Zhang, Y. Wang, Z. Sosic, L. Zang, S. Bergelson, W. Zhang, *Biochem* **2018**, *555*, 22.
- [115] V. Rayaprolu, S. Kruse, R. Kant, B. Venkatakrishnan, N. Movahed, D. Brooke, B. Lins, A. Bennett, T. Potter, R. McKenna, M. Agbandje-McKenna, B. Bothner, *J. Virol.* **2013**, *87*, 13150.
- [116] A. Bennett, S. Patel, M. Mietzsch, A. Jose, B. Lins-Austin, J. C. Yu, B. Bothner, R. McKenna, M. Agbandje-McKenna, *Mol. Ther. Methods Clin. Dev.* **2017**, *6*, 171.
- [117] S. Pacouret, M. Bouzelha, R. Shelke, E. Andres-Mateos, R. Xiao, A. Maurer, M. Mevel, H. Turunen, T. Barungi, M. Penaud-Budloo, F. Broucq, V. Blouin, P. Moullier, E. Ayuso, L. H. Vandenberghe, *Mol. Ther.* **2017**, *25*, 1375.
- [118] L. Rieser, M. Penaud-Budloo, M. Bouzelha, A. Rossi, R. Rieser, M. Penaud-Budloo, M. Bouzelha, A. Rossi, T. Menzen, M. Biel, H. Büning, E. Ayuso, G. Winter, S. Michalakis, *J. Pharm. Sci.* **2020**, *109*, 854.
- [119] L. Kondratova, O. Kondratov, R. Ragheb, S. Zolotukhin, *Mol. Ther. Methods Clin. Dev.* **2019**, *15*, 112.
- [120] M. Dawson, *BET White Paper*, Associates of Cape Cod, Inc., East Falmouth, MA **2017**, pp. 1.
- [121] J. Tordo, C. O'Leary, A. Antunes, N. Palomar, P. Aldrin-Kirk, M. Basche, A. Bennett, Z. D'Souza, H. Gleitz, A. Godwin, R. J. Holley, H. Parker, A. Y. Liao, P. Rouse, A. S. Youshani, L. Dridi, C. Martins, T. Levade, K. B. Stacey, D. M. Davis, A. Dyer, N. Clément, T. Björklund, R. R. Ali, M. Agbandje-McKenna, A. A. Rahim, A. Pshezhetsky, S. N. Waddington, R. M. Linden, B. W. Bigger, E. Henckaerts, *Brain* **2018**, *141*, 2014.
- [122] W. Y. Shen, Y. K. Lai, C. M. Lai, P. E. Rakoczy, *Vision Res.* **2004**, *44*, 339.
- [123] K. Borner, E. Kienle, L. Y. Huang, J. Weinmann, A. Sacher, P. Bayer, C. Stüllein, J. Fakhiri, L. Zimmermann, A. Westhaus, J. Beneke, N. Beil, E. Wiedtke, C. Schmela, D. Miltner, A. Rau, H. Erfle, H.-G. Kräusslich, M. Müller, M. Agbandje-McKenna, D. Grimm, *Mol. Ther.* **2020**, *28*, 1016.
- [124] M. Penaud-Budloo, E. Lecomte, A. Guy-Duche, S. Saleun, A. Roulet, C. Lopez-Roques, B. Tournaire, B. Cogné, A. Léger, V. Blouin, P. Lindenbaum, P. Moullier, E. Ayuso, *Hum. Gene Ther. Methods* **2017**, *28*, 148.
- [125] E. Lecomte, A. Leger, M. Penaud-Budloo, E. Ayuso, *Methods Mol. Biol.* **2019**, *1950*, 85.
- [126] L. H. Maynard, O. Smith, N. P. Tilmans, E. Tham, W. T. Hosseinzadeh, R. Leenay, A. P. May, N. K. Paulk, *Hum. Gene Ther. Methods* **2019**, *30*, 195.
- [127] J. Xie, Q. Mao, P. W. L. Tai, R. He, J. Ai, Q. Su, Y. Zhu, H. Ma, J. Li, S. Gong, D. Wang, Z. Gao, M. Li, L. Zhong, H. Zhou, G. Gao, *Mol. Ther.* **2017**, *25*, 1363.
- [128] L. V. Tse, K. A. Klinc, V. J. Madigan, C. Rivera, R. M., L. F. Wells, L. P. Havlik, J. K. Smith, M. Agbandje-McKenna, A. Asokan, *Proc. Natl. Acad. Sci. U. S. A.* **2017**, *114*, E4812.
- [129] P. J. Ogden, E. D. Kelsic, S. Sinai, G. M. Church, *Science* **2019**, *366*, 1139.



Jihad EL Andari has obtained a Ph.D. in Molecular Microbiology from the University of Freiburg (Germany). Following a postdoctoral stint at the Center of Synthetic Microbiology (SYNMIKRO) at the University of Marburg (Germany), he is now a senior postdoctoral fellow in the laboratory of Dirk Grimm at the medical faculty and BioQuant center of the University of Heidelberg (Germany). His current research focuses on AAV capsid engineering with the aim to develop novel synthetic vectors for safe and efficient therapeutic gene delivery to the human musculature and the central nervous system.



Dirk Grimm holds the Professorship for Viral Vector Technologies at the medical faculty of the University of Heidelberg (Germany). For over 25 years including a six-year postdoctoral stint at Stanford University (CA, USA), his research has been dedicated to the engineering of Adeno-associated virus (AAV) capsids and genomes towards novel human gene therapy vectors with superior efficiency, specificity and safety. To this end, his team including Dr. El Andari applies a wide variety of state-of-the-art technologies for AAV diversification, production, and high-throughput in vivo screening in small or large animals, comprising next-generation sequencing, barcoding, single-cell RNA sequencing, and machine learning.

Process evolution in cell and gene therapy from discovery to commercialization

Elizabeth Csaszar¹ | Sara Mills² | Peter W. Zandstra^{1,3,4}

¹Notch Therapeutics, Toronto, Ontario, Canada

²Dark Horse Consulting Group, Inc., Walnut Creek, California

³Michael Smith Laboratories, University of British Columbia, Vancouver, British Columbia, Canada

⁴School of Biomedical Engineering, University of British Columbia, Vancouver, British Columbia, Canada

Correspondence

Elizabeth Csaszar, Notch Therapeutics, Toronto, ON Canada.
Email: lcsaszar@notchtx.com

Abstract

The field of cell and gene therapy (CGT) is maturing at a rapid rate. Manufacturing remains a major challenge and manufacturing failures and limitations are a notable source of CGT products not meeting specification or being held back from regulatory approvals. To ensure that products remain compliant and competitive throughout their lifecycle, CGT process development requires both ongoing advancement of fit-for-purpose technologies to allow for and support well-designed development studies, and a methodology that enables these studies to occur effectively during focused product development campaigns. We describe a framework for ongoing innovation in CGT process development, manufacturing, and clinical testing, based on the quality by design (QbD) approach. We propose use of the concepts of process discovery, process characterization, and process development in an iterative way to refine the design space as a product matures. This strategy is enabled by the early implementation of broad and robust analytics, and a modular approach to accelerate optimization. With these strategies, CGT developers can prospectively plan for comparability studies and develop in a stage-appropriate manner, to allow for ongoing innovation and improvements from discovery through to commercialization.

KEYWORDS

cell analytics, cell therapy, manufacturing, process development, quality by design

1 | MANUFACTURING OF CELL AND GENE THERAPY PRODUCTS REQUIRES A FRAMEWORK TO SUPPORT CONTINUING INNOVATION

The field of cell and gene therapy (CGT) encompasses advanced therapeutics including living cells, tissues, viral vectors, and non-viral gene modifying components. The CGT industry is growing at a rapid rate. As of 2020, there were reported to be more than 1000 active CGT clinical trials^[1] and revenue in the CGT market is predicted to grow at a compound annual growth rate (CAGR) of more than 30% between 2019–2025.^[2] Much of this recent

growth comes from gene therapies targeting monogenic disorders, and gene modified cell therapies in the immune-oncology field, particularly chimeric antigen receptor T-cell (CAR-T cell) therapies. Through the past 5–10 years, positive clinical results and interest from investors and the pharmaceutical industry have led to an accelerated pace of activity as companies work to achieve aggressive milestones. A key challenge that has been created by this rapid growth is the need to manufacture CGT products in a robust and stage-appropriate manner throughout the product development lifecycle, while still allowing for the incorporation of innovation.

Manufacturing failures are a notable source of CGT products not meeting specification and not being

delivered to patients, and chemistry, manufacturing, and controls (CMC) concerns are a major reason for CGT products being held back from regulatory approvals. Several companies have publicly acknowledged recent CMC-related challenges in late-stage interactions with regulators,^[3] including the refusal to file that Bristol Myers Squibb received on their Biologics License Application (BLA) for their ide-cel CAR-T product in 2020.^[4] For autologous or patient specific products, a manufacturing failure can mean that the patient is unable to receive the therapeutic, or out-of-specification products may be administered without companies being reimbursed.^[5] Novartis has reported that their on-market CAR-T product, Kymriah, has an approximately 10% rate of products not shipping to patients, due to manufacturing failures or products being out-of-specification,^[6] with additional out-of-specification products being administered without reimbursement. For allogeneic CGT products, where large batches of products are produced to treat many patients, a manufacturing failure may not have immediate clinical repercussions, but it can have a large financial impact.^[7] Manufacturing innovations and the incorporation of new technology solutions during product development and clinical studies are important to ensure that when a product reaches market approval it remains compliant, competitive, and cost efficient.

Manufacturing solutions for CGT products are non-standard. They are still emerging and typically evolve with industry offerings and clinical stage. Further innovations around manufacturing are a focus area for academic and tool and reagent company research and development (R&D) and are an important differentiator amongst products and a core part of companies' pipeline and IP strategies. Several categories of manufacturing challenges are common across CGT products. CGT products often have a complex composition that is highly specific to the individual, some being comprised of a patient's own cells or a precisely matched donor. These living drugs are often made from highly variable cell-based raw materials and the manufacturing steps may require skilled manual manipulations and a strategy to address inherent biological variability in cell growth and characterization. The final cell or gene products are typically fragile, may have short shelf lives, and require a carefully controlled supply chain. The biological mechanisms of these products are also very complex and highly dependent on in vivo interactions upon delivery to the patient,^[8,9] making relevant manufacturing release criteria challenging to define.

As the field of CGT matures, approaches are being developed to reduce manufacturing complexity and variability in several ways. One example is the increased focus on allogeneic cell therapy products as a step

towards producing off-the-shelf products.^[10,11] These have the potential to simplify manufacturing by standardizing input material and reducing supply chain complexities. Raw material suppliers are evolving to focus on chemically defined and animal-component free products to improve consistency and ensure a sufficient standard of quality,^[12,13] and supply chain solutions are supporting wide-reaching distribution with appropriate traceability.^[14,15] Industrial bioprocess strategies adapted from more mature biologics fields are starting to be implemented in CGT manufacturing.^[16,17] The incorporation of these strategies with increased rigour are critical for the evolution of CGT to a more mature and robust field.

To complement the maturation of CGT manufacturing, the approach to process development must also mature. This will require both ongoing advancement of fit-for-purpose technologies to allow for and support well-designed development studies, and a methodology that enables these studies to occur effectively during focused product development campaigns. Here, we propose a framework for ongoing stage-appropriate innovation in CGT process development and manufacturing, based on the quality by design (QbD) approach and its inherent iterative nature to better allow for incorporation of both technology-based improvements and discovery biology-based insights throughout the product development and commercialization lifecycle.

2 | THE QbD STRUCTURE GUIDES ITERATIVE REFINEMENT OF PROCESS DESIGN SPACE THROUGH THE PRODUCT DEVELOPMENT LIFECYCLE

In the early development stages of CGT products, there is incomplete or limited knowledge of the mode of action (MoA) and the target product profile (TPP). Early clinical data is used to refine the TPP, allowing for ongoing enhancement of understanding of the product, and the ability to identify and hone the critical quality attributes (CQAs) of the manufacturing process. However, much of this knowledge does not come until quite late in the product's development cycle. In order to guide pre-clinical development, an initial early draft of the TPP and associated CQAs should be defined. However, the TPP and CQAs are not fixed from early development, but instead should undergo an iterative refinement where the initially very broad TPP₁ is refined and narrowed through iterative cycles, leading to TPP₂, TPP₃,... TPP_{final} as more data is collected and the understanding of the cell product increases (Figure 1A).

QbD is a useful framework to guide CGT development and manufacturing.^[18,19] Developers use the identified TPP and CQAs to establish the process design space. This refers to the parameter space over which a process can be optimized to achieve the CQAs. At the beginning of the product development cycle, this design space can be very large as specifics of the CQAs may be unknown or poorly understood. For example, developers may be exploring large ranges of cell densities, numerous media and additive compositions, and various feeding regimes for a cell culture process. In this initial phase, data should be collected to better understand how these process parameters impact cell yields, viabilities, phenotypes, gene expression profiles, and functional outputs. At this stage, the criteria for a minimally acceptable TPP are quite broad. As these correlations between process inputs and cell outputs are developed, critical process parameters (CPPs) can be identified (typically the parameters whose sensitivities most significantly impact the TPPs) and CQAs are further refined through a feedback cycle. This in turn reduces the size of the design space and the next iteration of process optimization can focus on refinement of a smaller number of parameters. Mirroring the refinement of the TPP, the design space also becomes more focused over time, although never narrowing so much as to leave no room for minor adjustments even in advanced manufacturing stages (Figure 1B). Although beyond the scope of this commentary, statistical frameworks for the design space optimization exist in other fields and may be applicable to CGT.^[20,21]

To support this approach of an evolving design space framework, three iterative CGT product development stages can be considered: (1) process discovery, (2) process

characterization, and (3) process development (Table 1). Process discovery refers to identifying key process parameters that impact the fundamental biology of the system. Process characterization includes building datasets of inputs and outputs of each unit operation and their sensitivity to process parameters. Finally, process development involves using the outcomes of process characterization to optimize a component of the manufacturing process such that CQAs are more robustly achieved (or conversely, that the process is made more efficient, more consistent, or more cost effective while maintaining current status of CQAs). In doing so, process knowledge is gained, and the design space becomes better defined and aligned with the TPP and CQAs. These steps can then be iterated on, beginning with this more refined design space and continuing to move through this cycle.

3 | BROAD AND HIGH-RESOLUTION ANALYTICS ARE THE CORNERSTONE TO ENABLE ITERATIVE DEVELOPMENT

Analytics are essential for process discovery, process characterization, and process development. Therapeutic developers are well served to put substantial effort into building cell and molecular analytics for all stages of their manufacturing process early in development. In initial stages, characterization assays need to be broad enough to span a large, multi-dimensional design space. It is useful to characterize on- and off-target cells, capture run-to-run variability and general system robustness, and explore all characteristics of cells that may impact

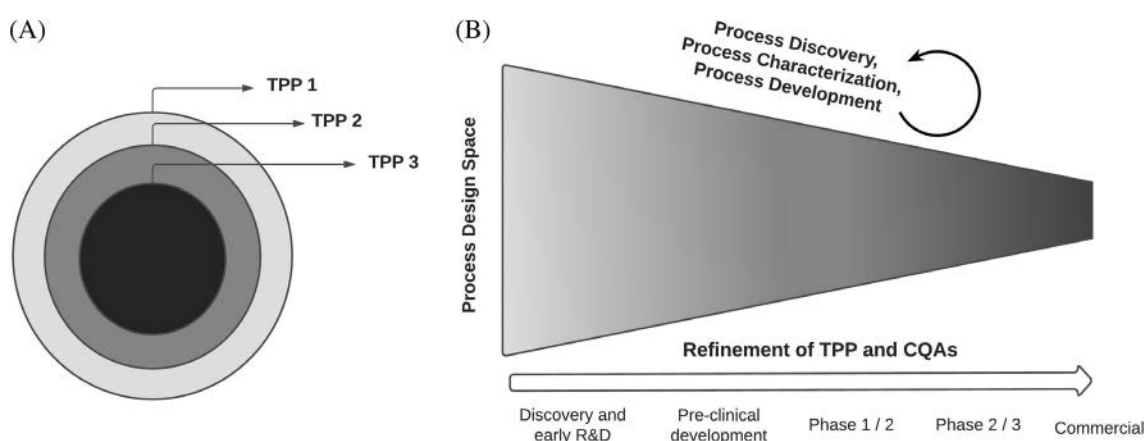


FIGURE 1 Iterative refinement of target product profile, critical quality attributes (CQAs), and process design space. (A) The target product profile (TPP) undergoes a series of refinements through the stages of process and product development. As clinical data is collected, understanding of the cell product increases and the TPP becomes more focused and directly tied to clinical efficacy (TPP1 → TPP2 → TPP3). (B) As the TPP and associated CQAs are refined, the process design space also narrows, allowing for the next iteration of more focused development

TABLE 1 Concepts to guide an iterative approach to development using QbD

Term	Definition	Example of this strategy being used in the development of a multi-stage differentiation process for a cell therapy product
Process discovery	Exploratory science to identify key process parameters that impact the fundamental biology of the system	Perform RNA-Seq on cell samples from many timepoints during a lengthy multi-stage differentiation process to identify the genomic signature of intermediate cell populations, and to trace product developmental lineage. Use computational tools to relate this data to developmental biology to inform strategies for new signalling pathways to modulate with the aim of improving differentiation efficiencies and identifying key intermediate developmental stages for modularity.
Process characterization	Generation of data of inputs and outputs of each unit operation or modular unit and their sensitivity to process parameters	Collect targeted PCR, flow cytometry data or similar during development studies to build datasets describing ranges of cell parameters responsive to process conditions and to determine run-to-run variability, process sensitivities, and impact on final cell output and function. Use this data in a risk-based approach to identify process parameters that require improved control.
Process development	Optimize a component of the manufacturing process such that CQAs are more robustly achieved, or the process is made more efficient, consistent, or cost effective while maintaining CQAs	Perform well-defined studies to evaluate and optimize process parameters, such as cell seeding densities, feeding regimes, or cytokine additions, to achieve the desired cell characteristics known to be important for cell function. Incorporate automation or new process technology using the quantitative framework developed.

Abbreviations: CQA, critical quality attribute; PCR, polymerase chain reaction; QbD, quality by design; RNA-Seq, RNA sequencing.

potency. Critical assays should be put in place and standardized to the greatest extent possible prior to process development activities so that assays are not evolving at the same time as process changes are being explored. Although assays used early in the R&D cycle are typically not qualified, it is important that they are sufficiently robust and consistent to ensure the ability to determine whether differences measured between process conditions are relevant and significant.

Cell characterization in the CGT field is often performed at quite a low throughput and low-resolution manner where bulk cell populations are tracked with a small number of parameters, such as surface marker expression by flow cytometry, without a good understanding of which parameters are responsive to process variability and process quality. In order to explore the design space more broadly in a detailed way, more sophisticated high resolution and single cell based analytic techniques, such as single cell RNA-Seq, and proteomic and metabolomic analysis of cells and culture components should be more routinely used by the CGT field.^[22–24] Using a broad range of analytics for characterization enables the discovery of the most relevant CQAs that can then be routinely monitored and serve as the basis of process development.

In addition to a diverse set of analytics, a robust testing panel should also be multi-dimensional in nature, leveraging multiple methods to assess the same CQAs. This orthogonal approach (i.e., using more than one independent method to measure similar attributes) is even more critical when developing an understanding and definition of drug product potency.

Robust analytics create the ability to implement tracking and trending of the process, in order to monitor CQAs through development and identify both intentional changes and unintentional drifts. These datasets form the basis of early process characterization and help to define the process optimization strategy. CGT developers may tend to defer process characterization to later stages of clinical development, but it is a valuable tool to implement early to build a development strategy. In pre-clinical development stages, simple studies and additional data collection can be incorporated to begin to build process understanding. By making this a focus in early process development work, it will be easier to make risk-based decisions on process changes and integrate technology solutions over time. During later product development, a very focused subset of these broad analytics will form the foundation of a minimal set of clinical

release assays. Additionally, if the product format allows, developers should retain samples from critical early development lots (e.g., those used in investigational new drug [IND]-enabling nonclinical and early clinical studies) to allow for retrospective analysis in the future, as product understanding and the quality and robustness of product analytical characterization improves during development.

Cell characterization data can also feed into process simulations as a complementary tool to explore and refine the design space.^[25–27] Outputs from computational models will help to identify key parameters more effectively and rapidly for experimentation and optimization by highlighting the sensitivity of the process to different parameters. For example, modelling of a differentiation process based on initial experimental conditions may lead to a hypothesis that maintaining a specific cell intermediate phenotype within upper and lower bounds is important for efficient subsequent differentiation and mature cell function. This then guides next experimental steps and constrains the design space around this refined target. Computational tools provide a way to move from multi-parameter high resolution data sets generated in the process discovery stage to a reduced number of specific parameters to be evaluated during experimental process development. Further formalization of how analytical and computational approaches can support design space refinement is an important area of ongoing strategic development for CGT.

4 | PROCESS MODULARITY ALLOWS FOR MORE RAPID ITERATIVE OPTIMIZATION

CGT manufacturing processes are often multistage processes with many unit operations, spanning several days to several months. In some cases, cells must pass through very specific intermediate stages, whether it be through a differentiation process, an activation step, or a selection or depletion of specific cell types. With increasing interest in off-the-shelf cell products, manufacturing process may include additional gene modification steps and lengthy cell expansion phases. Having a manufacturing process that is modular with well defined intermediates and process pause points is important to allow for innovation.

In a highly modular process, a complex manufacturing scheme can be thought of as a set of simplified building blocks which can each be independently optimized (Figure 2). To achieve this, each modular block must be clearly defined with CQAs governing its inputs and outputs. This allows for the improvements made to a single stage to be slotted into the full process with confidence

that re-optimization of subsequent stages is not likely to be required. Some process steps are easily suited to this modular consideration, such as a cryopreservation step or a magnetic cell enrichment. Multi-stage cell differentiation processes also benefit greatly from a modular optimization strategy. Enabling this approach requires sufficient knowledge of cell identity at each stage, and this requires high quality analytics (potentially including techniques like developmental lineage tracing^[28]) implemented early in a development program. The modular units can each be thought of as having a defined intermediate cell population as the output of the module, for which a target cell profile can be developed. This then enables the same iterative framework of design space refinement to be applied to these smaller process modules.

The process complexity of many CGT products also limits early R&D activities as research teams are limited in the quantity and consistency of material available for functional testing and detailed characterization. Modularity, and built-in in process pause points, provide a strategy for internal supply-chain optimization via the generation of consistent product or intermediates to be produced at greater quantity and/or robustness. Cell materials can be produced to feed into optimization studies at multiple points of the process such that input material supply does not limit discovery efforts.

5 | A STAGE-APPROPRIATE DEVELOPMENT STRATEGY MAINTAINS AGILITY WHILE CONTEMPLATING COMMERCIAL MANUFACTURING AND COMPARABILITY REQUIREMENTS

As CGT products progress through development stages, discovery teams generate new biological insights and learnings to enhance, modify, and improve therapies in development. The generation of pre-clinical and clinical data refines the understanding of the MoA and TPP of the drug product, allowing CGT developers to further innovate to improve the efficacy, safety, and/or consistency of their products. However, the benefits of iterative discovery biology can be hard to reconcile with the required structure and standardization of process development and manufacturing.

Due to the importance and challenges of developing robust manufacturing strategies for CGT products, the field has tended to promote a view that manufacturing solutions must be developed, implemented, and finalized as early as possible in the product development timeline. If substantial process changes are made, developers must be able to justify how these process changes will impact or alter the safety and efficacy profiles that were established

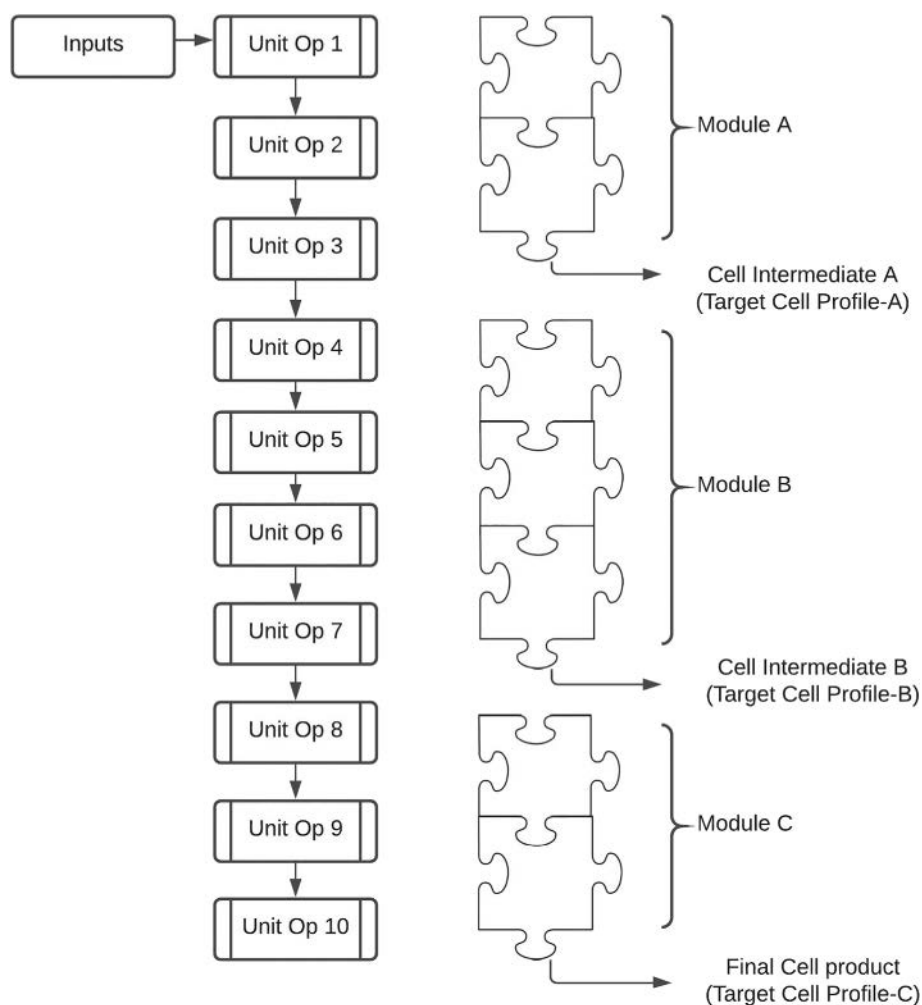


FIGURE 2 Modularity is beneficial for process development. In complex manufacturing processes, the process can be broken into modular units consisting of sets of unit operations for which a distinct intermediate input and output population can be defined. For each intermediate, a target cell profile can be determined that captures critical characteristics of the intermediate population's purity and identity. By aligning these intermediate populations with process pause points, each module can be independently and concurrently optimized

using the earlier process, and when the TPP and CQAs are still in development it can be difficult to identify the appropriate indicators by which to assess this impact. This burden to justify process changes becomes more onerous later into clinical development. As a result, CGT developers often avoid making substantial manufacturing changes or improvements.

However, this strategy of focusing on locking in manufacturing solutions creates notable limitations. CGT products often enter the market using manufacturing strategies that are suboptimal for the quantity, quality, and logistical needs to serve the intended patients, market size, and distribution, possibly limiting the potential clinical efficacy of the product. Newer manufacturing technologies that may introduce process consistencies through automation, enhanced monitoring and control, and improved data generation are not made use of even when they may provide an obvious benefit because of the onus of making the process change. New biological insights and discoveries may not be integrated into the product development because in typical process development approaches there is not a streamlined method to do so.

We propose that, in alignment with the ICH Guideline on Pharmaceutical Development,^[29] the CGT field should shift its thinking away from the idea that a final manufacturing process needs to be established as early as possible and instead use the iterative QbD framework of refining the process design space and CQAs through process discovery, process characterization, and process development. It is not necessary to design the product's commercial manufacturing process in early development. Instead, stage appropriate processes should be designed and then refined with a view towards later stage development and commercialization.

Rather than attempting to avoid the inevitable requirement to assess and determine comparability, the CGT field would benefit from planning the transition between stage-appropriate processes by prospectively designing their comparability study. Comparability does not require a piecemeal approach and multiple changes may be addressed simultaneously if the proper study design is assembled.^[30] The two most common misconceptions about comparability studies are that comparable should also be defined as identical and that setting

acceptance criteria for comparability on release specifications alone will be sufficient. The value of a diverse panel of orthogonal analytics is again highlighted when attempting to demonstrate comparability. This holds especially true with respect to the value of a matrices of analytics when building a narrative to describe potency (and MoA). The greater the knowledge of the design space gained from broad and high-resolution analytical characterization, the greater the confidence in product comparability. Furthermore, well understood in-process analytics will allow for real-time tracing of comparability throughout a modular process.

Planning a successful comparability study typically includes prospective communication with the regulatory authorities in order to gain early support of the proposed study design and statistical analysis plan. Obtaining such prospective concurrence will greatly mitigate the risk that the final data package is found to be insufficient to support a proposed process change. A final key consideration in planning for future comparability studies is maintenance of a robust retain program during early development. Retain samples will prove themselves invaluable in allowing for comparison of new process material to a larger number of old process lots, ideally including the specific lots used to gather critical nonclinical and early clinical data. Additionally, when introducing new or improved analytics, retain samples can be used to bridge data between two different test methods.

While the burden of comparability does increase with the stage of development, magnitude and anticipated impact of a particular change or change(s) and the strength of the available analytical package can make a significant impact on the nature (and magnitude) of a required comparability study. Process changes in early clinical development are quite common and generally addressable leveraging a paper-based and data driven justification. As clinical development progresses and a product enters phase 3 or pivotal trial, these changes can be much more challenging.

With the view that ongoing innovation in manufacturing development is beneficial and value adding, the costs and time to run well-staged comparability studies should be part of prospective planning. The QbD framework by which the TPP, CQAs, and design space are iteratively refined means that as the product matures and burden of comparability increases, the increased knowledge of the process enables a tightly controlled and focused comparability study guided by robust CQAs. Using these approaches, developers have a path to incorporate new technologies and new biological insights learned from current studies into the development and refinement of their process and CGT manufacturing can be open to allowing for ongoing innovation and improvements from discovery through to commercialization.

PEER REVIEW

The peer review history for this article is available at <https://publons.com/publon/10.1002/cjce.24141>.

REFERENCES

- [1] Alliance of Regenerative Medicine 2021 cell and gene state of the industry briefing, <http://alliancerm.org/wp-content/uploads/2021/01/SOTI-2021-pdf.pdf> (accessed: February 2021).
- [2] Cell & gene therapy market - global outlook and forecast 2020-2025, https://www.reportlinker.com/p05827567/Cell-and-Gene-Therapy-Market-Global-Outlook-and-Forecast.html?utm_source=GNW (accessed: February 2021).
- [3] 2020: The year the FDA ate our field for lunch (and why), <https://darkhorseconsultinggroup.com/2020-the-year-the-fda-and-why/> (accessed: February 2021).
- [4] FDA refuses to file BMS treatment over manufacturing concerns, <https://www.biopharma-reporter.com/article/2020/05/14/fda-refuses-to-file-bms-treatment> (accessed: March 2021).
- [5] A. Bersenev, S. Kili, *Cell and Gene Therapy Insights* **2018**, *4*, 1051.
- [6] Novartis still hasn't solved its CAR-T manufacturing issues, <https://www.biopharmadive.com/news/novartis-kymriah-car-t-manufacturing-difficulties-cell-viability/568830/> (accessed: February 2021).
- [7] T. D. P. Chilima, F. Moncaubeig, S. S. Farid, *Biochem. Eng. J.* **2018**, *137*, 132.
- [8] G. Moll, M. J. Hoogduijn, J. A. Ankrum, *Front. Immunol.* **2020**, *11*, 243.
- [9] M.-R. Benmebarek, C. H. Karches, B. L. Cadilha, S. Lesch, S. Endres, S. Kobold, *Int. J. Mol. Sci.* **2019**, *20*, 1283.
- [10] K. J. Caldwell, S. Gottschalk, A. C. Talleur, *Front. Immunol.* **2021**, *11*, 618427.
- [11] R. Lanza, D. W. Russell, A. Nagy, *Nat. Rev. Immunol.* **2019**, *19*, 723.
- [12] O. Karnieli, O. M. Friedner, J. G. Allickson, N. Zhang, S. Jung, D. Fiorentini, E. Abraham, S. S. Eaker, T. K. Yong, A. Chan, S. Griffiths, A. K. When, S. Oh, O. Karnieli, *Cytotherapy* **2017**, *19*, 155.
- [13] T. Fletcher, H. Harris, *BioPharm Int.* **2016**, *29*, 22.
- [14] Developing and implementing a supply chain management system for cellular therapy programs, <https://www.gotit-qs.com/developing-and-implementing-a-supply-chain-management-system-for-cellular-therapy-programs> (accessed: February 2021).
- [15] L. N. Chen, N. Collins-Johnson, N. Sapp, A. Pickett, K. West, D. F. Stroncek, S. R. Panch, *Transfusion* **2019**, *59*, 2506.
- [16] G. M. Pigeau, E. Csaszar, A. Dulgar-Tulloch, *Frontiers in Medicine* **2018**, *5*, 233.
- [17] K. M. Panchalingam, S. Jung, L. Rosenberg, L. A. Behie, *Stem Cell Res. Ther.* **2015**, *6*, 225.
- [18] A. Campbell, T. Brieval, L. Raviv, J. Rowley, K. Niss, H. Brandwein, S. Oh, O. Karnieli, *Stem Cell Transl. Med.* **2015**, *4*, 1155.
- [19] Y. Y. Lipsitz, P. Bedford, A. H. Davies, N. E. Timmins, P. W. Zandstra, *Cell Stem Cell* **2017**, *20*, 13.
- [20] G. W. Stockdale, A. Cheng, *Qual. Technol. Quant. M.* **2016**, *6*, 391.

- [21] M. von Stosch, R. Schenkendorf, G. Geldhof, C. Varsakelis, M. Mariti, S. Dessoy, A. Vandercammen, A. Pysik, M. Sanders, *Pharmaceutics* **2020**, *12*, 562.
- [22] S. Ghassemi, F. J. Martinez-Becerra, A. M. Master, S. A. Richman, D. Heo, J. Leferovich, Y. Tu, J. C. García-Cañaveras, A. Ayari, Y. Lu, A. Wang, J. D. Rabinowitz, M. C. Milone, C. H. June, R. S. O'Connor, *Molecular Therapy — Methods & Clinical Development* **2020**, *18*, 595.
- [23] A. Mizukami, C. H. Thomé, G. A. Ferreira, G. P. Lanfredi, D. T. Covas, S. J. Pitteri, K. Swiech, V. M. Faça, *Frontiers in Bioengineering and Biotechnology* **2019**, *7*, 154.
- [24] J. Acosta, D. Ssozi, P. van Galen, *Arterioscl. Throm. Vas.* **2021**, *41*, 1012.
- [25] D. C. Kirouac, G. J. Madlambayan, M. Yu, E. A. Sykes, C. Ito, P. W. Zandstra, *Mol. Syst. Biol.* **2009**, *5*, 293.
- [26] B. L. Puniya, R. G. Todd, A. Mohammed, D. M. Brown, M. Barberis, T. Helikar, *Front. Physiol.* **2018**, *9*, 878.
- [27] J. Vibert, V. Thomas-Vaslin, *PLoS Comput. Biol.* **2017**, *13*, e1005417.
- [28] K. Kretzschmar, F. M. Watt, *Cell* **2012**, *148*, 33.
- [29] ICH Harmonised Tripartite Guideline: Pharmaceutical Development Q8(R2), 2009, https://database.ich.org/sites/default/files/Q8_R2_Guideline.pdf (accessed: March 2021).
- [30] Q5E comparability of biotechnological/biological products subject to changes in their manufacturing process, <https://www.fda.gov/regulatory-information/search-fda-guidance-documents/q5e-comparability-biotechnologicalbiological-products-subject-changes-their-manufacturing-process> (accessed: March 2021).

How to cite this article: Csaszar E, Mills S, Zandstra PW. Process evolution in cell and gene therapy from discovery to commercialization. *Can J Chem Eng.* 2021;99:2517–2524. <https://doi.org/10.1002/cjce.24141>

Bioprocess characterization of virus-like particle production with the insect cell baculovirus expression system at nanoparticle level

Eduard Puente-Massaguer,^{a,*†} Irene González-Domínguez,^a Florian Strobl,^{b,c} Reingard Grabherr,^c Gerald Striedner,^c Martí Lecina^d and Francesc Gòdia^a



Abstract

Background. Virus-like particles (VLPs) are a multivalent platform showing great promise for the development of vaccines, gene therapy, diagnostic, and drug delivery approaches. Particularly, HIV-1 Gag VLPs provide a robust and flexible scaffold for the presentation of a variety of antigens. The insect cell baculovirus expression vector system (BEVS) is nowadays one of the reference systems to produce these complex nanoparticles, but information about VLP quality, quantity, stability, as well as cell performance is scarce, especially at bioreactor scale. **Results.** VLPs produced in the reference High Five and Sf9 insect cell lines share similar physicochemical properties, with VLPs produced in Sf9 cells showing lower levels of double stranded DNA and protein contaminants, and a higher degree of VLP assembly. Besides VLPs, other nanoparticle populations are divergently encountered in each cell line. Hi5 supernatants contain a higher load of extracellular vesicles, while Sf9 supernatants exhibit higher concentrations of baculovirus particles. Similar titers are achieved when comparing Gag to Gag-eGFP VLP production, with the size of most of the nanoparticles produced comprised at the 150–250 nm range. Eventually, Gag VLP production in a 2 L stirred tank bioreactor is successfully demonstrated, validating bioprocess transference to the final product candidate. **Conclusions.** This work provides two potentially valuable strategies for the production of HIV-1 Gag VLPs and a detailed analysis of the different nanoparticle populations produced.

© 2022 Society of Chemical Industry (SCI).

Supporting information may be found in the online version of this article.

Keywords: insect cells; virus-like particle; HIV-1; baculovirus; bioreactor; super-resolution fluorescence microscopy

INTRODUCTION

The baculovirus expression vector system (BEVS) has become one of the gold standards for recombinant protein production. Since its development in the early 1980s, the BEVS has experienced an unprecedented evolution¹ and is nowadays considered a robust technology to produce high levels of recombinant proteins in short times.² A variety of products have been produced with this system, ranging from very simple recombinant proteins³ to more complex products including adeno-associated virus vectors⁴ and virus-like particles (VLPs).⁵

VLPs are self-assembling nanoparticles made of one or several structural proteins of the native virus. These nanoparticles closely resemble the original virus structure but, unlike wild-type viruses, are devoid of viral genetic material.⁶ The main field of application of VLPs is in vaccine development since they have shown to elicit robust and broad immune responses that are capable of engaging B and T cells.⁷ Currently, several prophylactic VLP-based vaccines are commercially available for Hepatitis B, E, human papillomavirus, and malaria.⁸ The versatility of VLPs is

not restricted to vaccines, with successful results reported in gene therapy,^{9,10} drug delivery,^{11,12} theragnostic,¹³ and *in vitro* diagnostic approaches.¹⁴ Among the different VLP candidates available, Gag-based VLPs have shown great promise in a variety of

* Correspondence to: E Puente-Massaguer, Departament d'Enginyeria Química, Biològica i Ambiental, Universitat Autònoma de Barcelona, Barcelona, Spain. E-mail: eduard.puente-massaguer@mssm.edu

† Present address: Department of Microbiology, Icahn School of Medicine at Mount Sinai, 10029, New York, USA

a Departament d'Enginyeria Química, Biològica i Ambiental, Universitat Autònoma de Barcelona, Barcelona, Spain

b Austrian Centre of Industrial Biotechnology (acib GmbH), Vienna, Austria

c Department of Biotechnology, University of Natural Resources and Life Sciences, Vienna, Austria

d IQS School of Engineering, Universitat Ramon Llull, Barcelona, Spain

applications by providing a stable scaffold for membrane protein presentation against infectious diseases,¹⁵ as an active cancer immunotherapy,¹⁶ and for protein delivery.¹⁷

The production of enveloped VLPs is generally accomplished in mammalian or insect cell lines¹⁸ and through different expression systems,^{19,20} with the insect cell/BEVS being generally unrivalled.²¹ Sf9, a clonal isolate derived from the parental *Spodoptera frugiperda* cell line IPLB-Sf-21-AE, and High Five (Hi5, BTI-TN-5B1-4) insect cells are generally the choice to produce recombinant products with this system. Sf9 cells are known to achieve higher baculovirus (BV) titers, whereas Hi5 cells are typically used for recombinant protein production. Advances in the field of nanoparticle characterization and quantification have opened the opportunity to characterize the production of complex products at nanoparticle level. Moreover, progress made in the field of cell culture media development in recent years has put the basis for the intensification and standardization of recombinant protein production with the BEVS. In this sense, we recently assessed and optimized the production of Gag-eGFP VLPs with the BEVS in both insect cell lines cultured in shake flasks.^{22,23} Bioprocess validation using the final candidate product, its stability, and the transference to larger volumes are key aspects for the success of any given bioprocess. It has been a long time since the last attempts to transfer Gag VLP production with the BEVS to bioreactor scale,²⁴ and advances made in the field provide an excellent opportunity to explore the production and quality of these nanoparticles.

In this work, the physicochemical properties and stability of HIV-1 VLPs produced in insect cells is initially addressed. Next, the quantity and quality of the Gag-eGFP VLPs produced in Hi5 and Sf9 cells, and its comparison to Gag VLP production is analyzed at nanoparticle level. Finally, aiming to establish an insect cell platform for the rapid production of Gag VLPs, a proof of concept in bioreactor is conducted.

MATERIALS AND METHODS

Insect cell lines and culture conditions

Hi5 cells (cat. no. B85502, Thermo Fisher Scientific, Grand Island, NY, USA) and Sf9 cells (cat. no. 71104, Merck, Darmstadt, Germany) were grown in the low-hydrolysate animal component-free Sf900III medium (Thermo Fisher Scientific). Hi5 and Sf9 cells were subcultured three times a week at a cell density of $2\text{--}4 \times 10^5$ cells mL⁻¹²⁵ and $4\text{--}6 \times 10^5$ cells mL⁻¹²⁶ in 125 mL disposable polycarbonate Erlenmeyer shake flasks (Corning, Steuben, NY, USA), respectively. All cultures were grown in an orbital shaker at 130 rpm (Stuart, Stone, UK) and maintained at 27 °C. Cell count and viability were measured with the Nucleocounter NC-3000 (Chemometec, Allerød, Denmark) using acridine orange for cell detection and 4',6-diamidino-2-phenylindole (DAPI) (Chemometec) to quantify non-viable cells.

Recombinant BVs and infection conditions

The recombinant *Autographa californica* multicapsid nucleopolyhedrovirus (AcMNPV) encoding a Rev-independent full-length HIV-1 *gag* gene fused in frame to eGFP (Gag-eGFP)²⁷ was constructed using the BaculoGold BV expression system (BD Biosciences, San Jose, CA, USA). The recombinant AcMNPV encoding the full-length HIV-1 *gag* gene (GenBank accession no. K03455.1) codon-optimized for insect cell expression was developed with the Bac-to-Bac BV expression system (Thermo

Fisher Scientific).²⁸ Both genes were under the control of the polyhedrin (polh) promoter.

Sf9 cells were used for BV amplification by infection at 3×10^6 cells mL⁻¹ and a multiplicity of infection (MOI) of 0.1. BV containing supernatants were harvested at 96 h post infection (hpi) at $1000 \times g$ for 5 min. The number of infectious BV particles/mL was measured in Sf9 cells by the plaque assay method in 6-well plates (Nunc, Thermo Fisher Scientific).²²

Production of Gag-eGFP and Gag VLPs in shake flasks

Hi5 and Sf9 cells were infected with BV-Gag or BV-Gag-eGFP in 125 mL Erlenmeyer shake flasks with 15 mL of Sf900III medium at conditions previously optimized. Briefly, exponentially growing Hi5 cells were infected with a MOI of 2.5 at 2×10^6 cells mL⁻¹, and Gag or Gag-eGFP VLPs produced harvested at 69 hpi by centrifugation at $1000 \times g$ for 5 min.²² For Sf9 cells, BV infection was performed with a MOI of 0.01 at 3.7×10^6 cells mL⁻¹, with VLPs harvested at 80 hpi.²³

Production of Gag VLPs in bioreactor

A 2 L DASGIP® Bioblock glass bioreactor (Eppendorf, Hamburg, Germany) equipped with three Rushton impellers was used for Hi5 and Sf9 cell cultivation in 0.6 L working volume. Aeration was performed through a sparger to maintain the dissolved oxygen (DO) at 30% oxygen of air saturation. The air flow rate was set at 1 L h⁻¹ and temperature at 27 °C. Initial agitation conditions were set at 150 rpm for Hi5 cells and 100 rpm for Sf9 cells. Agitation conditions were automatically adjusted in cascade control to aeration by the DASware control software (Eppendorf) to maintain the DO setpoint at 30% oxygen of air saturation. The pH was fixed at 6.4 for Hi5 cells and 6.2 for Sf9 cells and controlled with 20% w/w H₃PO₄ and 7.5% w/w NaHCO₃. Antifoam C (Sigma Aldrich, Saint Louis, MO, USA) was added to the cell culture by pulses to prevent foam formation.

Hi5 and Sf9 cells previously grown in 1 L Erlenmeyer shake flasks (Corning) were inoculated in the bioreactor at a final concentration of 1×10^6 cells mL⁻¹. Hi5 and Sf9 cells were infected with BV-Gag at the same MOI used for shake flasks, when a viable cell concentration of 2×10^6 and 3.7×10^6 cell mL⁻¹ was attained respectively. Gag-VLPs were harvested by centrifugation at $1000 \times g$ for 5 min at the same conditions used in shake flasks.

Flow cytometry analysis of BV infection

The percentage of Gag-eGFP expressing cells was assessed using a BD FACS Canto II flow cytometer equipped with a 488 and 635 nm laser configuration (BD Biosciences, San Jose, CA, USA). For Gag expressing cells, a specific staining protocol was implemented. Shortly, cells were harvested at different times, washed, and fixed in 4% p-formaldehyde (Sigma) for 10 min at 4 °C. Afterwards, cells were washed and permeabilized using 0.1% (v/v) tween-20 (Sigma) for 15 min at room temperature (RT). Cells were washed again and blocked with 10% fetal bovine serum. After three washing cycles, cells were incubated with a rabbit anti-HIV-1 p24 primary antibody (EnoGene, New York, NY, USA) under mild rotation conditions for 1 h. Cells were then washed and incubated with a chicken anti-rabbit IgG secondary conjugated to Alexa Fluor 467 (Thermo Fisher Scientific) under continuous rotation for 2 h at RT in the dark. Cells were finally washed, resuspended in ice-cold phosphate buffered saline (PBS) solution and analyzed in the APC PMT detector of the flow cytometer. A total of 2×10^4 cells were analyzed per sample at a

flow rate of 10 $\mu\text{L min}^{-1}$. Single cells were gated according to side scatter (SSC-H) versus forward scatter (FSC-A) dot plots and Gag-eGFP (FITC-A) or Gag (APC-A) positive cells in comparison to a non-transfected control depending on their mean FITC-A or APC-A fluorescence intensity, respectively. Data acquisition and analysis was performed with the BD FACSDIVA software v.5.0 (BD Biosciences).

Gag-eGFP VLP characterization by ion exchange chromatography

An ÄKTA pure 25 M2 with an S9 sample pump and fraction collector F9-C (Cytiva, Marlborough, MA, USA) was used. Fifty milliliters and 43 mL of clarified cell culture supernatants containing Gag-eGFP VLPs produced in Hi5 and Sf9 cells, respectively, were filtered using a 0.8 μm Millex AA syringe filter (MilliporeSigma, Bedford, MA, USA) and loaded into 1 mL radial flow monolith column (CIMmultus™ QA, Sartorius, Göttingen, Germany).

Mobile phase A and B consisted in 50 mM HEPES, pH 7.2, and 50 mM HEPES, 2 M NaCl, pH 7.2, respectively. The column was equilibrated with 50 mM HEPES, 100 mM NaCl, pH 7.2 (5% v/v of buffer B) before loading. After column loading, a washing step with 15 column volumes (CV) of equilibration buffer (5% v/v of buffer B) was conducted. A 100–1000 mM NaCl (5–50% of buffer B) linear gradient at a flow rate of 1 mL min^{-1} was used to assess the VLP elution profile (50 CV). Samples were loaded into the column using the sample pump. Conductivity and ultraviolet (UV) absorbance at wavelengths of 280 and 260 nm were monitored using the software Unicorn (Cytiva).²⁹ Total protein concentration and double stranded DNA (dsDNA) quantification were conducted by the Bradford assay (BioRad Laboratories, Hercules, CA, USA) and QuantiTMM PicoGreen® dsDNA kit (Thermo Fisher Scientific) according to manufacturer's instructions.²⁹

Nanoparticle quantification and characterization

Nanoparticle tracking analysis

VLP and total nanoparticle concentrations were measured by nanoparticle tracking analysis (NTA) using a NanoSight NS300 (Malvern Panalytical, Malvern, UK). Fluorescent particles measured were considered as VLPs, whereas all light-scattered particles were considered as total nanoparticles. Shortly, samples from harvested supernatants at 3000 $\times g$ for 5 min were diluted in 0.22 μm -filtered DPBS and continuously injected into the device chamber through a syringe pump at an average concentration of 10^8 particles mL^{-1} (20–60 particles frame^{-1}). Videos of 60 s from independent triplicate measurements were analyzed with the NanoSight NTA 3.2 software (Malvern Panalytical).

Flow virometry

VLP and total nanoparticle concentrations were assessed by flow cytometry using a CytoFlex LX (Beckman Coulter, Brea, CA, USA). Gating of the different populations was made according to SSC-A versus FITC-A dot plots and using fresh DPBS and Sf900III medium samples as negative controls. Samples from supernatants harvested at 3000 $\times g$ for 5 min were diluted in 0.22 μm -filtered DPBS and triplicate measurements from independent samples were analyzed with the CytExpert 2.3 software (Beckman Coulter).

Super-resolution fluorescence microscopy

The different nanoparticle populations in Gag and Gag-eGFP supernatants were analyzed with a TCS SP8 confocal microscope equipped with the Huygens deconvolution and LAS X software

and GPU array (Leica Microsystems, Wetzlar, Germany) at Servei d'Anatomia Patològica from Hospital Sant Joan de Déu.³⁰ Briefly, nanoparticles were stained with 0.1% v/v of CellMask™ and 0.1% v/v of Hoechst 33342 or 0.05% v/v for Sf9-derived nanoparticles. Stained preparations were loaded onto a microscope slide and adsorbed to the surface of the cover glass (Linea LAB, Barcelona, Spain) for 30 min at RT. Analysis was conducted with 100 \times magnification (zoom 5) and a line average of 3 and 496 \times 496 pixels with a HC PL APO CS2 100 X/1.40 OIL objective in the HyVolution2 mode (Leica). Five fields of 13 sections per each biological triplicate were analyzed. Deconvolution was performed with the SVI Huygens Professional program and the best resolution strategy (Scientific Volume Imaging B.V., Hilversum, the Netherlands). Particle size distribution (PSD) analyses were performed with the 3D module package in Imaris 8.2.1 (Bitplane, Oxford Instruments, Zurich, Switzerland) at Servei de Microscòpia from Institut de Neurociències (Universitat Autònoma de Barcelona).²⁰ PSD histograms were created with Microsoft Excel 2016 (Redmond, WA, USA).

Gag-eGFP quantification

The supernatants of insect cells infected with the BV-Gag-eGFP were recovered by centrifugation at 3000 $\times g$ for 5 min. Green fluorescence was measured with a Cary Eclipse fluorescence spectrophotometer (Agilent Technologies, Santa Clara, CA, USA) at RT as follows: $\lambda_{\text{ex}} = 488$ nm (5 nm slit), $\lambda_{\text{em}} = 500$ –530 nm (10 nm slit). Relative fluorescence units were calculated by subtracting fluorescence unit values of fresh Sf900III medium.

Gag quantification

An HIV-1 p24 enzyme-linked immunosorbent assay (ELISA) kit (Sino Biological, Wayne, NJ, USA) was used to quantify the concentration of Gag polyprotein. Supernatants were harvested by centrifugation at 3000 $\times g$ for 5 min. Samples were incubated in SNCR buffer for 10 min at 70 °C, and in 1.5% Triton X-100 for 10 min at 100 °C. The substrate solution was prepared by dissolving a SIGMAFAST OPD substrate tablet and one urea hydrogen peroxide tablet (MilliporeSigma) at a final concentration of 0.4 mg mL^{-1} in deionized water. An HIV-1 p24 protein standard of known concentration was also included for absolute Gag quantification. The reaction was stopped by adding a 625 mM H_2SO_4 solution after 10 min incubation. The absorbance was measured at 492 nm with a reference wavelength at 630 nm in a Tecan Infinite 200 Pro reader (Tecan, Männedorf, Switzerland). p24 concentration values were corrected according to HIV-1 Gag molecular weight (55 kDa).

SDS-PAGE and western blot

Gag and Gag-eGFP VLP containing supernatants were examined by SDS-PAGE and western blot for HIV-1 p24 (A2-851-100, Icosagen, Tartu, Estonia) and GP64 (A2980, Abcam, Cambridge, UK) detection.³¹

Cryo-transmission electron microscopy

BV-Gag infected Sf9 and Hi5 cell supernatants at 80 and 69 hpi, respectively, were visualized with a cryo-transmission electron microscope. Two to three microliters of sample were blotted onto 400 mesh Holey carbon grids (Micro to Nano, Wateringweg, the Netherlands) previously subjected to glow discharge in a PELCO easiGlow discharge unit (Ted Pella Inc., Redding, CA, USA). Samples were subsequently plunged into liquid ethane at -180 °C using a Leica EM GP cryo workstation (Leica) and observed in a

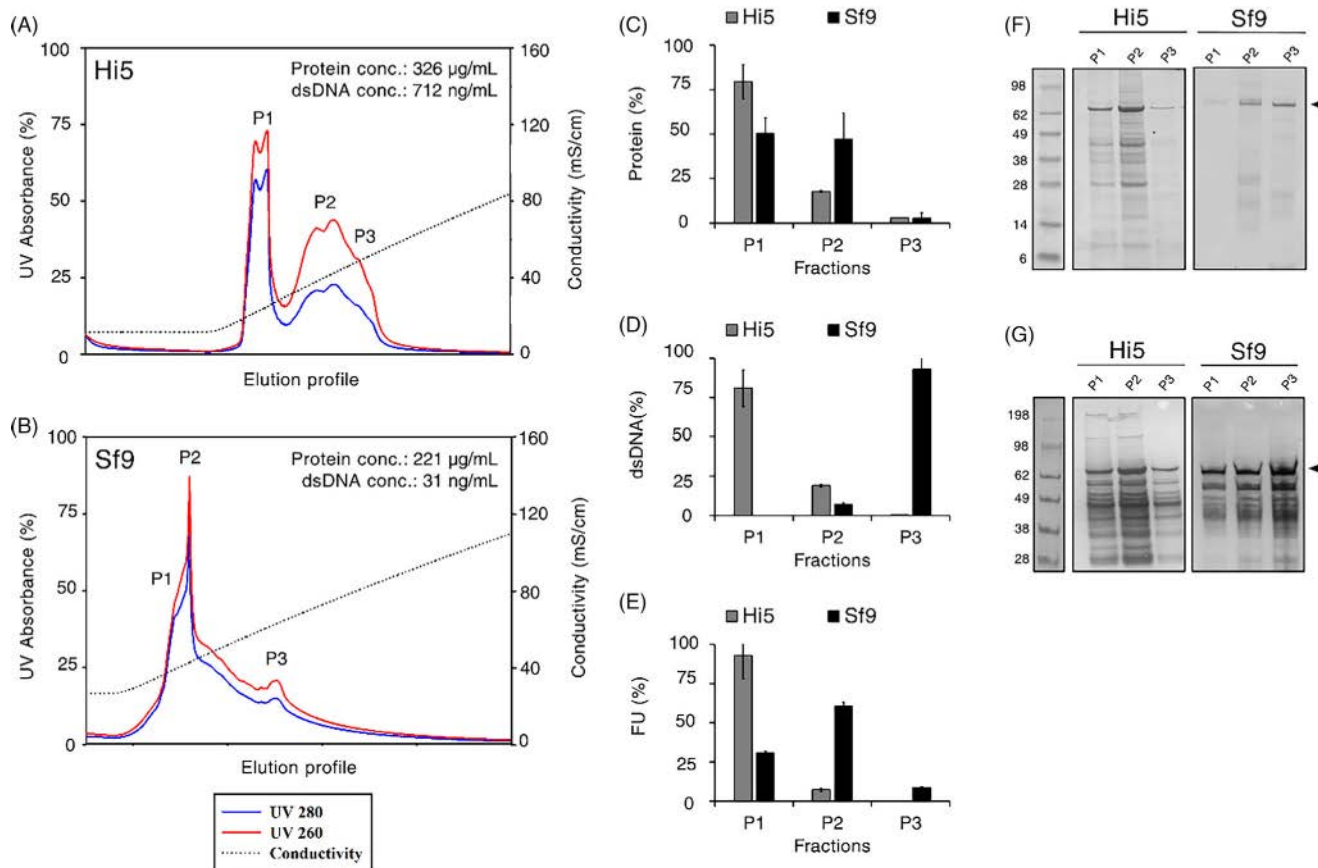


Figure 1. Characterization of Gag-eGFP VLPs produced in shake flasks. Elution profiles of infected Hi5 (A) and Sf9 cell (B) supernatants using a monolithic ion exchange column. The black dotted line in the chromatogram indicates conductivity, whereas blue and red lines refer to ultraviolet (UV) absorbance at 280 and 260 nm, respectively. Fluorescence (C), protein (D), and dsDNA distribution (E) in P1, P2, and P3 elution fractions. SDS-PAGE (F) and HIV-1 p24 western blot (G) analysis of P1, P2, and P3 elution fractions. The P1 fraction was diluted 1:2 before loading the SDS-PAGE and western blot. The black arrow corresponds to the band of the full-length Gag-eGFP polyprotein. Conc., concentration; FU, fluorescence units; dsDNA: double-stranded DNA.

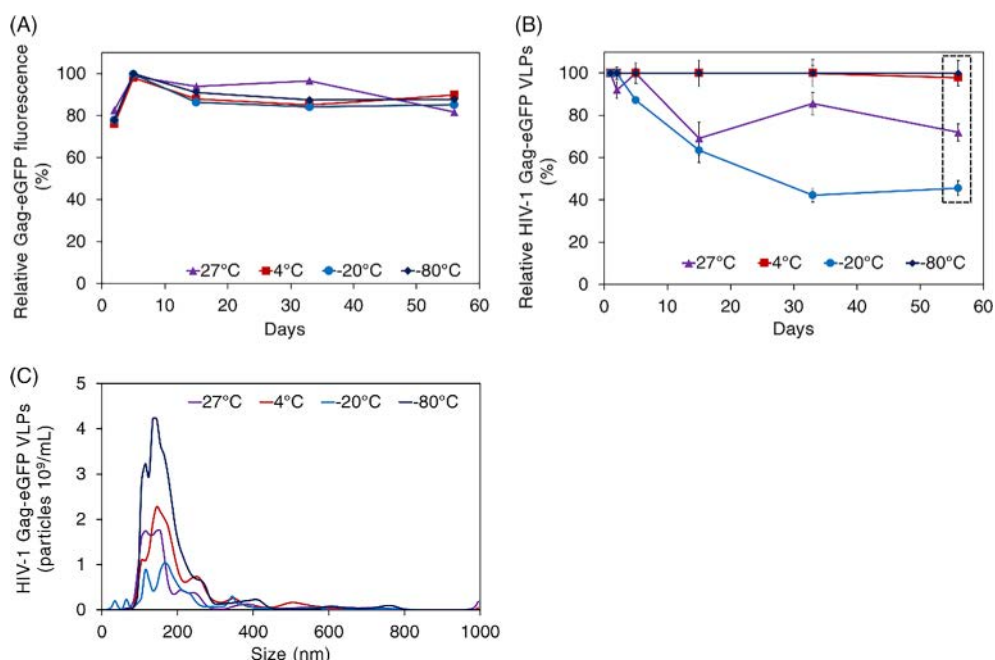


Figure 2. Stability profiles of Gag-eGFP VLPs in harvested supernatants stored at 27, 4, -20 and -80 °C. (A) Analysis of Gag-eGFP fluorescence by spectrofluorometry. (B) Analysis of VLP concentration by NTA. The first measurement in each condition was used as the reference to calculate relative percentages in subsequent readouts. (C) Size distribution of VLPs measured at day 56 post-freezing of the study [shown as a dashed square in Fig. 1(b)]. Fluorescent nanoparticles measured were considered as VLPs, whereas light-scattered particles were considered as total nanoparticles. NTA, nanoparticle tracking analysis; VLP, virus-like particle.

Jeol JEM-2011 TEM electron microscope operating at 200 kV (Jeol Ltd., Akishima, Tokyo, Japan). During imaging, samples were maintained at $-173\text{ }^{\circ}\text{C}$ and pictures were taken using a CCD multiscan camera model no. 895 (Gatan Inc., Pleasanton, CA, USA).

Analysis of insect cell metabolism

Glucose, lactate, and phosphate concentrations were measured by ion-exclusion chromatography using a sulfonated polystyrene divinyl benzene column (Aminex HPX-87H, Bio-Rad, Hercules, CA, USA) in an Agilent 1200 series HPLC system (Agilent). A 0.01 N H_2SO_4 solution was used as the mobile phase with a flow rate of 0.45 mL min^{-1} . All measurements were performed in an AZURA UV/VIS detector (Knauer, Berlin, Germany) with a refractive index detector temperature of $35\text{ }^{\circ}\text{C}$. The standard deviation of the technique was determined as 0.31% for glucose, 0.26% for lactate, and 1.01% for phosphate measurement. The phosphate uptake rate was calculated taking into consideration the amount of phosphate present in the medium and also the volume of H_3PO_4 added for pH control.

Amino acid concentrations were determined by HPLC after derivatization in a reversed-phase Eclipse Plus C18 column (Agilent) at $40\text{ }^{\circ}\text{C}$ according to manufacturer's instructions (Agilent). The flow rate was adjusted to 0.64 mL min^{-1} and two solvents (solution A and B) were used in the mobile phase. Solution A consisted of 10 mM K_2HPO_4 and 10 mM $\text{K}_2\text{B}_4\text{O}_7$, and solution B of a 45/45/10% v/v/v mix of acetonitrile, methanol and water, respectively. Amino acids were detected at 266/305 nm for fluorenylmethoxycarbonyl derivatives and at 450 nm for o-phthalaldehyde derivatives. The final amino acid concentration was quantified using an internal standard calibration. The standard deviation associated with the measurement of amino acid concentrations was $4 \pm 1\%$.

RESULTS AND DISCUSSION

Physicochemical properties and quality assessment of HIV-1 VLPs

We have recently proven that the BV infection conditions of Hi5²² and Sf9 cells²³ can be successfully optimized to produce high

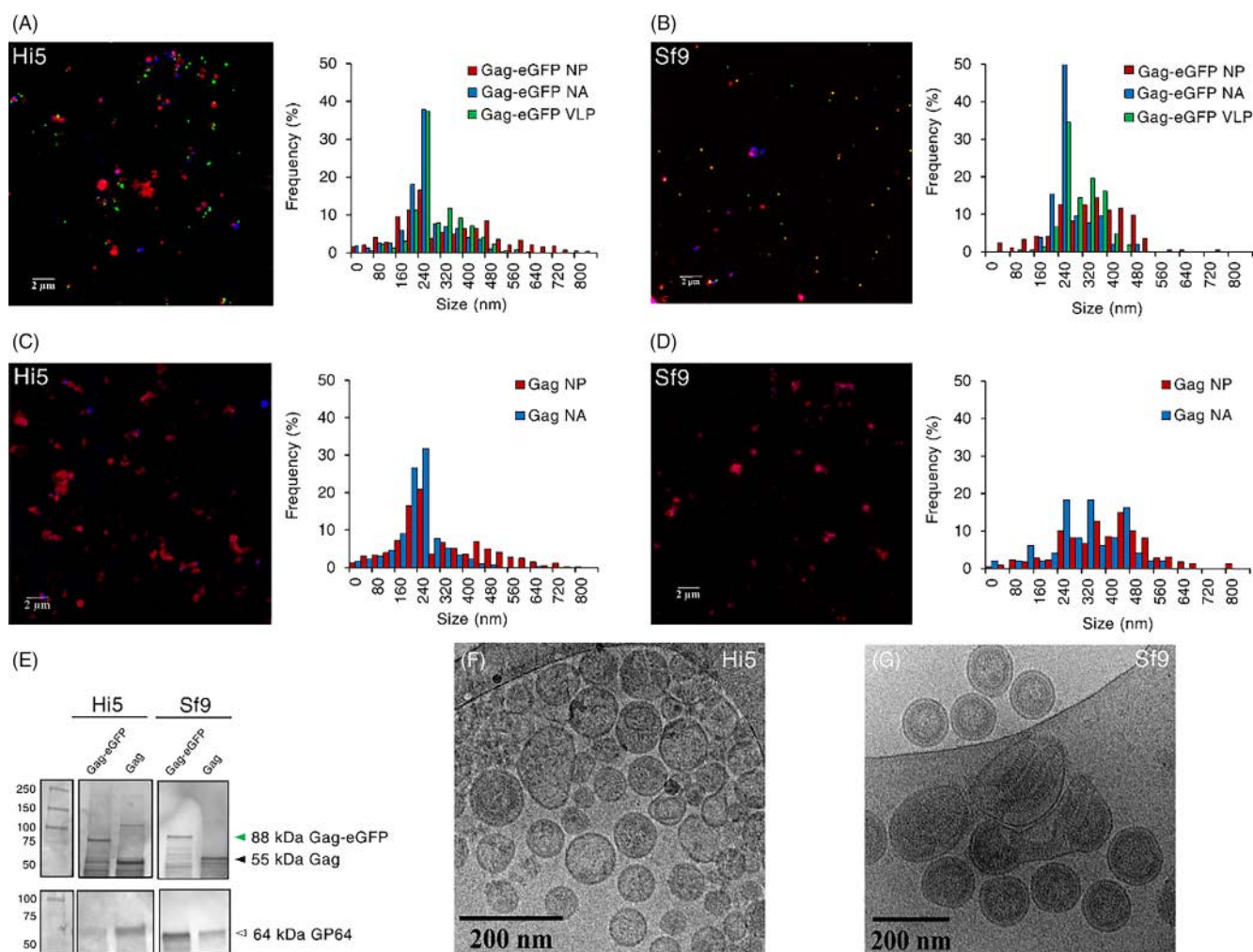


Figure 3. Analysis of Gag and Gag-eGFP VLPs. Imaging and assessment of size distribution by SRFM of the different nanoparticle populations in Hi5 (A) and Sf9 (B) supernatants infected with BV-Gag-eGFP. Nanoparticle lipid membranes were stained with CellMask™ (red) and nucleic acids with Hoechst (blue). Imaging and evaluation of size distribution by SRFM of the different nanoparticle populations in Hi5 (C) and Sf9 (D) supernatants infected with BV-Gag. (E) HIV-1 p24 (upper) and GP64 (lower) western blot analysis of Gag-eGFP and Gag VLP productions. The green mark indicates the Gag-eGFP band, the black mark shows the Gag band, and the white mark illustrates the GP64 band. Cryo-TEM micrographs of Gag VLPs produced in Hi5 (F) and Sf9 cells (G). NA, nucleic acid; NP, nanoparticle; SRFM, super-resolution fluorescence microscopy; VLP, virus-like particle.

HIV-1 VLP titers. However, the physicochemical properties and quality of these nanoparticles produced in both insect cell lines is still to be characterized. To this purpose, fluorescently tagged VLPs (Gag-eGFP VLPs) were used for an easier sample monitoring. Different parameters were assessed by ion exchange chromatography (IEX) in the unprocessed supernatant samples, including Gag-eGFP polyprotein (fluorescence units, FU), total protein concentration ($\mu\text{g mL}^{-1}$), and dsDNA concentration (ng mL^{-1}). A five-fold increase in FU was measured in Hi5 compared to Sf9 supernatants, with Sf9 supernatant samples exhibiting lower levels of contaminating protein and dsDNA (Fig. 1). The low Hi5 cell viability at harvest might explain the high amounts of dsDNA and proteins encountered in the supernatant. After IEX, there was no presence of VLPs in the flowthrough, supporting the complete capture of these nanoparticle by the monolith column (data not shown). Three different fractions, P1–P3, were pooled in each run according to UV 260 and 280 nm chromatograms. The three elution peaks were obtained at conductivities of 22, 38, and 51 mS cm^{-1} in the Hi5 supernatant [Fig. 1(A)], with similar conductivity values of 25, 31 and 51 mS cm^{-1} for P1–P3 in the Sf9 supernatant [Fig. 1(B)]. Most of the protein present in both Hi5 (80%) and Sf9 supernatants (50%) eluted at lower salt concentrations [Fig. 1(C)], whereas dsDNA eluted in P1 in the Hi5 and in P3 in the Sf9 supernatant, respectively [Fig. 1(D)]. The dsDNA elution profile of the Hi5 supernatant sample was comparable to that observed in Tnms42 cells,³² while it was similar to the elution profile measured in CHO cells for the Sf9 supernatant.³³ Considering the different level of contaminants in each unpurified supernatant, as well as the strong positive charge of the quaternary amine monolithic column, a competition for binding between negative charged dsDNA and VLPs could be the reason behind the differences in dsDNA elution profiles.

The presence of Gag-eGFP VLPs was analyzed by spectrofluorometry (FU), SDS-PAGE, and HIV-1 p24 western blot in each pooled fraction [Fig. 1(E)–(G)]. The Gag-eGFP polyprotein was detected in all fractions analyzed, most of it eluting at a low conductivity in the Hi5 supernatant (93%), and at a low-intermediate salt concentration in the Sf9 supernatant (60%). Differences in the

fluorescence elution pattern between cell lines could be attributed to the high ratio of unassembled Gag-eGFP monomer versus Gag-eGFP VLPs in the Hi5 supernatant,²² since free monomer has been reported to elute earlier than VLPs.²⁹ Apart from the different content of unassembled Gag-eGFP monomer between both cells, similar HIV-1 VLP elution profiles in monolithic columns were observed in this work compared to other production platforms, with HIV-1 VLPs produced in HEK 293, Tnms42 and CHO cells eluting at conductivities of 27–49, ~20–45, and 45–90 mS cm^{-1} , respectively.^{29,32,33}

Stability of HIV-1 VLPs

Product stability is an important parameter to consider towards extending the shelf-life of the product of interest. This is especially relevant when it comes to enveloped particulate products such as VLPs. To this purpose, the supernatant of VLPs produced with the BEVS was split, aliquoted, and maintained at four different conditions (27, 4, –20 and –80 °C) for 2 months. Gag-eGFP VLPs were used with the aim to discriminate VLPs from other nanoparticle populations co-expressed with the BEVS.²⁷ Different analytical techniques, including spectrofluorometry and NTA were employed (Fig. 2). VLP fluorescence was generally maintained over the 2-month period independently of the storage conditions used [Fig. 2(A)]. However, VLP characterization in native conditions by NTA revealed that the structural integrity of VLPs was only preserved at 4 and –80 °C [Fig. 2(B)], suggesting that VLPs stored at 27 and –20 °C were probably disassembling. Enhanced protease activity could explain the instability of VLPs stored at 27 °C, while particle disruption due to external and internal ice formation around the VLP envelope might explain the low stability at –20 °C.^{34,35} Additionally, changes in the morphology were detected in all conditions except –80 °C [Fig. 2(C)]. So far, it is still not well known whether variations in VLP morphology can alter their immunogenicity profile. In any case, this data indicates that Gag VLPs produced with the BEVS can be safely stored at 4 and –80 °C for mid to long term purposes without the need of further purification.

Table 1. Quantification of Gag and Gag-eGFP VLP production titers and baculovirus particles in Hi5 and Sf9 cells infected with the BEVS in shake flasks. Nanoparticle quantification was performed by NTA and flow virometry, and i baculovirus particles were measured by the plaque assay method

Condition	Quantification method	Product	Fluorescent particles (10^9 particles mL^{-1})	Total particles (10^9 particles mL^{-1})
Hi5	NTA	Gag	n.a.	495 ± 60
		Gag-eGFP	34 ± 2	426 ± 61
	Flow virometry	Gag	n.a.	5.9 ± 0.5
		Gag-eGFP	2.2 ± 0.1	9.5 ± 0.3
Sf9	NTA	Gag	n.a.	128 ± 24
		Gag-eGFP	37 ± 9	181 ± 15
	Flow virometry	Gag	n.a.	5.9 ± 0.3
		Gag-eGFP	3.3 ± 0.3	8.2 ± 0.9
Sf900III medium	NTA	n.a.	n.a.	44.8 ± 1.9
	Flow virometry			0.1 ± 0.0
Condition		Product	IBV particles (10^7 pfu mL^{-1})	
Hi5		Gag	10.0 ± 2.7	
		Gag-eGFP	6.0 ± 1.4	
Sf9		Gag	31.0 ± 13.5	
		Gag-eGFP	76.7 ± 51.3	

IBV, infectious baculovirus particle; n.a., not available.

Comparison of Gag-eGFP and Gag VLPs

Gag tagging with the fluorescent reporter protein eGFP is a useful strategy in bioprocess development since discrimination between other nanoparticle populations and VLPs is possible. This allows a better control and understanding of nanoparticle-based production platforms such as VLP expression with the BEVS. Nevertheless, once the bioprocess has been defined, the production of the final candidate without the fluorescent tag has to be assessed. Super-resolution fluorescence microscopy, a novel technique to characterize different nanoparticle populations simultaneously,²⁰ was applied to characterize Gag-eGFP and Gag VLP productions. Most of the Gag-eGFP VLPs produced in both insect cell lines were detected at the 150–250 nm range, as expected [Fig. 3(A) and (B)]. However, Sf9-derived Gag-eGFP VLPs proved to be more heterogeneous with a fraction of these VLPs with sizes in the 300–400 nm range. A higher number of nanoparticles was also measured at the 300–500 nm range in Sf9 supernatants. This could be related to the three to ten-fold higher

concentration of BV particles in Sf9 over Hi5 supernatants (Table 1) given that these cells generally produce higher amounts of BVs. This is in agreement with the higher frequency of nucleic acid detection in the 300–500 nm range since BVs contain large genomes up to 180 kb.³⁶

A similar size distribution was observed in Hi5 Gag VLP supernatants, with most of the nanoparticles located in the 150–250 nm size range [Fig. 3(C) and (D)]. Specific detection of Gag-eGFP and Gag in Hi5 and Sf9 supernatants was also confirmed by western blot, while the presence of the GP64 BV-associated protein also indicated the co-expression of BVs [Fig. 3(E)]. As Gag VLPs were not tagged, VLPs could not be differentiated from other nanoparticles, specifically extracellular vesicles (EVs), which fall in the same size range and have been described to be co-expressed with VLPs in animal cell lines.³⁰ These nanoparticles are generally produced at higher levels than VLPs, representing from 4 to 13-fold in Hi5 supernatants and from 2 to 5-fold in Sf9 supernatants,²⁶ with variability attributed to the quantification methodology employed

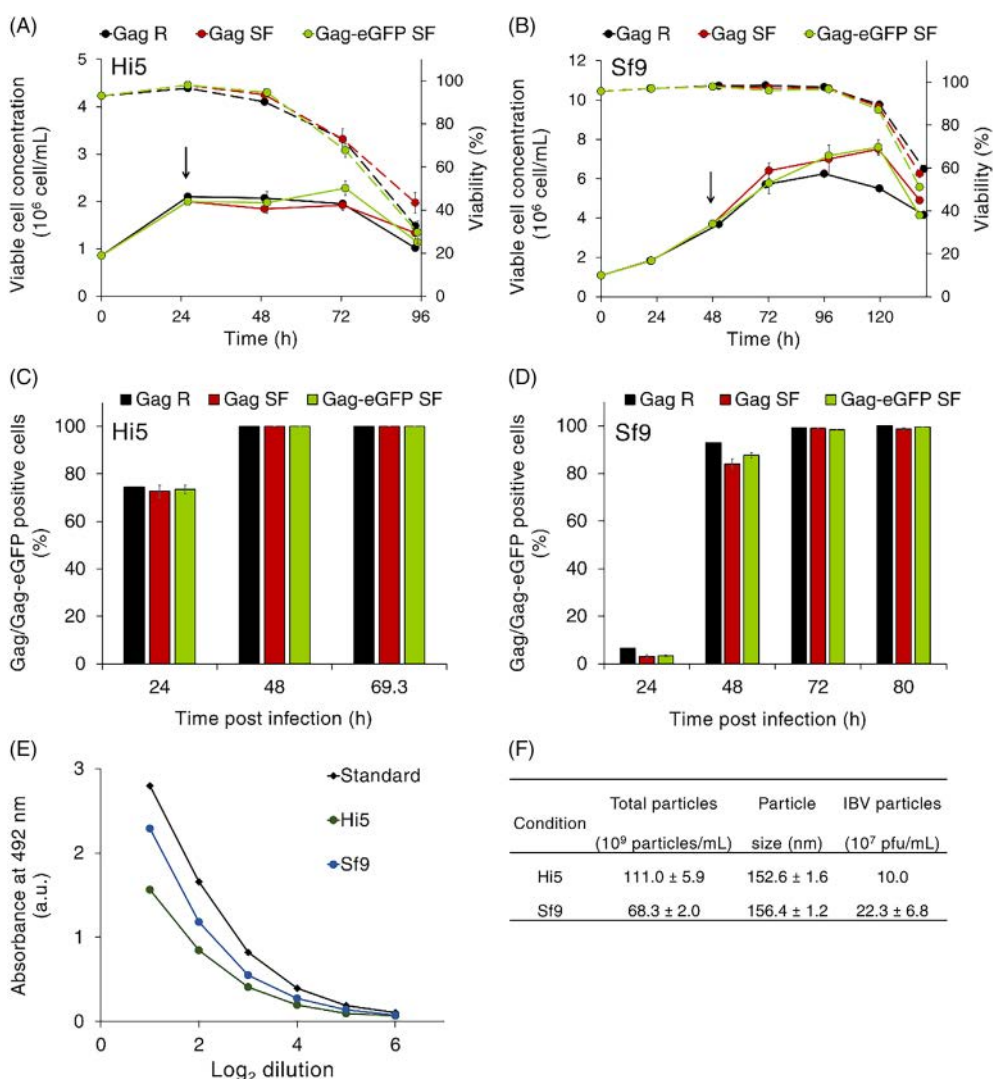


Figure 4. Transference of HIV-1 VLP production from shake flasks to bioreactor. Cell growth and viability profiles of Hi5 (A) and Sf9 cells (B). The black arrow indicates the time of recombinant baculovirus infection. Evolution of Gag and Gag-eGFP expression in Hi5 (C) and Sf9 cells (D) by flow cytometry after infection with recombinant baculoviruses. (E) Quantification of Gag production by enzyme-linked immunosorbent assay in the supernatant of infected insect cells cultured in bioreactor at the time of harvest. The HIV-1 p24 protein was included as standard of known concentration. (F) Measurement of total nanoparticles by NTA in the supernatant of infected insect cells cultured in bioreactor at the time of harvest. The concentration of infectious baculovirus particles in these conditions was also determined by the plaque assay method. IBV, infectious baculovirus; NTA, nanoparticle tracking analysis; R, bioreactor; SF, shake flask.

(Table 1). The higher load of BV particles in the Sf9 supernatant was also appreciated in Gag VLP preparations [Fig. 3(D)], with a larger nanoparticle population frequency in the 300–500 nm range compared to the Hi5 supernatant. Of note, it is possible that the concentration of BV particles was higher than the titers obtained by the plaque assay method due to the existence of defective BV particles.³⁷ The presence of nucleic acids in particles of similar sizes to VLPs was detected in Gag and Gag-eGFP preparations, possibly indicating that nanoparticles within this size range, VLPs, EVs or both, might contain or be associated with nucleotide molecules.^{38,39} Further studies are needed to discriminate which nanoparticle populations are subjected to incorporate or associate to nucleic acids.

Gag VLP supernatants from both insect cell lines were analyzed by cryo-transmission electron microscopy (cryo-TEM). The native structure of Gag VLPs could be observed but differentiation of VLPs from EVs was more difficult in the Hi5 supernatant [Fig. 3(F) and (G)]. This is possibly due to the higher load of EVs co-expressed in Hi5 cells and also to the larger amounts of proteins (Fig. 2), which increase the background signal and reduce the quality of the imaging. Compared to previous studies with Gag-eGFP VLPs, Gag VLPs proved to be less heterogenous and with a higher degree of internal arrangement.³⁰ The absence of the eGFP fusion protein might result in the formation of more structured nanoparticles closely resembling immature HIV-1 virions.

Gag VLP production in bioreactor

The production of Gag VLPs with the insect cell/BEVS was assessed in a stirred tank bioreactor to test the feasibility of this platform for large scale VLP manufacture. Similar cell growth and infection kinetics were measured between shake flasks and bioreactors for Gag as well as Gag-eGFP production, indicating the successful transference of the conditions optimized in shake flasks to bioreactor scale [Fig. 4(A)–(D)]. The higher MOI used in Hi5 cells completely arrested cell growth after infection, whereas Sf9 cells continued to grow for the next 48 hpi. The same reason applies to the earlier decrease in cell viability and also the faster infection kinetics

observed in Hi5 cells. After infection, an increase in stirring speed was observed in Hi5 cells, peaking at ~24 hpi, which could be related to a higher oxygen demand owing to the BV infection process since cell growth was completely arrested.⁴⁰ As for Sf9 cells, the maximum oxygen demand was recorded at ~40 hpi [Fig. 5 (A) and (B)], coinciding with the peak in viable cell concentration and complete infection. In these conditions, Hi5 and Sf9 cells yielded 1.86 and 1.28 mg L⁻¹ of Gag polyprotein, with a higher amount of contaminant BV particles in the latter [Fig. 4(E) and (F)]. VLP titers in both platforms were higher than those achieved in insect cells by stable gene expression,^{41–43} and transient transfection of plasmid DNA.^{44,45} On the other hand, a larger load of contaminant EVs in the same size range as VLPs was observed in Hi5 cell cultures. Despite several advances to separate these contaminant species from Gag VLPs have been accomplished in the last years,^{32,46} further research is still required. Moreover, it is not well known how these specimens might impact the final application of Gag VLPs, either by boosting their immunogenicity⁴⁷ or by reducing it.⁴⁸ If BV particles negatively impact the final application of Gag VLPs as a pharmaceutical product, Hi5 cells might be a better option for VLP production. If this is not the case, Sf9 cells might have an advantage since the presence of contaminating nucleic acids, host cell proteins and unassembled Gag, and EVs is lower, simplifying their purification. In any case, both platforms achieve superior Gag VLP yields in comparison to other systems employed to produce these nanoparticles at bioreactor scale,^{49–51} and a three- to four-fold increase with respect to the most recent optimization study for Gag VLP production with the insect cell/BEVS.⁵² Assuming a mouse is immunized with two doses of 5 µg of Gag VLPs in a prime-boost regimen¹⁶ and not considering losses in process purification, a 1 L bioreactor culture of Sf9 or Hi5 cells would enable to immunize around 100–200 mice, respectively.

The analysis of cell metabolism is an important aspect to consider in bioprocess development since strategies for process intensification can be implemented. To this end, the metabolism of both insect cell lines cultured at bioreactor scale after BV infection was analyzed. Hi5 cells consumed larger levels of all the different

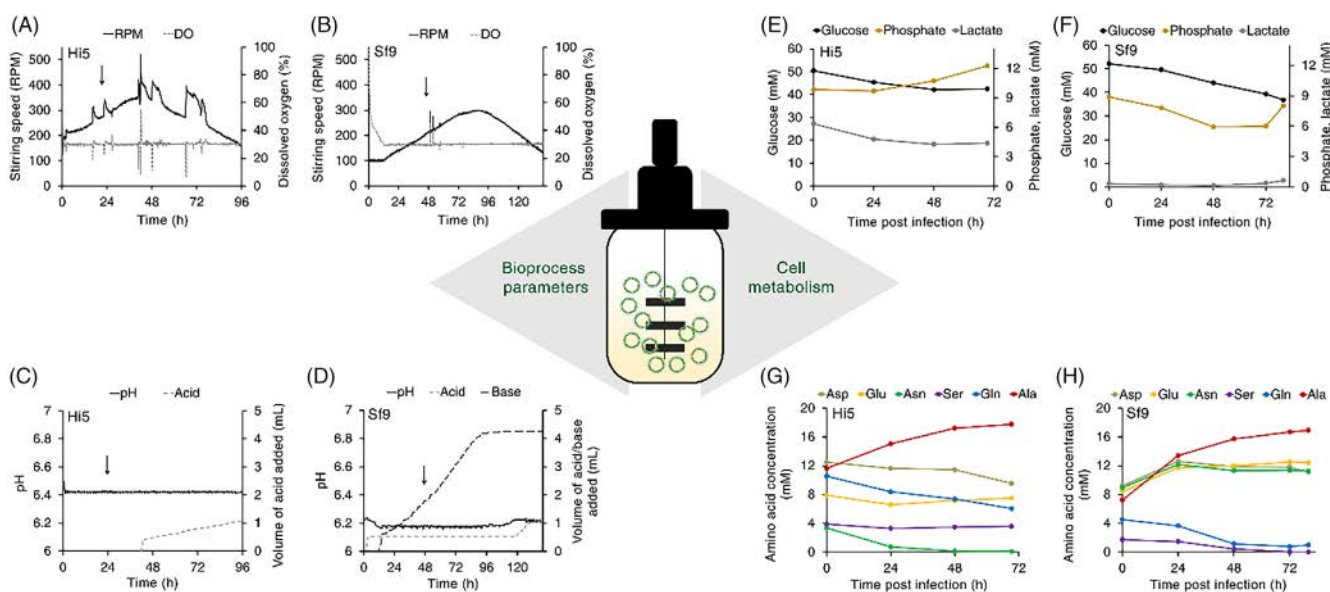


Figure 5. Analysis of bioreactor parameters with the insect cell/BEVS. Stirring speed, dissolved oxygen concentration, pH, and volume of acid/base added in Hi5 (A,C) and Sf9 cell (B,D) cultures. Black arrows indicate the time point of recombinant baculovirus infection. Profiles of glucose, lactate, phosphate (E,F) and main amino acids produced/consumed (G,H) in Hi5 and Sf9 cultures, respectively. Ala, alanine; Asn, asparagine; Asp, aspartic acid; DO, dissolved oxygen; Gln, glutamine; Glu, glutamic acid; RPM, revolutions per minute; Ser, serine.

metabolites assessed in comparison to Sf9 cells [Fig. 5(E)–(H)], with glucose, asparagine, and glutamine as the most highly consumed (Supporting Information, Fig. S1). Asparagine is reported as the principal nitrogen source for Hi5 cells and its uptake rate can be even higher than glucose.⁵³ After BV infection, asparagine was not consumed as rapid as previously observed,⁴¹ possibly due to the low concentration in the medium at the time of infection, resulting in complete asparagine exhaustion between 24–48 hpi and coinciding with the decline in cell viability. Sf9 cells exhibited a more balanced metabolism with reduced uptake fluxes of the different metabolites analyzed (Supporting Information, Fig. S1). Glucose, the principal carbon source, and glutamine, an important nitrogen source in insect cell cultures, were the main compounds consumed by Sf9 cells. None of them was limiting by the end of the production phase, though the low concentration of glutamine in the medium (~1 mM) could have possibly influenced its uptake by Sf9 cells. Interestingly, serine was depleted at 48 hpi, coinciding with the peak of maximum viable cell concentration and complete BV infection. Thus, asparagine and serine supplementation at the time of infection could be an option to extend the productive time of Hi5 and Sf9 cells, respectively, and further increase VLP yields.

The control of bioprocess parameters in the bioreactor was successfully achieved in both insect cell lines. However, differences in the behavior of Hi5 and Sf9 cells were observed [Fig. 5(C) and (D)]. The addition of sodium bicarbonate to the Sf9 cell culture by the software control loop at the beginning of the bioreactor operation indicated the acidification of the culture medium. The accumulation of organic acids derived from cell metabolism such as glutamic and aspartic acid, both with pKa values below the cell culture pH, and CO₂ production from cell respiration could be the reasons behind medium acidification. On the contrary, the addition of phosphoric acid to the Hi5 cell culture was detected. Ammonia formation, a by-product of insect cell metabolism, could explain medium basification since significantly higher asparagine and glutamine uptake rates were measured in this cell line.⁵⁴ Alanine was also produced in both bioreactor cultures peaking in the 15–20 mM range. The formation of this amino acid is a feature observed in animal cell metabolism under glucose excess conditions.⁵⁵ Lactate, another by-product of insect cell metabolism, was not produced after BV infection, which is probably associated to pH and dissolved oxygen concentration maintenance along the culture.⁵⁶

CONCLUSIONS

This study provides a detailed analysis of the insect cell/BEVS and shows the versatility of this system to produce HIV-1 VLPs. VLPs produced in the reference Hi5 and Sf9 insect cell lines exhibit similar physicochemical properties and are stable when stored at –80 °C for 2 months with little impact on their morphology. Gag VLP titers are similar to those obtained for Gag-eGFP VLPs, with nanoparticle sizes in the 150–250 nm range closely resembling immature HIV-1 virions. A high degree of heterogeneity and complexity is detected in VLP productions, with large concentrations of EVs, dsDNA and total protein content in Hi5 supernatants, whereas high loads of BV particles are encountered in Sf9 supernatants. The successful transference of Gag VLP production from shake flasks to stirred tank bioreactor is demonstrated, providing two different strategies to produce these complex nanoparticles in large volumes with controlled operational conditions.

ACKNOWLEDGEMENTS

The authors thank Alois Jungbauer (University of Natural Resources and Life Sciences, Vienna, Austria) for facilitating the access to ÄKTA pure system, and Paula Alves (Instituto de Biologia Experimental e Tecnológica, Oeiras, Portugal) for providing the Hi5 cell line. We also appreciate the support of Miriam Klausberger on the protocol for Gag staining, Krisztina Koczka for providing the BV-Gag stock, Sahar Masoumeh Ghorbanpour with ELISA quantification, Martí de Cabo (Servei de Microscòpia, Universitat Autònoma de Barcelona) with cryo-TEM, Mónica Roldán (Unitat de Microscòpia Confocal, Servei d'anatomia Patològica, Institut Pediàtric de Malalties Rares, Hospital Sant Joan de Déu) with SRFM, and Jorge Fomaro and Ángel Calvache (Beckman Coulter) for facilitating the access to the CytoFlex LX. Eduard Puente-Massaguer (FPU15/03577) and Irene González-Domínguez (FPU16/02555) are recipients of FPU grants from Ministerio de Educación, Cultura y Deporte of Spain. The research group is recognized as 2017 SGR 898 by Generalitat de Catalunya.

SUPPORTING INFORMATION

Supporting information may be found in the online version of this article.

REFERENCES

- 1 Stolt-Bergner P, Benda C, Bergbrede T, Besir H, Celie PHN, Chang C *et al.*, Baculovirus-driven protein expression in insect cells: a benchmarking study. *J Struct Biol* **203**:71–80 (2018).
- 2 Contreras-Gómez A, Sánchez-Mirón A, García-Camacho F, Molina-Grima E and Chisti Y, Protein production using the baculovirus-insect cell expression system. *Biotechnol Prog* **30**:1–18 (2014).
- 3 Weber W and Fussenegger M, *Insect Cell-Based Recombinant Protein Production*. Springer Heidelberg, Berlin, pp. 263–277 (2009).
- 4 Merten OW and Gaillet B, Viral vectors for gene therapy and gene modification approaches. *Biochem Eng J* **108**:98–115 (2016).
- 5 Dai X, Jian C, Na L, Wang X, Dai Y and Li D, Production and characterization of Hantaan virus-like particles from baculovirus expression system. *Biochem Eng J* **152**:107373 (2019).
- 6 Ding X, Liu D, Booth G, Gao W and Lu Y, Virus-like particle engineering: from rational design to versatile applications. *Biotechnol J* **13**:1–7 (2018).
- 7 Zepeda-Cervantes J, Ramírez-Jarquín JO and Vaca L, Interaction between virus-like particles (VLPs) and pattern recognition receptors (PRRs) from dendritic cells (DCs): toward better engineering of VLPs. *Front Immunol* **11**:1100 (2020).
- 8 Nooraei S, Bahrulolum H, Hoseini ZS, Katalani C, Hajzade A, Easton AJ *et al.*, Virus-like particles: preparation, immunogenicity and their roles as nanovaccines and drug nanocarriers. *J Nanobiotechnol* **19**:59 (2021).
- 9 Biddlecome A, Habte HH, McGrath KM, Sambanthamoorthy S, Wurm M, Sykora MM *et al.*, Delivery of self-amplifying RNA vaccines in vitro reconstituted virus-like particles. *PLoS One* **14**:e0215031 (2019).
- 10 Prel A, Caval V, Gayon R, Ravassard P, Duthoit C, Payen E *et al.*, Highly efficient in vitro and in vivo delivery of functional RNAs using new versatile MS2-chimeric retrovirus-like particles. *Mol Ther Methods Clin Dev* **2**:15039 (2015).
- 11 Finbloom J, Aanei I, Bernard J, Klass S, Elledge S, Han K *et al.*, Evaluation of three morphologically distinct virus-like particles as nanocarriers for convection-enhanced drug delivery to glioblastoma. *Nanomaterials* **8**:1007 (2018).
- 12 Peyret H, Gehin A, Thuenemann EC, Blond D, El Turabi A, Beales L *et al.*, Tandem fusion of hepatitis B core antigen allows assembly of virus-like particles in bacteria and plants with enhanced capacity to accommodate foreign proteins. *PLoS One* **10**:e0120751 (2015).
- 13 Enomoto T, Kawano M, Fukuda H, Sawada W, Inoue T, Haw KC *et al.*, Viral protein-coating of magnetic nanoparticles using simian virus 40 VP1. *J Biotechnol* **167**:8–15 (2013).
- 14 Theillet G, Martinez J, Steinbrugger C, Lavillette D, Coutard B, Papageorgiou N *et al.*, Comparative study of chikungunya virus-like particles and pseudotyped-particles used for serological detection

- of specific immunoglobulin M. *Virology* **529**:195–204 (2019). <https://doi.org/10.1016/j.virol.2019.01.027>.
- 15 Fontana D, Garay E, Cervera L, Kratje R, Prieto C and Gòdia F, Chimeric vlpS based on hiv-1 gag and a fusion rabies glycoprotein induce specific antibodies against rabies and foot-and-mouth disease virus. *Vaccine* **9**:251 (2021).
 - 16 Nika L, Cuadrado-Castano S, Arunkumar GA, Grünwald-Gruber C, McMahon M, Koczka K *et al.*, An HER2-displaying virus-like particle vaccine protects from challenge with mammary carcinoma cells in a mouse model. *Vaccine* **7**:1–19 (2019).
 - 17 Kaczmarczyk SJ, Sitaraman K, Young HA, Hughes SH and Chatterjee DK, Protein delivery using engineered virus-like particles. *Proc Natl Acad Sci U S A* **108**:16998–17003 (2011).
 - 18 Lavado-García J, Jorge I, Boix-Besora A, Vázquez J, Gòdia F and Cervera L, Characterization of HIV-1 virus-like particles and determination of gag stoichiometry for different production platforms. *Biotechnol Bioeng* **118**:2660–2675 (2021).
 - 19 Alvim RGF, Itabaiana I and Castilho LR, Zika virus-like particles (VLPs): stable cell lines and continuous perfusion processes as a new potential vaccine manufacturing platform. *Vaccine* **37**:6970–6977 (2019).
 - 20 González-Domínguez I, Puente-Massaguer E, Cervera L and Gòdia F, Quantification of the HIV-1 virus-like particle production process by super-resolution imaging: from VLP budding to nanoparticle analysis. *Biotechnol Bioeng* **117**:1929–1945 (2020).
 - 21 Puente-Massaguer E, Cajamarca-Berrezueta B, Volart A, González-Domínguez I and Gòdia F, Transduction of HEK293 cells with BacMam baculovirus is an efficient system for the production of HIV-1 virus-like particles. *Viruses* **14**:636 (2022).
 - 22 Puente-Massaguer E, Lecina M and Gòdia F, Integrating nanoparticle quantification and statistical design of experiments for efficient HIV-1 virus-like particle production in high five cells. *Appl Microbiol Biotechnol* **104**:1569–1582 (2020).
 - 23 Puente-Massaguer E, Lecina M and Gòdia F, Application of advanced quantification techniques in nanoparticle-based vaccine development with the Sf9 cell baculovirus expression system. *Vaccine* **38**:1849–1859 (2020).
 - 24 Cruz PE, Cunha A, Peixoto CC, Clemente J, Moreira JL and Carrondo MJT, Optimization of the production of virus-like particles in insect cells. *Biotechnol Bioeng* **60**:408–418 (1998).
 - 25 Puente-Massaguer E, Lecina M and Gòdia F, Nanoscale characterization coupled to multi-parametric optimization of Hi5 cell transient gene expression. *Appl Microbiol Biotechnol* **102**:10495–10510 (2018).
 - 26 Puente-Massaguer E, Saccardo P, Ferrer-Miralles N, Lecina M and Gòdia F, Coupling microscopy and flow cytometry for a comprehensive characterization of nanoparticle production in insect cells. *Cytometry A* **97**:921–932 (2020).
 - 27 Hermida-Matsumoto L and Resh MD, Localization of human immunodeficiency virus type 1 Gag and Env at the plasma membrane by confocal imaging. *J Virol* **74**:8670–8679 (2000).
 - 28 Nika L, Wallner J, Palmberger D, Koczka K, Vorauer-Uhl K and Grabherr R, Expression of full-length HER2 protein in Sf9 insect cells and its presentation on the surface of budded virus-like particles. *Protein Expr Purif* **136**:27–38 (2017).
 - 29 Pereira Aguilar P, González-Domínguez I, Schneider TA, Gòdia F, Cervera L and Jungbauer A, At-line multi-angle light scattering detector for faster process development in enveloped virus-like particle purification. *J Sep Sci* **42**:2640–2649 (2019).
 - 30 González-Domínguez I, Puente-Massaguer E, Cervera L and Gòdia F, Quality assessment of virus-like particles at single particle level: a comparative study. *Viruses* **12**:223–235 (2020).
 - 31 Steppert P, Burgstaller D, Klausberger M, Kramberger P, Tover A, Berger E *et al.*, Separation of HIV-1 gag virus-like particles from vesicular particles impurities by hydroxyl-functionalized monoliths. *J Sep Sci* **40**:979–990 (2017).
 - 32 Reiter K, Aguilar PP, Grammelhofer D, Joseph J, Steppert P and Jungbauer A, Separation of influenza virus-like particles from baculovirus by polymer grafted anion-exchanger. *J Sep Sci* **43**:2270–2278 (2020).
 - 33 Steppert P, Burgstaller D, Klausberger M, Berger E, Aguilar PP, Schneider TA *et al.*, Purification of HIV-1 gag virus-like particles and separation of other extracellular particles. *J Chromatogr A* **1455**:93–101 (2016).
 - 34 Lynch A, Meyers AE, Williamson A-L and Rybicki EP, Stability studies of HIV-1 Pr55gag virus-like particles made in insect cells after storage in various formulation media. *Virology* **9**:210 (2012).
 - 35 González-Domínguez I, Lorenzo E, Bernier A, Cervera L, Gòdia F and Kamen A, A four-step purification process for gag vlps: from culture supernatant to high-purity lyophilized particles. *Vaccine* **9**:1154 (2021).
 - 36 van Oers M and Vlaskovits J, Baculovirus genomics. *Curr Drug Targets* **8**:1051–1068 (2007).
 - 37 Wickham TJ, Davis T, Granados RR, Hammer DA, Shuler ML and Wood HA, Baculovirus defective interfering particles are responsible for variations in recombinant protein production as a function of multiplicity of infection. *Biotechnol Lett* **13**:483–488 (1991).
 - 38 Valley-Omar Z, Meyers AE, Shephard EG, Williamson A-L and Rybicki EP, Abrogation of contaminating RNA activity in HIV-1 gag VLPs. *Virology* **8**:462 (2011).
 - 39 Fatima F and Nawaz M, Vesiculated long non-coding RNAs: offshore packages deciphering trans-regulation between cells, cancer progression and resistance to therapies. *Noncoding RNA* **3**:10 (2017).
 - 40 Lecina M, Soley A, Gràcia J, Espunya E, Lázaro B, Cairó JJ *et al.*, Application of on-line OUR measurements to detect actions points to improve baculovirus-insect cell cultures in bioreactors. *J Biotechnol* **125**:385–394 (2006).
 - 41 Puente-Massaguer E, Grau-García P, Strobl F, Grabherr R, Striedner G, Lecina M *et al.*, Accelerating HIV-1 VLP production using stable high five insect cell pools. *Biotechnol J* **16**:1–12 (2021).
 - 42 Puente-Massaguer E, Grau-García P, Strobl F, Grabherr R, Striedner G, Lecina M *et al.*, Stable Sf9 cell pools as a system for rapid HIV-1 virus-like particle production. *J Chem Technol Biotechnol* **96**:3388–3397 (2021).
 - 43 Vidigal J, Fernandes B, Dias MM, Patrone M, Roldão A, Carrondo MJT *et al.*, RMCE-based insect cell platform to produce membrane proteins captured on HIV-1 gag virus-like particles. *Appl Microbiol Biotechnol* **102**:655–666 (2018).
 - 44 Puente-Massaguer E, Gòdia F and Lecina M, Development of a non-viral platform for rapid virus-like particle production in Sf9 cells. *J Biotechnol* **322**:43–53 (2020).
 - 45 Puente-Massaguer E, Strobl F, Grabherr R, Striedner G, Lecina M and Gòdia F, PEI-mediated transient transfection of high five cells at bioreactor scale for HIV-1 VLP production. *Nanomaterials* **10**:1–16 (2020).
 - 46 Reiter K, Aguilar PP, Wetter V, Steppert P, Tover A and Jungbauer A, Separation of virus-like particles and extracellular vesicles by flow-through and heparin affinity chromatography. *J Chromatogr A* **1588**:77–84 (2019).
 - 47 Heinimäki S, Tamminen K, Malm M, Vesikari T and Blazevic V, Live baculovirus acts as a strong B and T cell adjuvant for monomeric and oligomeric protein antigens. *Virology* **511**:114–122 (2017).
 - 48 Thompson CM, Petiot E, Mullick A, Aucoin MG, Henry O and Kamen A, Critical assessment of influenza VLP production in Sf9 and HEK293 expression systems. *BMC Biotechnol* **15**:1–12 (2015).
 - 49 Sakuragi S, Goto T, Sano K and Morikawa Y, HIV type 1 Gag virus-like particle budding from spheroplasts of *Saccharomyces cerevisiae*. *Proc Natl Acad Sci U S A* **99**:7956–7961 (2002).
 - 50 Fernandes B, Vidigal J, Correia R, Carrondo MJT, Alves PM, Teixeira AP *et al.*, Adaptive laboratory evolution of stable insect cell lines for improved HIV-Gag VLPs production. *J Biotechnol* **307**:139–147 (2020).
 - 51 Fernandes B, Correia R, Sousa M, Carrondo MJT, Alves PM and Roldão A, Integrating high cell density cultures with adapted laboratory evolution for improved Gag-HA virus-like particles production in stable insect cell lines. *Biotechnol Bioeng* **118**:2536–2547 (2021).
 - 52 Pillay S, Meyers A, Williamson AL and Rybicki EP, Optimization of chimeric HIV-1 virus-like particle production in a baculovirus-insect cell expression system. *Biotechnol Prog* **25**:1153–1160 (2009).
 - 53 Monteiro F, Bernal V and Alves PM, The role of host cell physiology in the productivity of the baculovirus-insect cell system: fluxome analysis of *Trichoplusia ni* and *Spodoptera frugiperda* cell lines. *Biotechnol Bioeng* **114**:674–684 (2017).
 - 54 Rhiel M, Mitchell-Logean CM and Murhammer DW, Comparison of *Trichoplusia ni* BTI-Tn-5b1-4 (high five) and *Spodoptera frugiperda* Sf-9 insect cell line metabolism in suspension cultures. *Biotechnol Bioeng* **55**:909–920 (1997).
 - 55 Benslimane C, Elias CB, Hawari J and Kamen A, Insights into the central metabolism of *Spodoptera frugiperda* (Sf-9) and *Trichoplusia ni* BTI-Tn-5B1-4 (Tn-5) insect cells by radiolabeling studies. *Biotechnol Prog* **21**:78–86 (2005).
 - 56 Strobl F, Ghorbanpour SM, Palmberger D and Striedner G, Evaluation of screening platforms for virus-like particle production with the baculovirus expression vector system in insect cells. *Sci Rep* **10**:1065 (2020).

HEK293 Suspension Cell Culture Using the BioFlo® 320 Bioprocess Controller with BioBLU® 3c Single-Use Bioreactors

Jorge L. Escobar Ivirico and Ma Sha
Eppendorf, Inc., Enfield, CT, USA

Contact: bioprocess-experts@eppendorf.com

Abstract

Mammalian cells cultivated *in vitro* represent one of the most important manufacturing platforms for vaccine and gene therapy developers. Especially, human embryonic kidney 293 (HEK293) cells are an attractive and reliable host for numerous biotherapeutic platforms. HEK293 cells have a wide variety of advantages including low-maintenance, rapid proliferation, and convenient application to both, transient and stable expression. Furthermore, they are easy to transfect and can produce large amounts of recombinant proteins and virus particles. However, a major limitation of the cell line is its tendency to clump when converted to suspension format and there-

fore has been limited to adherent cell culture. To achieve large scale protein production, a new suspension-adapted HEK293 cell line, Expi293F™, was developed by Thermo Fisher. The new HEK293 cell line appears to be a robust suspension cell line capable of achieving greater per cell productivity in high density culture without clumping. In this study, we evaluated the cell line using bioreactor batch culture. We used a BioFlo® 320 bioprocess control system and a BioBLU® 3c Single-Use Bioreactor to carry out Expi293F batch culture in 2 L scale. In addition we monitored and analyzed the metabolites as well as cell density and viability during 11 days of culture.

Interested in more bioprocess information?

Our quarterly Bioprocess Spotlight newsletter keeps you up to date about educational material, events, and product news related to your cell culture bioprocess workflow.



You can conveniently unsubscribe from the newsletter at any time.

Subscribe here: www.eppendorf.group/bioprocess-spotlight



Introduction

Developing innovative preventive solutions through new vaccine technologies or gene therapy platforms that respond to new diseases is an important challenge in present day biotechnology. The gene therapy market is projected to reach more than \$ 3 billion by 2023 and the global vaccine market is expected to reach \$46 billion by 2022, pushing them to the apex of the biotechnology food chain [1-3]. To produce high-quality biotherapeutics, process development involves several demanding components including cost, cell line development, small scale exploration, effective scaling, and optimization of upstream/downstream processes.

The selection of the host cell is a key factor based on its capabilities and properties, including its ability to grow in suspension or adhere to a substrate. HEK293 is one of the most versatile mammalian cell lines with a wide range of applications including expression of recombinant proteins, antibodies and viruses. The HEK293 cell line was immortalized in 1973 by the integration of a ~4.3 kbp adenoviral 5 (Ad5) genome fragment containing the E1A and E1B genes, located on chromosome 19 [4,5]. E1A and E1B are essential helper factors for adeno-associated virus (AAV) manufacture, making these cells a popular host platform for AAV particles production [6]. Our goal in this project was to evaluate the suspension culture of Expi293F cell line using Eppendorf bioprocess equipment and assess its suitability in virus production.

HEK293 in gene therapy

Gene therapy involves the transfer of functional genes into cells to replace absent genes or correct defective ones. In a typical protocol, the cells are extracted from the donor and genetically modified by introducing a new or modified gene to inactivate or to replace a disease-causing gene. These modified cells are then reimplanted in the subject (ex vivo strategy). In addition, a well-established cell culture platform, such as HEK293, can be used to produce viral or non-viral delivery vehicles to introduce the gene of interest (GOI).

A well-established method (transient transfection) is frequently employed to produce different vectors using adherent human HEK293 cells cultivated in T-flasks or bioreactors. Prominent examples include lentivirus [7, 8], adenovirus [9,10], non-viral vectors [11], and AAV [12,13]. AAV represents one of the leading platforms for gene therapy due to its ability to provide in vivo long-term gene expression. Nearly 200 AAV clinical trials and biotherapeutic protocols are in different stages of FDA review, in which the transient transfection of adherent HEK293 cells has been the predominant

platform [14,15]. We believe that the Expi293F cell line is a significant improvement over traditional HEK293 cell lines due to its robust growth under suspension culture conditions as well as its property of stable expression in addition to transient expression.

HEK293 in vaccine production

During the last century, vaccines saved billions of lives throughout the world. Vaccine technology has distinguished itself as the most important development in the history of medicine. This unparalleled success has driven researchers to explore new and more efficient platforms to meet the constantly expanding demands of the industry.

Conventional vaccines usually contain whole weakened or inactivated viruses or protein subunits made by the pathogen to trigger an immune response. The cell-based vaccine platform is a well-established technology [16], offering several notable advantages:

- > cell lines are well characterized and may be easily stored for future applications,
- > their use avoids dependence on embryonated chicken eggs (ECE), whose quality is highly and unpredictably variable, despite their being the most common method used to develop vaccines,
- > some viruses grow better in cells reducing the time to achieve high growth profiles [17],
- > compared to ECE, viruses propagated in mammalian cells have shown an antigenic profile similar or identical to that of the field virus [18], and
- > scalability is superior to the ECE production platform [19].

Although numerous mammalian cell lines have been evaluated for vaccine production [20-24], and performance in gene therapy protocols, the HEK293 cell line is one of the most widely used cell platforms for these demands. Specifically, high yield adenoviral vectors (~4 × 10¹⁵ viral particles) have been obtained in stirred-tank bioreactor systems using microcarriers [25,26]. Adherent HEK293 cells are easy to cultivate at laboratory scale, and require less expert bioengineering know-how, but when biotherapeutics production increases, suspension cell lines offer advantages in terms of scalability and robustness, using established stirred-tank bioreactor platforms. Eppendorf bioprocess systems, including BioFlo 320, are not medical devices and cannot be directly used for Gene Therapy and Vaccine production without special approval process. However, it can be used for effective HEK293 suspension cell culture and virus production research including research in the Gene Therapy and Vaccine production field at R&D level. To this end,

APPLICATION NOTE | No. 447

Expi293F cells (a suspension adapted HEK293 cell line) can accelerate the therapeutics development by enabling rapid, high yield and scalable production of proteins, viral antigens and AAV particles.

In this study, we used a BioBLU 3c Single-Use Bioreactor for Expi293F cell expansion and a BioFlo 320 as the bioprocess control system (Figure 1). We analyzed the cell growth, the viability as well as the metabolic activity (levels of glucose, ammonia and lactate in the medium).



Fig. 1: BioBLU 3c Single-Use Bioreactor (left) and BioFlo 320 bioprocess control system (right).

Technical Features

In this study, pH, DO, and temperature were controlled online. Get to know more about the possibilities for bioprocess control with the BioFlo 320.



www.eppendorf.group/bioflo320

Material and Methods

Cell line and medium

We cultured the suspension Expi293F cell line (Thermo Fisher Scientific, USA) in Expi293 Expression Medium (Thermo Fisher Scientific, USA) formulated with GlutaMAX-I reagent. Expi293 Expression Medium is a chemically defined, serum and protein-free medium, ready to use without need for additional supplements.

Inoculum preparation

We rapidly thawed the cryovial containing 1 mL of Expi293F cells (Thermo Fisher Scientific, A14527) at 1×10^7 cells/mL, from a previously prepared cell bank, using a ThawSTAR® CFT2 instrument (MedCision®, USA). Just before the cells

were completely thawed we decontaminated the vial wiping it with 70% alcohol before opening it in a laminar flow hood. We transferred the entire content of the cryovial into a 125 mL disposable, sterile and vented shaker flask containing 30 mL (24 % of the total volume) of pre-warmed Expi293 Expression Medium (Thermo Fisher Scientific, A1435101). We cultured the cells in a New Brunswick™ S41i CO₂ incubator Shaker (Eppendorf, Germany) at 37 °C, 8 % CO₂ and at agitation speed of 125 rpm. We cultured the cells for 4 days after thawing and then determined the cell viability and total viable cells using a Vi-CELL XR cell viability analyzer (Beckman Coulter). We then performed the subsequent passages when the viable cell density reached around 3×10^6 cells/mL (typically 4 days after shaker flask inoculation) reaching more than 900×10^6 cells in the third passage. During the expansion process we kept the inoculation density, percentage fill of the shake flasks and other parameters constant. Finally, we prepared the inoculum containing 800×10^6 cells in 200 mL of Expi293F Expression Medium. The cell expansion workflow is shown in Figure 2.

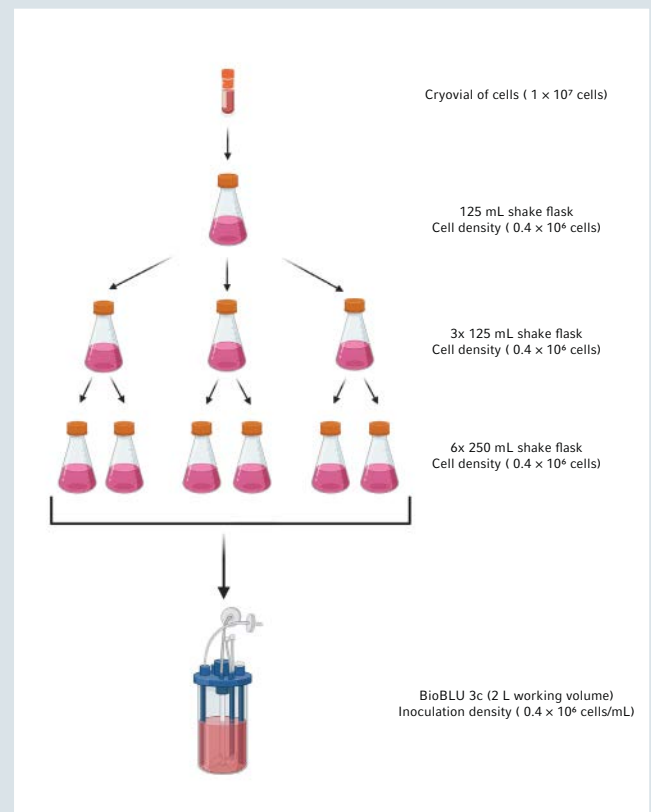


Fig. 2: Inoculum preparation.

Created with: BioRender.com.

Bioreactor control

We used a BioFlo 320 bioprocess control station to perform two batch cultures using BioBLU 3c Single-Use Bioreactors equipped with a single pitched-blade impeller. The bioreactor unit is equipped with two universal port connectors for pH (port 1) and DO (port 2) sensors, an heat blanket connection providing precise temperature control, agitation control and a gas module that includes 3 TMFC, high-flow sparge drawer with a gas flow range of 0.04 – 20 SLPM.

Sensor calibration

Prior to the preparation of the BioBLU 3c Single-Use Bioreactors, we connected the gel-filled pH sensor to the BioFlo 320 bioprocess controller. The software automatically detects the connected sensors to support an efficient workflow. We performed the calibration process according to the operation's manual using buffer solutions of pH 7 and pH 4 as "zero" and "span" respectively. Then, we disconnected the pH sensor and sterilized it in an autoclavable pouch.

BioBLU 3c Single-Use Bioreactor preparation and process parameters

We equipped the BioBLU 3c with a magnetic drive, the previously sterilized pH sensor, inserted in a spare PG 13.5 port under aseptic conditions in the Biosafety Cabinet, a polarographic DO sensor (Mettler Toledo®), an exhaust condenser, a 3-gas mixing line connected to the gas sparge port, and 3 liquid addition ports (one for inoculation/glucose addition, one for base addition and another for the addition of 0.1 % of antifoam (Pluronic®-F68 surfactant, Life Technologies®, 24040-032). Then, we controlled the temperature using a heat blanket. Finally, we introduced the 1.8 L of Expi293F Expression Medium into each bioreactor and conditioned for at least 24 hours under the parameters and setpoints listed in Table 1.

Table 1: Process parameters and setpoints of the first and second experiments.

Parameters	Setpoints
Starting volume	1.8 L
Ending volume	2 L
Initial agitation	120 rpm (0.4 m/s tip speed)
Temperature	37 °C
Inoculation density	0.4 x 10 ⁶ cell/mL
Cell culture medium	Expi293™ Expression Medium
DO Setpoint	40% (P=0.1; I=0.001)
pH Setpoint	7.0 (deadband = 0.2), cascade to CO ₂ (acid) and cascade to 0.45 M sodium bicarbonate (base)
Gassing range	Air flow: 0.04 SLPM -1 SLPM O ₂ flow: 0 SLPM -1 SLPM

Expi293FTM cells culture on BioBLU 3c Single-Use Bioreactor

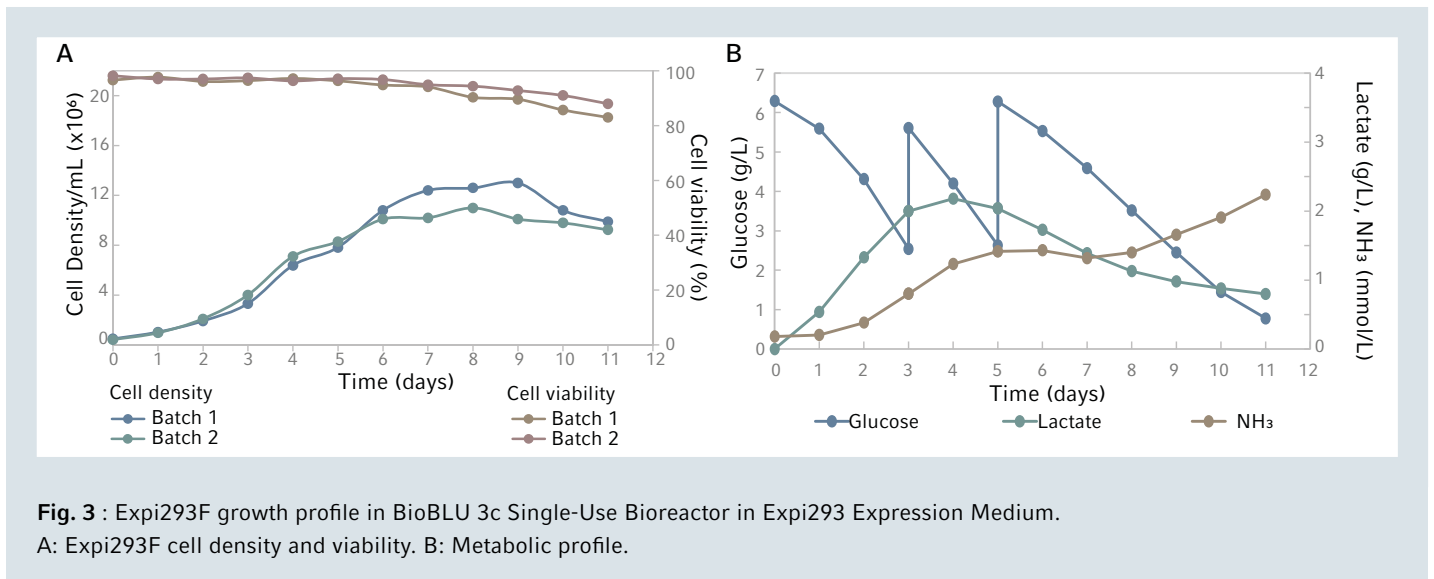
We inoculated the BioBLU 3c Single-Use Bioreactors with the inoculum described above (see section "Inoculum preparation") reaching 2 L as working volume with a cell density around 0.4 x 10⁶ cell/mL and more than 95 % of cell viability. We monitored the temperature at 37 °C and controlled the dissolved oxygen (DO) at 40 % using the 3-Gas Auto mode. In addition, we limited the oxygen flow to 0 – 1 SLPM and the air flow to 0.04 – 1 SLPM in the controller setup screen to avoid high gas flow that can cause DO fluctuation and excessive foaming in the beginning stage of the cells culture. In addition to the gas flow limit, we added Pluronic-F68 surfactant as needed. We used a gel-filled pH sensor to control the pH during the cell culture run at 7.0 (deadband = 0.2), using a cascade to CO₂ (acid) and 0.45 M sodium bicarbonate (base). We took a sample from the bioreactor daily and measured the pH, the cell viability and density as well as the concentration of various metabolites offline.

Cell viability and metabolic activity

We collected samples on a daily basis from the BioBLU 3c Single-Use Bioreactors to determine the cell viability, cellular density, and the concentration of metabolites (glucose, ammonia (NH₃) and lactate), by connecting a sterile 5 ml syringe to the Luer Lock sample port. Then, we discarded 5 mL of dead volume and collected again 3 mL (using a new 5 mL sterile syringe) as a viable sample for analysis. We used 1 mL to measure the metabolite levels employing a Cedex® Bio Analyzer (Roche, USA), 1 mL to measure the cell viability and density using a Vi-Cell® XR Viability Analyzer (Beckman Coulter®, USA) and 1 mL to check the pH offline using an Orion Star A211 pH meter (Thermo Fisher Scientific, USA), which we calibrate daily using standard pH buffers.

Results and Discussion

To evaluate the Expi293F suspension culture robustness, we performed two bioreactor batch culture runs using BioBLU 3c Single-Use Bioreactors controlled by BioFlo 320 bioprocess controller. We used Expi293 Expression Medium with additional glucose supplementation to extend the growth phase and increase the peak cell density. The inoculum was ready after the cell expansion in the New Brunswick S41i CO₂ incubator Shaker at 37 °C and 8 % CO₂ and agitation speed of 125 rpm. We then inoculated the BioBLU 3c Single-Use Bioreactor with an initial cell density of 0.4 x 10⁶ cells/mL under a controlled environment (see Table 1).



In addition, we added Pluronic-F68 surfactant (0.1 %) to the medium in the bioreactor to decrease foaming produced by the gas introduced through the sparger.

As shown in Figure 3A, we observed a rapid increase of cell growth between days 1 and 9 of culture, reaching a peak in viable cells density at 13×10^6 cells/mL, followed by a decrease in cell density and viability as anticipated. Furthermore, we determined the consumption of glucose and production of lactate and NH_3 while at the same time maintaining the concentration of lactate and NH_3 below 2 g/L and 2 mmol/L respectively during the whole run (See Figure 3B). We performed bolus glucose supplementation (to maintain target concentration > 2 g/L in both runs) at days 3 and 5 to extend the growth phase. The ammonia concentration gradually increased every day up to 2.2 mmol/L on day 11. We believe the depletion of glucose and other nutrients contributed to the decrease of the cell density, starting from day 9. Overall, cell growth increased around 32-fold.

Conclusions

Using the BioFlo 320 bioprocess control system and BioBLU 3c Single-Use Bioreactors, we demonstrated the feasibility of applying glucose-enhanced batch culture technique to expand Expi293F cells rapidly up to 13 million cells/mL within 9 days. The efficient and straightforward configuration of the BioFlo 320 allows precise control of the cell culture environment, leading to reliable cell expansion. Although the experiments were conducted as feasibility studies and no optimization of conditions was attempted, we observed vigorous growth of Expi293F in suspension culture at a pace and simplicity close to Chinese hamster ovary (CHO) cells, the accepted industry standard. We believe that the Expi293F cell line has great potential in both vaccine and gene therapy method development when used in conjunction with Eppendorf's advanced stirred-tank bioreactors.

APPLICATION NOTE | No. 447

Literature

- [1] Grand View Research, "Gene Therapy Market Size, Share & Trends Analysis," 2019.
- [2] Markets and Markets, "Gene Therapy Market by Vectors," 2019.
- [3] Vaccines Market by Indication, Type, Route of Administration & Geography / Global Vaccines Market Forecasts 2018-2025 / ResearchandMarkets.com/CoherentMarketInsights, 2018.
- [4] Graham FL, Smileyt J, Russell WC, Nairn R. Characteristics of a Human Cell Line Transformed by DNA from Human Adenovirus Type 5. *J. gen. Virol* 1977; 36:59–7.
- [5] Louis N, Eveleigh C, Graham FL, 1997. Cloning and Sequencing of the Cellular– Viral Junctions from the Human Adenovirus Type 5 Transformed 293 Cell Line. *Virology* 1997; 233:423–429.
- [6] Clément N, Grieger JC. Manufacturing of recombinant adeno-associated viral vectors for clinical trials. *Mol. Ther. Methods Clin. Dev.* 2016; 3:16002.
- [7] McCarron A, Donnelley M, McIntyre C, Parsons D. Transient Lentiviral Vector Production in HEK 293T Cells Using the BioFlo® 320 Control Station with a BioBLU® 5p Single-Use Packed-Bed Vessel. *Application Note* 2019; App-411.
- [8] Ferreira CB, Sumner RP, Rodriguez-Plata MT, Rasaiyaah J, Milne RS, Thrasher AJ, Qasim W, and Towers GJ. Lentiviral Vector Production Titer Is Not Limited in HEK293T by Induced Intracellular Innate Immunity. *Molecular Therapy: Methods & Clinical Development.* 2020; 17:209-219.
- [9] Feng L, Wang Q, Shan C, Yang C, et al. An adenovirus-vectored COVID-19 vaccine confers protection from SARS-COV-2 challenge in rhesus macaques. *Nat Commun.* 2020; 11:4207.
- [10] Fedosyuk S, Merritt T, Peralta-Alvarez MP, Morris SJ, et al. Simian adenovirus vector production for early-phase clinical trials: A simple method applicable to multiple serotypes and using entirely disposable product-contact components. *Vaccine.* 2019; 37:6951–6961.
- [11] Patil S, Gao YG, Lin X, et al. The Development of Functional Non-Viral Vectors for Gene Delivery. *Int J Mol Sci.* 2019; 20:5491.
- [12] Wang D, Tai PWL, Gao G. Adeno-associated virus vector as a platform for gene therapy delivery. *Nat Rev Drug Discov.* 2019; 18:358–378.
- [13] Li C, Samulski RJ. Engineering adeno-associated virus vectors for gene therapy. *Nat Rev Genet.* 2020; 21:255–272.
- [14] Rumachik NG, Malaker SA, Poweleit N, et. Methods Matter: Standard Production Platforms for Recombinant AAV Produce Chemically and Functionally Distinct Vectors. *Molecular Therapy: Methods & Clinical Development.* 2020; 18:98-118.
- [15] Grimm D, Kern A, Rittner K, Kleinschmidt JA. Novel tools for production and purification of recombinant adeno-associated virus vectors. *Hum. Gene Ther.* 1998; 9:2745–2760.
- [16] Le Ru A, Jacob D, Transfiguracion J, Ansoorge S, Henry O, Kamen AA. Scalable production of influenza virus in HEK-293 cells for efficient vaccine manufacturing. *Vaccine.* 2010; 28:3661–3671.
- [17] Jung EJ, Lee KH, Seong BL. Reverse genetic platform for inactivated and live-attenuated influenza vaccine. *Exp Mol Med.* 2010; 42:116-21.
- [18] Donis RO. The Influenza Cell Culture Working Group. Performance characteristics of qualified cell lines for isolation and propagation of influenza viruses for vaccine manufacturing. *Vaccine.* 2014; 32:6583-90.
- [19] Hegde NR. Cell culture-based influenza vaccines: A necessary and indispensable investment for the future. *Hum Vaccin Immunother.* 2015; 11:1223–1234.
- [20] Rimmelzwaan GF, Baars M, Claas ECJ, Osterhaus ADME. Comparison of RNA hybridization, hemagglutination assay, titration of infectious virus and immunofluorescence as methods for monitoring influenza virus replication in vitro. *Journal of Virological Methods.* 1998; 74:57–66.
- [21] Voeten JTM, Brands R, Palache AM, et al. Characterization of high-growth reassortant influenza A viruses generated in MDCK cells cultured in serum-free medium. *Vaccine.* 1999; 17:1942–1950.
- [22] Pau MG, Ophorst C, Koldijk MH, Schouten G, Mehtali M, Uytdehaag F. The human cell line PER.C6 provides a new manufacturing system for the production of influenza vaccines. *Vaccine.* 2001; 19:2716–2721.
- [23] Kistner O, Barrett PN, Mundt W, Reiter M, Schober-Bendixen S, Dorner F. Development of a mammalian cell (Vero) derived candidate influenza virus vaccine. *Vaccine.* 1998; 16:960–968.
- [24] Youil R, Su Q, Toner TJ, et al. Comparative study of influenza virus replication in Vero and MDCK cell lines. *Journal of Virological Methods.* 2004; 120:23–31.
- [25] Vemula SV, Mittal SK. Production of adenovirus vectors and their use as a delivery system for influenza vaccines. *Expert Opinion on Biological Therapy.* 2010; 10:1469–1487.
- [26] Fuenmayor Garcés J, Gutiérrez Granados S, Gòdia Casablanca F, Cervera Gracia L. Cell line and plasmid influence on the efficiency of HEK293 cells transient transfection for the production of VLP-based vaccines. *New Biotechnology.* 2016; 33:S32-S33.

APPLICATION NOTE | No. 447

Ordering information

Description	Order no.
BioFlo® 320 , base control station, no water connection	1379962911
BioFlo® 320 , left-handed orientation/four front-mounted peristaltic pumps (3 @ 5 – 25 rpm/1 @ 20 – 100 rpm)	1379963211
BioFlo® 320 , sparge gas option, 3 TMFC (0.04 – 20 SLPM)	1379501311
Accessories	
Touchscreen Monitor Bundle , includes desk mount and 1 meter cable set, for BioFlo® 320	M1379-9906
Bioreactor	
Single-Use Vessel Bundle , for BioFlo® 320, for BioBLU® 3c/5c	M1379-0322
BioBLU® 3c , 1.25 L - 3.75 L, Microsparger, 1x pitched-blade	1386000100
BioBLU® 3c , 1.25 L - 3.75 L, Macrosparger, 1x pitched-blade	1386000300
BioBLU® 3c , 1.25 L - 3.75 L, Microsparger, 2x pitched-blade	1386120000
BioBLU® 3c , 1.25 L - 3.75 L, Macrosparger, 2x pitched-blade	1386121000

Your local distributor: www.eppendorf.com/contact
 Eppendorf SE · Barkhausenweg 1 · 22339 · Hamburg · Germany
eppendorf@eppendorf.com · www.eppendorf.com

www.eppendorf.com/bioprocess

FlowStar® and MedCision® are registered trademarks of MedCision Inc., USA. Mettler Toledo® is a registered trademark of Mettler-Toledo AG, Switzerland. Pluronic® and Life Technologies® are registered trademarks of Life Technologies Corp. USA. Cedex® is a registered trademark of Roche Diagnostics GmbH, Germany. VI-Cell® and Beckman Coulter® are registered trademarks of Beckman Coulter, Inc., USA. BioBLU®, Eppendorf® and the Eppendorf Brand Design are registered trademarks of Eppendorf SE, Germany. BioFlo® is a registered trademark of Eppendorf Inc., USA. Expi293F™ and Thermo Scientific™ are trademarks of Thermo Fisher Scientific Inc., USA. All rights reserved, including graphics and images. Copyright © 2022 by Eppendorf SE.

eBook: It's All About Stem Cells

This eBook covers various topics from modern medicine to novel foods. With an interesting editorial about how stem cell research can change the world, application notes on hiPSC-derived cardiomyocytes and exosome production, and a Q&A with Prof. Mark Post - CEO from MosaMeat, this eBook is a must-read for everyone who is working in stem cell research.

Get your free copy now!
<https://eppendorf.group/stemcell-bioprocessing>

